Wissenschaftliche Reihe
Fahrzeugtechnik Universität Stuttgart

RESEARCH

Francesco Cupo

Modeling of Real Fuels and Knock Occurrence for an Effective 3D-CFD Virtual Engine Development

IVK

Springer Vieweg

Wissenschaftliche Reihe Fahrzeugtechnik Universität Stuttgart

Reihe herausgegeben von

Michael Bargende, Stuttgart, Deutschland

Hans-Christian Reuss, Stuttgart, Deutschland

Jochen Wiedemann, Stuttgart, Deutschland

Das Institut für Fahrzeugtechnik Stuttgart (IFS) an der Universität Stuttgart erforscht, entwickelt, appliziert und erprobt, in enger Zusammenarbeit mit der Industrie, Elemente bzw. Technologien aus dem Bereich moderner Fahrzeugkonzepte. Das Institut gliedert sich in die drei Bereiche Kraftfahrwesen, Fahrzeugantriebe und Kraftfahrzeug-Mechatronik. Aufgabe dieser Bereiche ist die Ausarbeitung des Themengebietes im Prüfstandsbetrieb, in Theorie und Simulation. Schwerpunkte des Kraftfahrwesens sind hierbei die Aerodynamik, Akustik (NVH), Fahrdynamik und Fahrermodellierung, Leichtbau, Sicherheit, Kraftübertragung sowie Energie und Thermomanagement – auch in Verbindung mit hybriden und batterieelektrischen Fahrzeugkonzepten. Der Bereich Fahrzeugantriebe widmet sich den Themen Brennverfahrensentwicklung einschließlich Regelungs- und Steuerungskonzeptionen bei zugleich minimierten Emissionen, komplexe Abgasnachbehandlung, Aufladesysteme und -strategien, Hybridsysteme und Betriebsstrategien sowie mechanisch-akustischen Fragestellungen. Themen der Kraftfahrzeug-Mechatronik sind die Antriebsstrangregelung/Hybride, Elektromobilität, Bordnetz und Energiemanagement, Funktions- und Softwareentwicklung sowie Test und Diagnose. Die Erfüllung dieser Aufgaben wird prüfstandsseitig neben vielem anderen unterstützt durch 19 Motorenprüfstände, zwei Rollenprüfstände, einen 1:1-Fahrsimulator, einen Antriebsstrangprüfstand, einen Thermowindkanal sowie einen 1:1-Aeroakustikwindkanal. Die wissenschaftliche Reihe „Fahrzeugtechnik Universität Stuttgart“ präsentiert über die am Institut entstandenen Promotionen die hervorragenden Arbeitsergebnisse der Forschungstätigkeiten am IFS.

Reihe herausgegeben von

Prof. Dr.-Ing. Michael Bargende
Lehrstuhl Fahrzeugantriebe
Institut für Fahrzeugtechnik Stuttgart
Universität Stuttgart
Stuttgart, Deutschland

Prof. Dr.-Ing. Hans-Christian Reuss
Lehrstuhl Kraftfahrzeugmechatronik
Institut für Fahrzeugtechnik Stuttgart
Universität Stuttgart
Stuttgart, Deutschland

Prof. Dr.-Ing. Jochen Wiedemann
Lehrstuhl Kraftfahrwesen
Institut für Fahrzeugtechnik Stuttgart
Universität Stuttgart
Stuttgart, Deutschland

Weitere Bände in der Reihe http://www.springer.com/series/13535

Francesco Cupo

Modeling of Real Fuels and Knock Occurrence for an Effective 3D-CFD Virtual Engine Development

Springer Vieweg

Francesco Cupo
Institute of Automotive Engineering IFS,
Chair of Vehicle Drives
University of Stuttgart
Stuttgart, Germany

Dissertation University of Stuttgart, 2020

D93

ISSN 2567-0042 ISSN 2567-0352 (electronic)
Wissenschaftliche Reihe Fahrzeugtechnik Universität Stuttgart
ISBN 978-3-658-31627-3 ISBN 978-3-658-31628-0 (eBook)
https://doi.org/10.1007/978-3-658-31628-0

© The Editor(s) (if applicable) and The Author(s), under exclusive license to Springer Fachmedien Wiesbaden GmbH, part of Springer Nature 2021
This work is subject to copyright. All rights are solely and exclusively licensed by the Publisher, whether the whole or part of the material is concerned, specifically the rights of translation, reprinting, reuse of illustrations, recitation, broadcasting, reproduction on microfilms or in any other physical way, and transmission or information storage and retrieval, electronic adaptation, computer software, or by similar or dissimilar methodology now known or hereafter developed.
The use of general descriptive names, registered names, trademarks, service marks, etc. in this publication does not imply, even in the absence of a specific statement, that such names are exempt from the relevant protective laws and regulations and therefore free for general use.
The publisher, the authors and the editors are safe to assume that the advice and information in this book are believed to be true and accurate at the date of publication. Neither the publisher nor the authors or the editors give a warranty, expressed or implied, with respect to the material contained herein or for any errors or omissions that may have been made. The publisher remains neutral with regard to jurisdictional claims in published maps and institutional affiliations.

This Springer Vieweg imprint is published by the registered company Springer Fachmedien Wiesbaden GmbH part of Springer Nature.
The registered company address is: Abraham-Lincoln-Str. 46, 65189 Wiesbaden, Germany

A Mamma e Papà.

Preface

This work was realized during my activities as a research associate at the Institute of Automotive Engineering (IFS) at the University of Stuttgart.

First of all, I would like to thank Prof. Dr.-Ing. M. Bargende for the outstanding scientific support and inspiration showed during these years. My deep gratitude goes to also to Prof. Dr.-Ing. F. Millo for showing interest in my work and for joining the doctoral committee.

Furthermore, I want to thank Dr. Marco Chiodi, Dr. Andreas Kächele, Oliver Mack, Edoardo Rossi, Rodolfo Tromellini, Antonino Vacca, Dr. Marlene Wentsch, Marcel Eberbach, Hubert Fuesshoeller and all other colleagues at the IFS/FKFS for the pleasant collaboration and the wonderful working atmosphere.

I would like to thank Dr. Donatus Wichelhaus and Dr. Daniel Koch for their extensive support in different projects during the past years.

I am very grateful to all my friends (better known as Politopi) for sharing with me a big passion and for all unforgettable and noisy moments together.

Finally, I am extremely grateful to my family and Alina Askadullina (aka Ruskaja). Without your support and encouragement, none of this would have been possible.

Stuttgart Francesco Cupo

Contents

Figures

Tables

Abbreviations

0D	Zero dimensional
1D-CFD	One dimensional computational fluid dynamic
3D-CFD	Three dimensional computational fluid dynamic
a.TDC	After Top Dead Center
b.TDC	Before Top Dead Center
BC	Boundary condition
BEV	Battery Electric Vehicle
CFD	Computational Fluid Dynamics
CI	Compression Ignition
CNG	Compressed natural gas
CPU	Central processing unit
DI	Direct Injection
DI-SI	Direct-Injected Spark-Ignited
DNS	Direct numerical simulation
DWI	Direct water injection
EGR	Exhaust gas recirculation
EOI	End Of Injection
EV	Electric Vehicle
FKFS	Forschungsinstitut für Kraftfahrwesen und Fahrzeugmotoren Stuttgart
FTDC	Firing Top Dead Center
GHG	Greenhouse gas
HCCI	Homogeneous Charge Compression Ignition

ICE	Internal Combustion Engine
IDT	Ignition delay time
IFS	Institut für Fahrzeugtechnik Stuttgart
IMEP	Indicated Mean Effective Pressure
IP	Ignition point
IWI	Indirect water injection
KRAT	Knock ratio
LES	Large eddy simulations
LFS	Laminar flame speed
LHV	Lower Heating Value
LLNL	Lawrence Livermore National Laboratory
LVK	Technical University of Munich - Chair of Internal Combustion Engines
MFB	Mass Fraction Burned
MON	Motor Octane Number
MPI	Manifold Port Injection
NTC	Negative temperature coefficient
OEM	Original equipment manufacturer
PRF	Primary Reference Fuel
RANS	Reynolds Averaged Navier-Stokes
RON	Research Octane Number
SACI	Spark Assisted Compression Ignition
SI	Spark Ignition
SOI	Start Of Injection
SPI	Single-Point Injection
TDC	Top Dead Center

TRF	Toluene Reference Fuel
TUM	Technische Universität München
WEC	World Endurance Championship
WP	Working process
WRC	World Rally Championship

Symbols

	Latin Letters	
c_f	Long-range process term in conservation equation	-
c_p	Specific heat at constant pressure	J/kgK
F	Extensive variable in conservation equation	-
f	Density / intensive variable in conservation equation	-
G	Gravitational energy	J/kg
H_E	Exhaust enthalpy	J
h_f	Heat of formation	J/kg
H_I	Intake enthalpy	J
H_L	Leakage enthalpy	J
h_{tc}	Thermo-chemical enthalpy	J/kg
h	Enthalpy	J/kg
H_{tot}	Total enthalpy	J
$\vec{j}$	Diffusive mass flux	kg/m^{2}s
K	Wrinkling factor	-
M	Molar mass	kg/kmol
m	Mass	kg
m_B	Fuel mass	kg
m_C	Cylinder mass	kg
m_E	Exhaust gas mass	kg
m_I	Intake mass	kg
m_l	Leakage mass	kg
$\dot{m}$	Mass flow	kg/s
p	Pressure	Pa
p_2	Intake gas pressure	Pa
p_3	Exhaust gas pressure	Pa
p_{ref}	Reference pressure	Pa
$\overline{\overline{P}}$	Second order stress tensor	N/^{2}

Q_B	Fuel heat release	J
Q_W	Wall heat transfer	J
R_s	Specific gas constant	J/kgK
Re	Reynolds number	-
s	Entropy	J/K
s_f	Source or sink term in conservation equation	-
S_L	Laminar Flame speed	m/s
S_T	Turbulent flame speed	m/s
T	Temperature	K
t	Time	s
T_2	Intake gas Temperature	K
T_3	Exhaust gas Temperature	K
t_e	final integration step	-
T_{ref}	Reference temperature	K
T_{unb}	Unburned mass temperature	K
U	Internal energy	J
$\vec{V}$	Diffusive fluid velocity	m/s
V	Volume	m^3
$\vec{v}$	Fluid velocity	m/s
W	Work	J
w	Mass fraction	-
w_{Air_B}	Mass fraction of vaporized fuel that has previously EGR	%
w_{Air_U}	Mass fraction of fresh air	%
w_B	Burned Mass fraction	%
$w_{EGR\_Air\_U}$	Mass fraction of air that has previously produced EGR	%
$w_{EGR\_F\_U}$	Mass fraction of vaporized fuel that has previously EGR	%
w_{F_B}	Mass fraction of vaporized fuel that has previously produced burned gas	%
w_{F_U}	Mass fraction of fresh vaporized fuel	%
w_{Water_B}	Mass fraction of water that has previously produced burned gas	%
w_{Water_U}	Mass fraction of water	%
x_{exh}	EGR concentration	%

	Greek Letters	
λ	Lambda	-
ω_i	Molar formation rate of species i	kmol/m^{3}s
φ	Crank Angle	°CA
$\vec{\Phi}_f$	Flux of the intensive variable f in the conservation equation	-
ϕ_{st}	Stoichiometric air to fuel ratio	-
$\overline{\overline{\Pi}}$	Second order shear stress tensor	N/m^2
ρ	Mass density	kg/m^3
τ	Ignition delay time	s

	Indices
stoich	Stoichiometric
ref	Reference

Abstract

The reduction of both harmful emissions (CO, HC, NO_x, etc.) and gases responsible for greenhouse effects are mandatory aspects to be considered in the development process of any propulsion concept. The main development topics are today not only the reduction of harmful emissions, the increase of thermodynamic efficiency, etc. but also the decarbonization of fuels which offers the highest potential for the reduction of emissions. Accordingly, the development of future ICEs will be strictly linked to the development of CO_2 neutral fuels (e.g. biofuels and e-fuels) as they will be part of a joint development process. This evolution implies an increase in development complexity, which needs the support of engine simulations.

3D-CFD simulation is one of the most detailed approaches for the investigation of the engine operating cycle. However, due to the lack of phenomena understanding at the fundamental physical level, inaccurate mathematical formulations, numerical dependencies on the mesh structure, etc., the models used are often not able to ensure a high level of reliability in reproducing and predicting the requested engine processes. Among others, fuel modelling is one of the most relevant elements affecting the combustion processes of any engine.

For a better investigation of both innovative fuels and complex combustion processes, it is necessary to have an accurate description of real fuel characteristics, which in many cases cannot be ensured by the traditional PRF/TRF (Primary Reference Fuel and Toluene Reference Fuel, respectively) surrogates. The use of detailed fuel description can significantly improve simulation predictability and allow a better and more reliable validation with experimental measurements, especially when several fuel batches with similar compositions are intensively tested. Moreover, such chemical calculations can be used to support fuel investigations by selecting those compositions that better fit the requirements of the considered engine application.

This work aims to enhance the simulation environment of the 3D-CFD tool QuickSim which has been developed and continuously enhanced over the years at the FKFS/IFS in Stuttgart. The introduction of a more accurate fuel descrip-

tion and new combustion models enabled the virtual investigation of alternative fuels and detection of knock occurrence.

In the first part of this work, the 3D-CFD models adopted in QuickSim and the approaches used for the implementation of fuel-specific properties are described. According to the results of the fuel investigations performed on commercial and high-performance fuels, it is shown that to accurately reproduce a wide range of fuel characteristics, an extended surrogate formulation is needed. This requisite implies the necessity to include, in the surrogate, at least one chemical species for each relevant hydrocarbon group present in the fuel. Depending on their concentration, components like cycloalkanes, oxygenates and olefins can have a substantial impact on fuel behaviour.

In QuickSim, to optimise simulation time, the working fluid is described by few scalars, and no detailed chemical reaction mechanism is directly implemented. Consequently, a tabulated approach is used to import thermodynamic properties of the fluid and to characterise fuel properties. The look-up tables describing laminar flame speed and ignition delay time of the fuel are prepared using a tool developed in Cantera. Here, the influence of the following parameters is considered: temperature, pressure, EGR concentration, EGR composition, water concentration and lambda. Among them, water is of particular importance to take into account the influence of air humidity and analyse water injection strategies.

Since no detailed chemical reaction mechanism is directly implemented in the 3D-CFD environment, to reproduce phenomena like autoignition of fresh charge, dedicated models must be implemented. The ignition delay time calculated with Cantera is used as input for a locally-distributed autoignition model based on the well-known Livengood and Wu integral formulation. Differently from the original formulation, the integral is solved in every 3D-cell of the simulation domain and not according to average cylinder conditions. This approach brings to a more precise estimation of radicals formation and gives the possibility to calculate location and quantity of charge in autoignition conditions so that phenomena like knock can be correctly detected.

In the second part of this work, three recent investigations conducted with the support of the newly developed models are presented.

In the first, three fuels with different ethanol content are compared through 3D-CFD engine simulations and their differences in knock behaviour, efficiency and performance potential are discussed. The goal is to understand which are the advantages and disadvantages of ethanol-based fuels.

In the second analysis, the potential benefits of water injection in SI engines are investigated. In this section, it is shown how 3D-CFD simulations can, by utilising the previously introduced models, correctly predict the influence of water on combustion processes and therefore allow the optimisation of water injection strategies.

Finally, a fuel investigation on a single-cylinder research engine operating with the innovative SACI (Spark Assisted Compression Ignition) combustion concept is presented. The study is conducted virtually at the FKFS of Stuttgart and experimentally at the engine laboratory of the Technische Universität München with the support from Volkswagen Motorsport GmbH. Different high-performance fuels are virtually investigated in order to find the best composition that can maximise engine power at constant fuel consumption.

Kurzfassung

Die Reduzierung der schädlichen Emissionen (CO, HC, NO_x, etc.) sowie der für den Treibhauseffekt verantwortlichen Gase sind Kernaspekte, die bei der Entwicklung von Antriebskonzepten zu berücksichtigen sind. Mit Fokus auf den Verbrennungsmotor sind die Hauptentwicklungsthemen heute nicht nur die Reduzierung der Schadstoffemissionen, die Erhöhung des thermodynamischen Wirkungsgrades usw., sondern auch die Dekarbonisierung von Kraftstoffen, welche das größte Potenzial zur CO_2-Emissionsreduzierung bietet. Dementsprechend wird die Entwicklung von zukünftigen Verbrennungsmotoren eng mit der Entwicklung CO_2-neutraler Kraftstoffe (z.B. Biokraftstoffe und e-Kraftstoffe) verbunden sein, da sie Teil eines gemeinsamen Entwicklungsprozesses sind. Dies bedeutet eine Erhöhung der Entwicklungskomplexität, die ohne die Unterstützung durch Motorsimulationen kaum bewältigt werden kann.

Die 3D-CFD-Simulation ist einer der detailliertesten Ansätze zur Untersuchung des Verbrennungsmotors. Aufgrund des unvollständigen Phänomenverständnisses auf der grundlegenden physikalischen Ebene, ungenauer mathematischer Formulierungen, numerischer Abhängigkeiten von der Netzstruktur usw. sind die verwendeten Modelle jedoch oft nicht in der Lage, ein hohes Maß an Zuverlässigkeit bei der Reproduktion und Vorhersage der geforderten Motorprozesse zu garantieren. Unter anderem die Kraftstoffmodellierung ist eines der wichtigsten Elemente, die die Verbrennungsprozesse von Motoren beeinflussen.

Für eine bessere Untersuchung, sowohl von innovativen Kraftstoffen als auch komplexen Verbrennungsprozessen ist eine genaue Beschreibung der tatsächlichen Verbrennungseigenschaften erforderlich, die in vielen Fällen nicht durch die üblichen PRF/TRF-Surrogate (Primary Reference Fuel bzw. Toluene Reference Fuel) gewährleistet werden kann. Eine detaillierte Kraftstoffbeschreibung ermöglicht eine bessere und zuverlässigere Validierung mit experimentellen Messungen am Prüfstand (insbesondere wenn mehrere Kraftstoffchargen mit ähnlicher Zusammensetzung intensiv getestet werden) und kann die Vorhers- agbarkeit der Simulation erheblich verbessern. Darüber hinaus können

solche detaillierte Kraftstoffbeschreibung verwendet werden, um Kraftstoffe auszuwählen, deren Zusammensetzung die Anforderungen der jeweiligen Motoranwendung am besten entspricht.

Ziel dieser Arbeit ist es, die Simulationsumgebung des 3D-CFD-Tools QuickSim zu verbessern, welches im Laufe der Jahre am FKFS/IFS in Stuttgart entwickelt wurde. Die Einführung einer genaueren Kraftstoffbeschreibung und neuer Verbrennungsmodelle ermöglichte die virtuelle Untersuchung alternativer Kraftstoffe und die Detektierung von Verbrennungsklopfen.

Im ersten Teil dieser Arbeit werden die in QuickSim übernommenen 3D-CFD-Modelle und die Ansätze zur Umsetzung kraftstoffspezifischer Eigenschaften beschrieben. Nach den Ergebnissen der Untersuchungen an kommerziellen und hochleistungs-Kraftstoffen wird gezeigt, dass zur genauen Reproduktion eines breiten Spektrums von Kraftstoffeigenschaften eine erweiterte Ersatzformulierung erforderlich ist. Dies impliziert die Notwendigkeit, mindestens eine chemische Spezies für jede relevante Kohlenwasserstoffgruppe, die im Kraftstoff vorhanden ist, in die Ersatzformulierung aufzunehmen. Je nach Konzentration können Komponenten wie Cycloalkanen, Olefinen und sauerstoffhaltige Bestandteile das Kraftstoffverhalten stark beeinflussen.

In QuickSim wird zur Optimierung der Simulationszeit das Arbeitsmedium durch wenige Spezies beschrieben und es wird kein detaillierter chemischer Reaktionsmechanismus direkt implementiert. Folglich wird ein tabellarischer Ansatz verwendet, um thermodynamische Eigenschaften des Fluids zu importieren und die Kraftstoffeigenschaften zu charakterisieren. Die Nachschlagetabellen, welche die laminare Flammengeschwindigkeit und die Zündverzugszeit des Kraftstoffs beschreiben, werden mittels detaillierte Reaktioskinetik erstellt. Dabei wird der Einfluss der folgenden Parameter berücksichtigt: Temperatur, Druck, AGR-Konzentration, AGR-Zusammensetzung, Wasserkonzentration und Lambda. Wasser ist von besonderer Bedeutung, um den Einfluss der Luftfeuchtigkeit und potenziellen Wassereinspritzstrategien zu analysieren.

Da in der 3D-CFD-Umgebung zur Reduktion der Rechenzeit kein detaillierter chemischer Reaktionsmechanismus implementiert ist, muss ein spezielles Modell implementiert werden, um Reaktionen wie die Selbstzündung der Frischladung zu reproduzieren. Die mit der Reaktionskinetik berechnete Zündverzugszeit wird als Grundlage für ein Selbstzündungsmodell mit räumlicher Auflö-

sung verwendet, das auf dem bekannten Livengood und Wu Integral basiert. Anders als bei der ursprünglichen Formulierung wird das Integral in jeder Zelle der 3D-Simulationsdomäne gelöst und nicht mit gemittelten Zylinderbedingungen. Ein solcher Ansatz führt zu einer lokalen Abschätzung der Radikalbildung und gibt die Möglichkeit, den Ort und die Ladungsmenge unter Selbstzündungsbedingungen zu berechnen, so dass Phänomene wie Klopfen korrekt erkannt werden können.

Im zweiten Teil dieser Arbeit werden drei aktuelle Untersuchungen vorgestellt, die mit Unterstützung der neu entwickelten Modelle durchgeführt wurden.

Im ersten Schritt werden drei Kraftstoffe mit unterschiedlichem Ethanolgehalt durch 3D-CFD-Motorsimulationen verglichen und ihre Unterschiede in Klopfverhalten, Effizienz und Leistungspotenzial diskutiert. Ziel ist es, die Vor- und Nachteile von Kraftstoffe auf Ethanolbasis zu verstehen.

In der zweiten Analyse werden die potenziellen Vorteile der Wassereinspritzung in Ottomotoren untersucht. In diesem Abschnitt wird gezeigt, wie 3D-CFD Simulationen unter der Verwendung der zuvor vorgestellten Modelle den Einfluss von Wasser auf Verbrennungsprozesse korrekt abbilden und somit eine Optimierung der Wassereinspritzstrategien ermöglichen.

Abschließend wird eine Kraftstoffuntersuchung an einem Forschungsmotor mit dem innovativen Verbrennungskonzept SACI (Spark Assisted Compression Ignition) vorgestellt. Die Untersuchung wurde virtuell am FKFS Stuttgart und experimentell im Motorenlabor der Technischen Universität München mit der Unterstützung der Volkswagen Motorsport GmbH durchgeführt. Verschiedene Hochleistungs-Kraftstoffe wurden virtuell untersucht, um, bei vorgegebenem Kraftstoffverbrauch, die Höchste Motorleistung zu erzielen.

1 Introduction

1.1 Background and Global Prospect

In recent times, we witnessed a radical change in the automotive industry with many new technologies that principally aim to reduce the emission of greenhouse gases. More stringent regulations, especially for corporate average CO_2 emissions, created a general scepticism towards the internal combustion engine, which moved the focus toward other forms of propulsion such as fuel cells and electric powertrains. Nevertheless, it is proved that the combination of high-efficiency internal combustion engines and alternative fuels can retain significant potential in reducing overall emissions.

To reduce CO_2 emissions, OEMs are currently testing various solutions, which can be grossly divided into:

- Development of new combustion methods such as homogeneous charge compression ignition, premixed charge compression ignition, controlled auto ignition and many others. All these solutions have in common to try to achieve better performances and fewer emissions by performing a better combustion and by approximating the ideal rapid combustion at low temperatures.
- Electrification or hybridizing of ICE. This second solution tries to enhance the performances of the engine by coupling it with electrical devices (electrification) or electric motor and battery (hybridizing) in order to exploit the strengths of both engines. One of the main advantages of solutions like plug-in hybrid electric vehicles is that the use of the ICE can be restricted to those operating conditions in which its efficiency is the highest. Thus, reducing fuel consumption and emissions considerably.
- Electric vehicles (EV), also called battery electric vehicles (BEV) whose greatest advantage is that, during their operation, they do not produce any GHG and pollutant. For this reason, in recent years, the politics of many European countries proposed to shift to a mobility completely based on BEV.

© The Editor(s) (if applicable) and The Author(s), under exclusive license to Springer Fachmedien Wiesbaden GmbH, part of Springer Nature 2021
F. Cupo, *Modeling of Real Fuels and Knock Occurrence for an Effective 3D-CFD Virtual Engine Development*,Wissenschaftliche Reihe Fahrzeugtechnik Universität Stuttgart, https://doi.org/10.1007/978-3-658-31628-0_1

Many forecasts see that the EV will gain a greater percentage in small and light cars for city use where the characteristics of the electric motor, such as regenerative braking, are more interesting. The main critical points of a BEV are the limited range, the long charging time and the weight and the cost of the current batteries.

- Development of biofuels and e-fuels which combine the advantage of a reliable and cost-effective technology with a drastic reduction of well-to-wheel CO_2 emissions.

1.1.1 Bio-Fuels

If the entire process of energy flow, from the mining of the energy source to a vehicle being driven, is considered (Well-To-Wheel analysis), the combination of alternative fuel and efficient Internal Combustion Engine (ICE) represents a very attractive solution due to the possibility of achieving a CO_2 neutral balance between production, refining and combustion.

A biofuel is a type of fuel whose energy is derived from the biological reduction of atmospheric inorganic carbon to organic compounds by living organisms. The most common and commercially available are bioethanol, biodiesel and biogas.

Bioethanol is one of the most used, and it is mainly blended with standard gasoline to both improve the quality of the gasoline and to reduce its price (i.e low quality fuel can reach the desired RON by adding Ethanol). Thanks to the ability of ethanol to mix homogeneously with gasoline, it is common in many countries, also in some European one, to find at the pump station the possibility to choose gasolines that are blended with a 5% (E5), 10% (E10) or 15% (E15) of ethanol. The advantages are a reduction of the cost of gasoline at the pump, a reduction of the greenhouse emission, lower dangerous air pollutant emissions (due to the absence of those species like aromatics which increase soot formation), higher octane number and the reduction of the crude's import.

1.1.2 E-Fuels

The biggest problem in the energy system is how to deal with the randomness of power production; it is indeed common that Eolic turbines or solar panels have to be shut down during a period of particular high production or low request. To solve these problems, it is fundamental to find ways to stock energy conveniently in order to use all the possible energy that renewable sources can produce and keep it stocked until the request increases or production drops. Many solutions have been proposed, among which there is the possibility to use excess electricity to produce hydrogen via water electrolysis (a technology called Power-to-gas). Once hydrogen is produced it can be used in fuel cells, or it can be used to produce fuels by reaction with CO_2. Such fuels are called e-fuels or synthetic fuels.

Up to now, the most produced e-fuel is methane but, as many types of research show, it will be soon possible to develop many other kinds of fuels. The downside of e-fuels is that it is hard to think of a scenario dominated by renewable sources with enough energy to produce an amount of synthetic fuels that can supply the fraction of the transportation sector depending on liquid fuels.

As for biofuels, e-fuels do not require significant modifications in the ICE nor in the distribution system, do not cause any instability on the infrastructure and reduce the dependence on fossil fuels. Moreover, due to their inherent flexibility in the production process, e-fuels and biofuels created the new idea of "fuel design". In fact, the last stage of the production process can be theoretically adapted to create different fuels according to customer needs. This possibility opens new scenarios toward a joint development of engine and fuels, which would favour the investigation of innovative combustion strategies.

1.2 Motivation and Objectives

The engine of the future must be efficient, with very low exhaust emissions and fuel consumption. To reach such goals and to reduce engine development cost and time, the support of simulations is mandatory.

Until a few years ago, the basic models for standard fuels have shown to be sufficiently reliable in most of the conditions. However, if the research on alternative fuels is added to the development process, current simulations capabilities are quite limited due to over-simplified surrogates and not adequate combustion models which are not able to predict how specific compositions can affect the engine performance.

Due to the increase in fuel complexity and diversity, a more accurate modelling of real fuels is mandatory. When talking about fuel modelling, find a surrogate that could better represent a specific fuel is not sufficient. Most of the models used in engine simulations are affected by fuel properties and, therefore, they must be improved and adapted to the new fuel characterization. Considering the combustion, both laminar flame speed and autoignition reactions depend not only on local thermodynamic conditions (pressure, temperature) but also on charge composition. Accordingly, not only the fuel composition but also the presence of EGR, water or other substances must be taken into consideration.

The goal of this work is to introduce, in the 3D-CFD tool QuickSim, new fuel and combustion models able to enhance simulation predictability especially when innovative strategies (like SACI operation and water injection) and alternative fuels are investigated.

In the following Chapter 2 the fundamentals on fuel modelling, knock analysis, and numeric simulations are reported. It follows, in Chapter 3, a detailed introduction to the simulation environments used in this work, with particular attention to the 3D-CFD Tool QuickSim which is used for simulation of internal combustion engines.

To accurately describe the influence of any fuel on the combustion process, it necessary to have both adequate combustion models and fuel description. Independently from the models used, the results can be precise only if their inputs (i.e. fuel description) are accurate. As discussed in Chapter 4, a detailed fuel description is a mandatory starting point for an effective virtual fuel investigation and, as shown, it is crucial to identify and correctly reproduce the contribution of the most important hydrocarbon groups.

Thanks to a more accurate estimation of laminar flame speed and ignition delay time, the development and improvement of different combustion models was

possible. The locally-resolved autoignition model implemented in QuickSim, and the knock detection criterion derived from it, are described in detail in Chapter 5.

The models here presented were successfully used in the past years to conduct numerous engine investigations, some of which are discussed in chapters 7, 8 and 9.

Chapter 7 reports the investigation conducted on a downsized, DI engine in which fuels with different ethanol content are compared to estimate the influence of ethanol on knock occurrence.

It follows, in Chapter 8, an investigation on water injection in SI engines. Here is shown that thanks to the newly developed models, simulations can be successfully used to evaluate the benefits of different water injection strategies adequately.

Finally, in Chapter 9 the fuel investigation conducted in collaboration with Volkswagen Motorsport GmbH and Technische Universität München (TUM) is reported. In this work, a virtual fuel development is carried out with the scope to maximize the performance of a WRC derived engine, running with the innovative SACI (Spark Assisted Combustion Ignition) combustion.

2 Fundamentals

The development of more efficient forms of internal combustion engine is requiring a greater symbiotic relationship between the engine and the fuel that burns within it. In particular, fuel resistance to auto-ignition and laminar flame speed are among the most important characteristics affecting the combustion of any engine type (SI, CI, HCCI, etc..) and they must be correctly reproduced in any engine simulation.

In this Chapter, the fundamentals regarding the numerical implementation of fuel modelling, laminar flame speed and ignition delay time are reported. It follows a brief introduction on knock occurrence in SI engines, which is strictly connected to autoignition phenomena. Finally, the basics of internal combustion engine simulations are briefly discussed with particular focus on real working process, 1D-CFD and 3D-CFD simulations.

2.1 Fuel Modelling for CFD Simulations

The combustion process of a common gasoline fuel involves more than 7000 chemical species which means that experimental and computational investigations of fuel reaction kinetic during combustion is virtually impossible for practical applications. In CFD simulations, fuels are usually represented by surrogates of simple molecular composition and the combustion processes are then described by simplified reaction schemes which include only a limited number of relevant species.

As described in the literature [31, 40], surrogates are usually composed by some of the most representative species of the main hydrocarbons groups present in the fuel, like those listed in Table 2.1.

© The Editor(s) (if applicable) and The Author(s), under exclusive license to Springer Fachmedien Wiesbaden GmbH, part of Springer Nature 2021
F. Cupo, *Modeling of Real Fuels and Knock Occurrence for an Effective 3D-CFD Virtual Engine Development*,Wissenschaftliche Reihe Fahrzeugtechnik Universität Stuttgart, https://doi.org/10.1007/978-3-658-31628-0_2

Table 2.1: Few of the most representative chemical species used for gasoline surrogates.

Hydrocarbon Group	Representative Species
n-alkanes	n-heptane, n-pentane
iso-alkanes	isooctane, isopentane
cycloalkanes	Cyclohexane, Cyclopentane
Aromatics	Benzene, Toluene
Olefins	2-methyl-2-butene, Cyclopentene
Oxygenates	Ethanol, ETBE

Different methodologies can be used to determine surrogate composition. The most widely used surrogates for gasoline fuels are a mixture of n-heptane and isooctane, commonly called primary reference fuel (PRF), or a ternary mixture of PRF plus toluene (i.e. TRF). Experimental researches show that these simple compositions are suitable to reproduce with sufficient accuracy properties like the laminar flame speed of commercial fuels, but their ability in describing fuel characteristics is limited. In particular, it is not possible to accurately reproduce the behaviour of those fuels with a high concentration of olefins and cycloalkanes. For these reasons, a more complex surrogate including at least one chemical species for each relevant hydrocarbon group should be used.

Two approaches can be used to numerically describe the thermodynamic properties and the chemical reactions occurring in the working fluid during combustion. One consists in implementing a sufficiently detailed mechanism (with more than 100 species) within the 3D-CFD simulation environment. As shown in [2, 41], this methodology can ensure sufficiently reliable results but with a considerable increase in CPU-time. Generally speaking, the higher is the number of species and reactions contained in a chemical mechanism, the higher is the calculation time. On the other side instead, too simplified mechanisms may not be able to describe the real fuel behaviour properly. Alternatively, to reduce the calculation burden, thermodynamic properties of the mixture and information on chemical reactions (such as laminar flame speed and ignition timings) can be read from external databases which are prepared separately with dedicated software. A similar approach is used in [28]. Another advantage of this

method is that the databases can be prepared with detailed mechanisms which are more accurate than those generally used within 3D-CFD simulations due to CPU time constrains.

2.2 Ideal Laminar Premixed Flame

A flame is the mechanism by which combustion of hydrocarbons can occur and it can be identified as the region where the initial breakdown of the fuel molecules happen. There are two different types of flame: premixed flames and diffusion flames. Premixed flames occur in any homogeneous mixture where the fuel and the oxidant are mixed prior to the reaction. In diffusion flames instead, the rates of reaction are not controlled by the laminar flame speed but by the rate at which the fuel and air can be brought together to form a combustible mixture.

The structure of a one-dimensional, premixed and adiabatic flame can be divided into three areas according to the chemical composition of the mixture: unburned, reaction and burned zones (Figure 2.1). Locally, the temperature increases smoothly from the initial to the final state, and the concentration of intermediate and final products increase similarly. Whereas, the concentrations of fuel and oxidant show a corresponding decrease. The visible part of the flame is located in the reaction zone, and the emission is mainly due to electronically excited species, such as CH, CN, C_2 and CHO emitting light, as they return to their ground state [21].

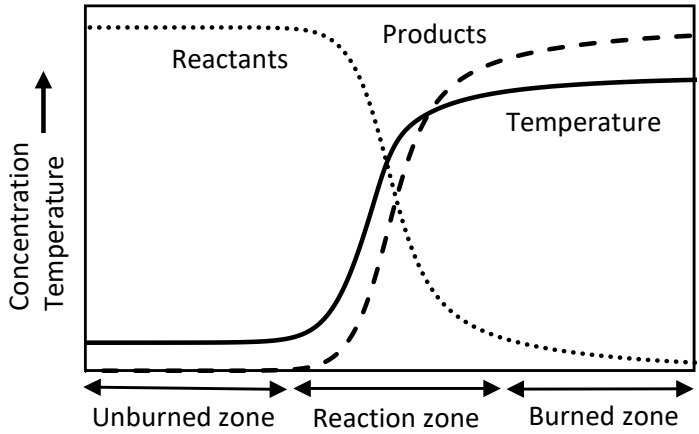

Figure 2.1: Change in temperature and mass composition in a one-dimensional, premixed and adiabatic flame.

The physical phenomena occurring in the flame can be described as follows: heat flows, by conduction, from the burned products zone (b) towards the unburned reactants zone (u), while the gas flows from u to b. A mass element passing from left to right at first receives more heat by conduction from the downstream products than it loses by conduction to the reactants, and hence its temperature increases. In the reaction zone, the mass element now loses more heat to the upstream elements than it receives from the products, but its temperature continues to increase because of the exothermic reaction taking place within the element. In the burned zone, the chemical reaction is complete and there is no further change in temperature [58].

The laminar burning velocity of a given fuel + oxidant mixture is defined in a formal way as the velocity with which a plane flame front moves normal to its surface through the adjacent unburned gas. The fuel + oxidant ratio has a marked effect on the burning velocity, which has its maximum value in a marginally fuel-rich mixture. In contrast, it shows only a small dependence on the pressure and temperature of the reactant gases, usually increasing at reduced pressures or elevated temperatures. Flame temperatures are notoriously difficult to determine and, in many cases, the quality of the thermodynamic data

available is sufficiently high for calculations of the adiabatic flame temperature to be more reliable than experimental measurements [21].

Laminar flame speed can be experimentally measured in different ways. One example is the flat flame method approach used in [12, 31, 50], which is able to reproduce a one-dimensional flat flame free of stretch. The main limiting factors are the thermodynamic conditions at which the experiment can be conducted. Most of the experimental investigations found in the literature are indeed conducted at environmental pressure and for temperatures lower than 400 K. These constraints limit the validation possibilities of chemical reaction schemes exactly in those ranges of temperature and pressure, which are of interest for ICE engines.

2.3 Autoignition Chemistry

The auto-ignition of a commercial hydrocarbon fuel occurs when thermal and chemical conditions are such to favourite those chain-branching reactions that can cause very fast energy release with consequent local increase in temperature and pressure. Of the thousands reactions occurring during this process, the following can be considered to be the most relevant [44, 56]:

$$H\bullet + O_2 + M \rightarrow HO_2\bullet + M \qquad \text{eq. 2.1}$$

$$RH + HO_2\bullet \rightarrow R\bullet + H_2O_2 \qquad \text{eq. 2.2}$$

$$H_2O_2 + M \rightarrow OH\bullet + OH\bullet + M \qquad \text{eq. 2.3}$$

Where atoms with $\bullet$ denote a radical (atom with unpair electron), RH is an alkane, $R\bullet$ is an alkyl radical, and M is a third body. Those in eq. 2.1 and eq. 2.2 are chain propagating reactions, which have the same number of radicals among both the reactants and the products. The reaction in eq. 2.3, instead, is a chain branching reaction, where the number of radicals in the product is higher than in the reactants.

Figure 2.2 shows the reaction processes that occur at ignition. H_2O_2 is produced as the fuel molecules degenerate. In the first stage, the concentration of

H_2O_2 increases since this molecule is rather stable at low temperature. When the temperature reaches 900 to 1000 K, the third reaction becomes dominating. Thus, H_2O_2 decomposes quickly to OH radicals and triggers the ignition of the main heat release.

Hydrocarbons mainly differ in low-temperature reactions (T< 800 K). Those favouring the production of HO_2 radicals will show less resistance to autoignition. Every reaction occurring during the compression is therefore very important since it will affect the temperature history and the combustion phasing. The reactions in eq. 2.1, eq. 2.2 and eq. 2.3 play an important role in every type of combustion: they determine the autoignition in HCCI and Diesel engine and they are the cause of knock in SI engine.

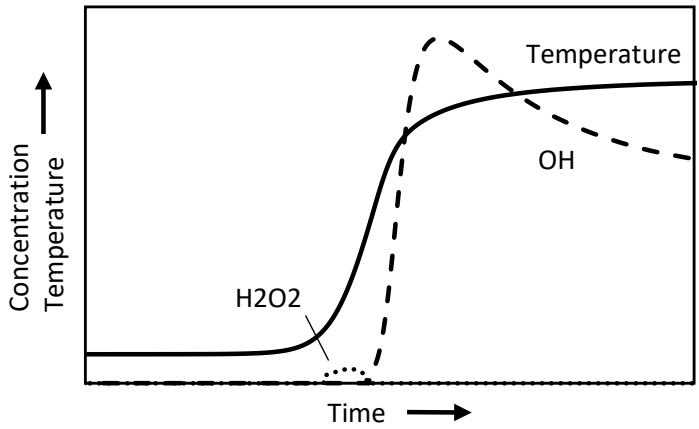

Figure 2.2: Change in Temperature and concentration of OH and H2O2 during autoignition.

The time necessary to complete these chemical reactions is known as induction time, which can be experimentally measured in shock tubes [26, 40], or rapid compression machines [11] or calculated by solving chemical reaction schemes. Differently from laminar flame speed, ignition delay time can be measured for a wide range of temperature and pressure, allowing a more reli-

able validation of reaction models. Experiments with temperatures up to 1200 K and pressures up to 50 bar can be found in the literature [15].

2.3.1 Factors Affecting Autoignition and Cool Flame

The main factors influencing the autoignition behaviour of hydrocarbons is the carbon chain length and the C-H bond type. If the reference fuels used for the octane scale are considered (Figure 2.3), it can be noticed that isooctane (rated with a RON of 100) has a short branched structure and n-heptane (rated with a RON of 0) has a long straight structure.

The carbon-hydrogen that breaks the easiest is the ternary C-H bond (the carbon atom is bonded to three other carbon atoms and just one hydrogen) while the strongest bond is the primary C-H bond (the carbon atom is bonded to just one carbon atom and three hydrogen atoms). Consequently, long straight chains are more prone to auto-ignite than short and branched chains.

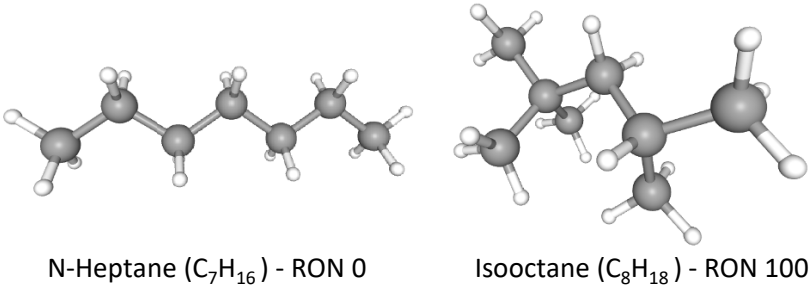

Figure 2.3: Atomic structure of isooctane and n-heptane.

Reactions in eq. 2.1, eq. 2.2 and eq. 2.3 do not explain why hydrocarbons have different auto-ignition quality but they rather give information on how autoignition is triggered. To explain the differences among fuels, it is necessary to consider other important reactions that occur in the early phase of compression. These reactions, result in a first stage of heat release at low temperatures and they are often referred to as cool flames.

At temperatures as low as 393 K, some fuel-air mixtures react chemically, and very little heat is released. During this phase, the reaction has not gone to complete combustion; instead the molecules break down and recombine to produce a variety of stable chemical compounds including alcohols, acids, peroxides, aldehydes and carbon monoxide [38]. After cool flame occurs, the overall reaction rate decreases with increasing temperature leading to an increased resistance to autoignition.

An example of this phenomena can be seen in Figure 2.4, which reports the calculated ignition delay time for n-Heptane, isooctane and toluene at 50 bar and stoichiometric air to fuel ratio (A/F). For knock occurrence, for example, the highest possible autoignition delay time is desirable. It should be noticed that, for both alkanes (n-heptane and isooctane), the autoignition delay time does not decrease monotonically with an increase in inlet temperature. These species show a drastic change in behaviour as the temperature increases and at high temperatures, their actual delay time is at least two orders of magnitude larger than that expected for a system with linear response. The region where this change in behaviour occurs is referred to as negative temperature coefficient (NTC).

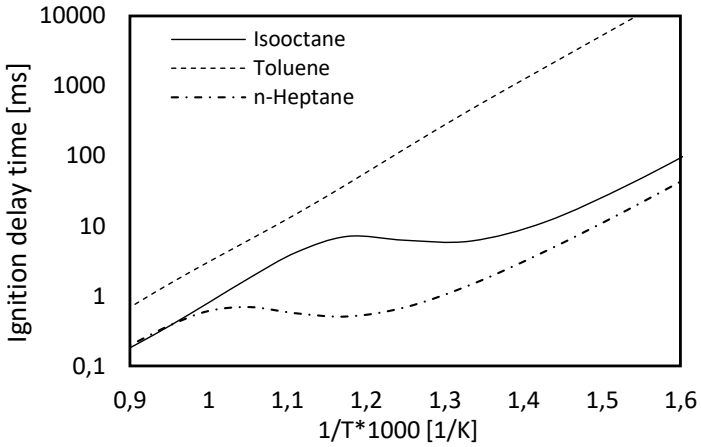

Figure 2.4: Ignition delay time of n-Heptane, Isooctane and Toluene at 50 bar and lambda 1.

Cool flame heat release occurs preferentially under fuel-rich conditions during degenerate branching reactions in early combustion. The phenomena are not only dependent on fuel type but also on engine conditions as different reaction pathways become dominant at different temperatures. This behaviour is typical of alkanes and many additives can be added to fuels to either inhibit (for SI engines) or favourite (for Diesel engines) low-temperature reactions.

2.3.2 Empirical Auto-Ignition Modelling

Most of the auto-ignition models developed in the past 20 years are generally based on the evaluation of an integral representing the pre-reaction state of the unburned mixture. The formulation reported in eq. 2.4 was originally proposed by Livengood and Wu [33] and they proved that the ignition delay time of an air-fuel mixture in motored and firing SI engines could be estimated by evaluating an integral representing the degree of chemical reaction progress and thus the pre-reaction state of the mixture.

$$1 = \int_{t=0}^{t=t_e} \frac{1}{\tau} dt \qquad \text{eq. 2.4}$$

Where t is the elapsed time $[s]$, t_e is the time at the end of the integration $[s]$ and τ is the ignition delay to auto-ignition of the mixture at the current boundary conditions $[s]$. Hence, if the ignition delay times τ are known at every integration step, it is possible to predict when the ignition delay time of a mixture in a firing engine will occur (end of integration t_e). Ignition delay time τ can be either measured in a rapid compression machine or calculated using detailed kinetic reaction mechanisms.

One of the main benefits of Livengood and Wu approach is its low calculation time. This formulation was successfully used to predict the auto-ignition delay of air-mixture in internal combustion engines for decades. In contrast, the implementation of a kinetic reaction mechanism would lead to a significant increase in computational time, and it can be challenging to combine it with engine simulation software.

This approach tries to apply a single reaction rate to a global reaction but, as already mentioned, the auto-ignition chemistry is very complex. The reaction

mechanism of a simple binary fuel already contains thousands of reactions, and each of them is dominating in different temperatures and pressures regimes. Due to this simplification, it is not possible to have an understanding of what is actually happening chemically in the unburned mixture. In this context, in the course of their research in 1955, Livengood and Wu noted that interfering effects might arise and impair the prediction quality of Equation eq. 2.4. For the case of a low-temperature heat release occurring before the auto-ignition for instance, they proposed a separate integration for each ignition stage in succession [33]. Accordingly, different two-stage ignition models, like the one developed by Fandakov [14], have been intensively investigated.

Another import aspect to consider is that autoignition chemistry is strongly dependent on local mixture conditions (temperature, a/f ratio, EGR and water concentrations). If the integral is calculated by using, as input, global values (e.g. average mixture conditions in the cylinder) significant simplifications can be introduced as the mixture may not be in perfect homogenised conditions and the mass ahead of the flame as different temperatures according to the distance from the flame itself. Moreover, by considering local mixture conditions, it would be possible to estimate with greater accuracy the exact amount of energy released in auto-ignition.

According to Authors opinion, simplifications on mixture condition lead to more significant errors than neglecting low-temperature heat release phenomena. The last, by strongly depending on fuel composition and operating conditions, it may not be significant in certain situations (more information are reported in Chapter 2.3.1). This work focus on improving the accuracy of the inputs used fo the calculation of the integral. Nevertheless, more research is required to fully evaluate the influence of two-stage ignition phenomena, especially for future fuel compositions.

2.4 Knock in SI Engines

Knocking combustion in spark-ignition (SI) engines is an abnormal combustion phenomenon which can limit engine performance, thermal efficiency and, in extreme cases, it can result in permanent engine damages. As the flame

propagates across the combustion chamber, the unburned mixture ahead of the flame (end gas) is compressed, causing its pressure, temperature, and density to increase. This causes an acceleration of the chemical reactions previously introduced. These reactions may lead to a rapid release of chemical energy, which can be from 5 to 25 times faster than normal flame propagation combustion [25, 57, 59]. Hence, knock occurs when the flame front is not fast enough to consume the end gas before auto-ignition occurs. The propagation of the resulting pressure waves causes high-frequency pressure oscillations inside the cylinder (Figure 2.5) that produce the sharp metallic noise known as "knock".

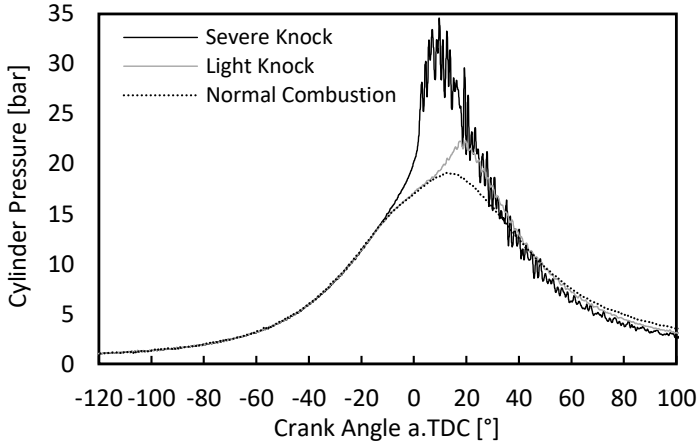

Figure 2.5: Cylinder pressure under different knock conditions.

Many factors like operating conditions, fuel composition and engine design affect engine knock tendency of an engine. High compression ratios and charge density, for example, are known to increase knock occurrence while high in-cylinder turbulence mitigates it by increasing flame propagation velocity.

The most common ways used to detect knock are by using vibration sensors (used in commercial engines) or by a piezoelectric transducer to trace the in-cylinder pressure trace (used on research test benches).

One standard criterion used to define the knock boundary is the evaluation of the knock frequency (number of cycles with knock divided by the total number of cycles measured). Accordingly, it is possible to determine if an engine operating point is in severe, light or close to knock.

The resistance to knock of standard fuels is conventionally measured in specific single-cylinder engines by its Research Octane Number (RON) and Motor Octane Number (MON). In these tests, the knock intensity of the fuel is compared to that of isooctane and n-heptane blends. These two kinds of paraffin also represent the ends of the scale, being zero for n-heptane and 100 for isooctane. Fuel with an octane number of 95, for example, has the same knock intensity of a blend with 95% of isooctane and 5% of n-heptane. RON and MON measurements mainly differ for intake air temperature and engine speed used in the test and they are both higher for MON method making it the most severe of the two (MON number is lower than RON number).

2.5 Simulation of Internal Combustion Engines

Numerical engine investigations are mainly performed by three tools: real working-process analyses (WP), One-Dimensional fluid dynamic simulations (1D-CFD) and three-dimensional fluid-dynamics simulations (3D-CFD). The first, is a zero-dimensional (0D) approach in which the engine operating cycle analysis is based on the energy conservation equations where temperatures and concentration distributions are not considered. 1D-CFD simulation instead is a combination of thermodynamic analysis for the cylinder and a simplified fluid dynamic simulation for all pipes (intake and exhaust system). Finally, the 3D-CFD simulation is a complete fluid motion analysis where the real geometries are discretized in finite volumes and the conservation equations are solved for each of them. These approaches differ considerably in terms of results predictability and computing time. Of all of them, the last is the most detailed approach, with the highest predictability capabilities but also the highest computational time. More details about each approach are reported in the following chapters.

2.5.1 Real Working Process Analysis

Thanks to their very low computational time, working process analyses are very important calculation tools for real time evaluation of engine operating cycles at the test bench. Engine working cycles are here analysed by the conservation of energy and mass in cylinder as reported in eq. 2.5 and eq. 2.6 [4, 51].

By writing the conservation of energy in differential form, it is possible to describe the variation internal energy U in function of the time (or degree crank angle φ):

$$\frac{\mathrm{d}Q_B}{\mathrm{d}\varphi}+\frac{\mathrm{d}Q_W}{\mathrm{d}\varphi}+\frac{\mathrm{d}H_I}{\mathrm{d}\varphi}+\frac{\mathrm{d}H_E}{\mathrm{d}\varphi}+\frac{\mathrm{d}W}{\mathrm{d}\varphi}+\frac{\mathrm{d}H_L}{\mathrm{d}\varphi}=\frac{\mathrm{d}U}{\mathrm{d}\varphi} \qquad \text{eq. 2.5}$$

Where the fuel heat release energy Q_B, wall heat transfer Q_W, intake enthalpy H_I, exhaust enthalpy H_E, leakage enthalpy H_L and work W. The variation in cylinder mass in the cylinder can be expressed as:

$$\frac{\mathrm{d}m_C}{\mathrm{d}\varphi}=\frac{\mathrm{d}m_I}{\mathrm{d}\varphi}+\frac{\mathrm{d}m_E}{\mathrm{d}\varphi}+\frac{\mathrm{d}m_L}{\mathrm{d}\varphi}+[\frac{\mathrm{d}m_B}{\mathrm{d}\varphi}]_{DI} \qquad \text{eq. 2.6}$$

Where m_c is the cylinder mass, m_i the intake mass, m_e the exhaust gas, m_l the leakage mass due to blow-by and m_b the fuel mass.

In addition to the conservation equations, the ideal gas equation is used to relate pressure p, volume V, mass m, specific gas constant R_s and temperature T:

$$p\cdot V=m\cdot R_s\cdot T \qquad \text{eq. 2.7}$$

During compression, intake and exhaust phases the thermodynamic modelling is base on a one-zone approach, by which the working fluid inside the cylinder is assumed to have a uniform composition and thermodynamic state (p, T, R,..).

During combustion instead, burned and unburned masses are separated in two or more zones according to the combustion type. A two-zones approach is typically used for SI-engines while a more complex n-zones is used for DI and stratified engine where the charge is not homogeneously mixed. Furthermore, combustion process models like the Vibe function are used to characterise the

combustion profile. These models need to be calibrated for each operating point, limiting the predictive capability of this calculation approach.

2.5.2 1D-CFD Simulation

In 1D-CFD simulations, the combustion chamber is modelled with a real working process analysis but, in addition to this, the simulation domain is extended to intake and exhaust systems. The flow components are discretized in volumes and the conservation equations (continuity, momentum and energy) are used to calculate a one-dimensional flow field [7]. Other components like turbochargers, fuel injectors, lambda sensors, etc., can be integrated by dedicated models or characteristic maps.

In the past, numerous phenomenological and quasi-dimensional models have been developed in order to consider the influence of different factors like in-cylinder motion (tumble and swirl) and combustion chamber geometry. These models can be adapted to the change in engine operating conditions, reducing the necessity in calibration effort [4].

Among the disadvantages of these simulations, it is important to consider the necessity to calibrate combustion models and the flow field simplifications, which limit the predictability of complex phenomena like mixture formation and scavenging. Nevertheless, thanks to their relatively low computational time and good results predictability, 1D-CFD simulations are an essential tool for engine development processes. They can be successfully used to optimise valve timing, intake and exhaust system layout, simulate transient engine behaviour and investigate vehicle integration.

2.5.3 3D-CFD Simulation

Three-dimensional simulation approach allows to reproduce with more accuracy the flow field of complex geometries but at very high computational time. For this reason, the simulation domain is often limited to parts where complex phenomena take place (e.g. combustion chamber, valve and intake channels). However, the smaller is the simulation domain, the higher is the influence of boundary conditions on results accuracy [7].

In 3D-CFD simulations, the domain is divided infinite volumes in which partial differential equations for conservation of mass, species concentration, momentum (Navier-Stokes' Equation) and energy are solved. Fluid properties and thermodynamic state within a cell are considered to be homogeneous (finite volume approximation) and its centre is used to represent the discretised volume itself.

In the following, an overview of the main fundamental equations is reported. For a more detailed description, please refer to [1, 6, 39].

Fundamentals Equations

According to Euler formulation, conservation equations of mass, momentum and energy can be derived from:

$$\frac{\partial f}{\partial t} + div\vec{\Phi}_f = s_f + c_f \qquad \text{eq. 2.8}$$

Where $f(\vec{x},t) = dF/dV$ is the density or intensive variable of the extensive variable $F(t)$ in the cell at position $\vec{x}$. According to the equation, a variation in the density variable $\frac{\partial f}{\partial t}$ can be caused by flux through the volume surface $\vec{\Phi}_f$, by a source or sink S_f or a long-range processes C_f.

For the mass conservation, the extensive variable F(t) corresponds to the mass m, the density variable $f(\vec{x},t)$ corresponds to the mass density ρ. The terms S_f and C_f are here set to 0 since no mass is formed or destroyed and there are no long-range terms. The eq. 2.8 can be reformulated as follows:

$$\frac{\partial \rho}{\partial t} + div(\rho\vec{v}) = 0 \qquad \text{eq. 2.9}$$

If i species are present, the following considerations can be made:

$$f = \rho_i = \rho w_i \qquad \text{eq. 2.10}$$

$$\vec{\Phi}_f = \rho_i\vec{v}_i = \rho_i(\vec{v}_i + \vec{V}_i) = \rho_i\vec{v}_i + \vec{j}_i \qquad \text{eq. 2.11}$$

$$s_f = M_i\omega_i \qquad \text{eq. 2.12}$$

$$c_f = 0 \qquad \text{eq. 2.13}$$

Where the source term s_f is given by the molar mass M_i multiplied for the molar fraction rate of species i due to chemical reactions, $w_i = m_i/m$ is the fraction of species i and the local flow velocity $\vec{v}_i$ is substituted by the mean flow velocity $\vec{v}$ and the diffusion velocity $\vec{V}_i$, which generates a species diffusion mass flux $\vec{j}_i$. Therefore, the conservation equation becomes:

$$\frac{\partial \rho w_i}{\partial t} + div\,(\rho w_i \vec{v}) + div\,\vec{j}_i = M_i \omega_i \qquad \text{eq. 2.14}$$

The specific energy content of a fluid can be generally expressed as:

$$\rho e = \rho \left(u + \frac{1}{2}|\vec{v}|^2 + G + h_f \right) \qquad \text{eq. 2.15}$$

where u is the internal energy, $\frac{1}{2}|\vec{v}|^2$ is the kinetic energy, G the gravitational energy and h_f is the enthalpy of formation of the mixture. For the conservation equation, the following can be applied:

$$f = \rho e \qquad \text{eq. 2.16}$$

$$\vec{\Phi}_f = \rho e \vec{v} + \overline{\overline{P}}\vec{v} + \vec{j}_q \qquad \text{eq. 2.17}$$

$$s_f = 0 \qquad \text{eq. 2.18}$$

$$c_f = q_r \qquad \text{eq. 2.19}$$

Where the long term c_f is given by the contributions of radiations or magnetic fields q_r, $\vec{\Phi}_f$ is composed by the sum of convective term $\rho e \vec{v}_i$, energy transport term $\overline{\overline{P}}\vec{v}$ due to pressure and shear stresses and the energy transport term $\vec{j}_q$ due to heat conduction. Consequently, the conservation equation is expressed as:

$$\frac{\partial\,(\rho h_{tc})}{\partial t} - \frac{\partial p}{\partial t} + div\left(\rho h_{tc}\vec{v} + \vec{j}_q\right) + \overline{\overline{P}} : grad(\vec{v}) - div(p\vec{v}) = q_r \qquad \text{eq. 2.20}$$

where the thermal-chemical enthalpy h_{tc} is the sum of thermal and chemical contribution, respectively h and h_f:

$$h_{tc} = h + h_f \qquad \text{eq. 2.21}$$

For the conservation of momentum, the following considerations can be made:

$$f = \rho \vec{v} \qquad \text{eq. 2.22}$$

$$\vec{\Phi}_f = \rho\vec{v}\otimes\vec{v} + \overline{\overline{P}} \qquad \text{eq. 2.23}$$

$$s_f = 0 \qquad \text{eq. 2.24}$$

$$c_f = \rho\vec{g} \qquad \text{eq. 2.25}$$

where $\rho\vec{v}$ is the momentum density, the momentum flux $\vec{\Phi}_f$ is composed by a convective term $\rho\vec{v}\otimes\vec{v}$ and a second-order stress tensor $\overline{\overline{P}}$, the long term c_f is given by gravitation contribution $\rho\vec{g}$.

The second-order stress tensor $\overline{\overline{P}}$ describes the variation in momentum due to viscous effects $\overline{\overline{\Pi}}$ and the pressure p. The momentum flux $\vec{\Phi}_f$ can be, therefore, also expressed as:

$$\vec{\Phi}_f = \rho\vec{v}\otimes\vec{v} + \overline{\overline{P}} = \rho\vec{v}\otimes\vec{v} + p\bar{\bar{I}} + \overline{\overline{\Phi}} \qquad \text{eq. 2.26}$$

Accordingly, the conservation equation of momentum can be formulated as follows:

$$\frac{\partial(\rho\vec{v})}{\partial t} + div(\rho\vec{v}\otimes\vec{v}) + div(\overline{\overline{\Pi}}) - gradp = \rho\vec{g} \qquad \text{eq. 2.27}$$

Turbulence Modelling

It is well known that many of the engine processes (like mixture formation, wall heat transfer and combustion) are heavily dependent on local turbulences. Unfortunately, the turbulent phenomena occurring in internal combustion engines are very complex and cannot be measured with sufficient accuracy by any device. Consequently, there is no possibility to validate turbulence models directly, and this represents a very critical factor in the simulation of internal combustion engines.

Three main turbulence models are available, and they mainly differ on the turbulence length that they can describe. The most detailed approach is the direct numerical simulation (DNS) in which the Navier-Stokes equations are numerically solved without any turbulence model. In this way, it is possible to calculate also the smallest vortices directly, but it requires a very detailed mesh and small simulation time step [7]. Due to its high computational time, this approach is only used for pure research activities.

The same can be said for the large-eddy simulations (LES) although it has a much lower computational burden. The main difference between the two simulations is that LES does not solve Navier–Stokes equations for the smallest length scales, but dedicated models estimate their effect [7, 16, 49]. To reduce computational time of simulations within acceptable limits, Reynolds Averaged Navier-Stokes (RANS) equations are typically used. Here, the turbulent flow is entirely described by models, which give approximate time-averaged solutions to the Navier–Stokes equations [46].

Modelling of Working Fluid and Chemical Reactions

As mentioned in Chapter 2.5.1, the thermodynamic properties of the working fluid are fundamental terms in the conservation equations and the accuracy of the results. The exact estimation of the chemical composition of the working fluid is not mandatory. Empiric formulation for the calculation of R (real gas constant) and H_{tot} (total enthalpy of the mixture) would be sufficient to solve the conservation equations. In the past, also properties like the laminar flame speed of the fuel have been estimated through empirical formulations but this approach is limited to those fuels for which experimental coefficient has been determined. Therefore, for better simulation flexibility and capabilities, a chemical composition of the working fluid is necessary.

As already mentioned, to solve the mass conservation (eq. 2.14), information about chemical source term $r_i = M_i \omega_i$ is required. If the combustion process of common gasoline fuels is considered, it involves more than 7000 chemical species and more than thousand reactions whose influence is not fully understood yet. Due to such complexity, it is not practically possible to consider all reaction paths and only simplified chemical reaction schemes can be used. The combustion can then be described by considering only the most relevant species and reactions. However, to have acceptable computational time, extremely simplified schemes are often used, significantly affecting simulation accuracy.

Engine Specific Models

Many of the phenomena occurring in an ICE, like spark ignition, combustion, self-ignition, wall heat transfer and injector spray are not fully understood and cannot be correctly described by mathematical formulations, which means that specific models are required. To properly reproduce these important phenomena, many phenomenological and empirical approaches have been developed in the last 30 years [3, 22].

This work mainly focus on this last aspect. Fuel chemical composition and reaction schemes are analysed with the purpose to better reproducing thermodynamic characteristic of the fuel during combustion (i.e. laminar flame speed and ignition delay time).

3 Simulation Environments

The 3D-CFD numerical investigations presented in this work are carried out with the ICE-specific tool QuickSim while the chemical kinetics calculations, used to estimate fuel properties, are conducted with Cantera.

In the following, the main features of these tools are described.

3.1 3D-CFD Tool QuickSim

Using the commercial software STAR-CD as a solver, QuickSim code has been developed in the last 20 years at the Research Institute of Automotive Engineering and Vehicle Engines Stuttgart (FKFS) and at the Institute of Automotive Engineering (IFS) by the University of Stuttgart.

By using ICE-adapted and improved computational models, coarser meshes compared to traditional 3D-CFD approaches can be used without sacrificing the quality of the simulation results. As a result of this, the time expense for a simulation is highly minimized (2 hours for an operating cycle of a full engine on a 12 cores CPU) [7]. Typical simulations time scale is showed in Figure 3.1.

This approach not only allows the extension of the simulation domain to a full engine but also the calculation of several successive operating cycles (up to transients) in a reasonable time frame. As a result, a stable flow field can evolve (depending on the operating point, usually after 5-10 cycles) and the influence of user-defined fluid initial conditions can be reduced significantly [8].

© The Editor(s) (if applicable) and The Author(s), under exclusive license to Springer Fachmedien Wiesbaden GmbH, part of Springer Nature 2021
F. Cupo, *Modeling of Real Fuels and Knock Occurrence for an Effective 3D-CFD Virtual Engine Development*,Wissenschaftliche Reihe Fahrzeugtechnik Universität Stuttgart, https://doi.org/10.1007/978-3-658-31628-0_3

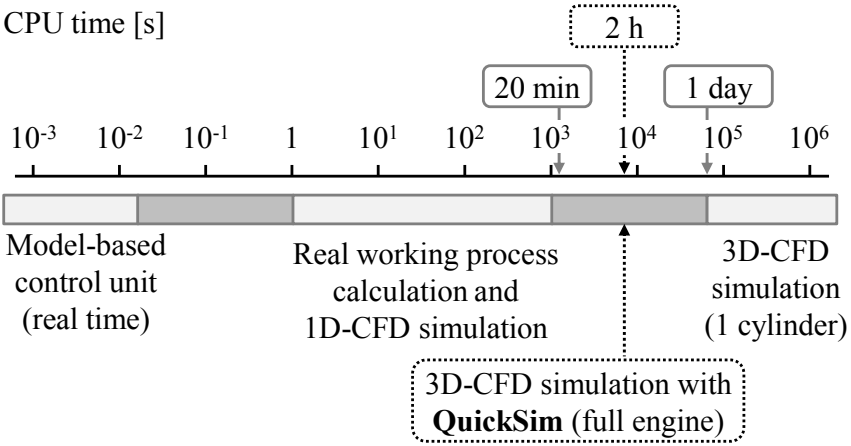

Figure 3.1: Typical simulations time scale.

Another important aspect to consider in 3D-CFD simulations is the influence of boundary conditions which are used to describe the fluid-dynamic conditions in the missing part of the engine (the region outside the simulation domain). If, for example, the simulation domain is limited to cylinder, intake and exhaust channels, the necessary boundary conditions can be obtained by measurements at the test bench (pressure traces) or 1D-flow models. The main problem about this approach is that is it practically impossible to apply locally resolved boundary conditions over the channel section and, therefore, a fluid homogeneity assumption across the section is required. Such simplification can induce significant calculation errors as complex fluid phenomena, like backflow and pressure waves, cannot be correctly reproduced. As schematically shown in Figure 3.2, to drastically reduce the influence of boundary conditions, the simulation domain in QuickSim is usually expanded to the full engine (also including 0D turbocharger model). In this way, constant ambient conditions can be used as boundary condition, and no fluid simplification is introduced.

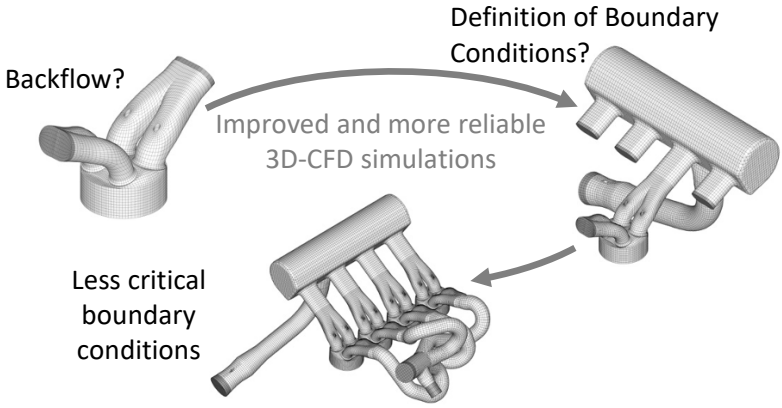

Figure 3.2: Extension of the simulation domain in QuickSim.

Regarding the possible engine configurations that can be investigated with QuickSim, there are no limitations to what concerns:

- Engine layout: any cylinder number, comb. chamber geometry, intake and exhaust system geometry, and any injection system (DI, SPI, MPI, etc.) with arbitrary injector geometry can be realized.
- Ignition type: spark-ignition, compression ignition, homogeneous charge compression ignition (HCCI) and spark-assisted compression ignition SACI. The autoignition HCCI model was calibrated using a highly variable free-piston linear generator [47, 48].
- Fuel type: gasoline, diesel, compressed natural gas (CNG), biofuels and e-fuels.
- Valve and piston motion.

In the following, some of the main simulation models are briefly introduced. For more information, please refer to [7].

3.1.1 Description of the Thermodynamic Properties of the Working Fluid

Differently from traditional approaches, in QuickSim the working fluid is described by few scalars which are not directly related to molecules but to "groups of interest" (fresh charge, EGR and burned gas). In Figure 3.3 is depicted an example of cell composition during combustion. The scalars can also be divided into two zones, burned and unburned. This distinction allows to have a clear representation of the flame front within the cell.

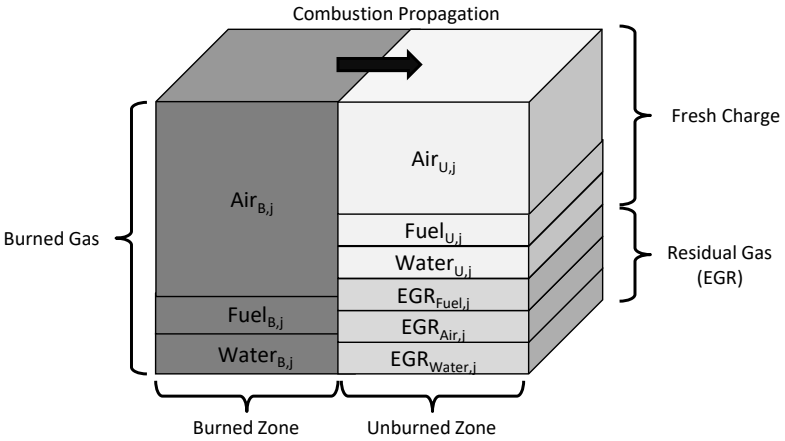

Figure 3.3: Fluid cell discretization in QuickSim.

A detailed description of the scalars is reported in Table 3.1.

The distinction between burned gas and EGR is used to distinguish the exhaust gas in front of the flame (i.e. EGR) to the one generated from the combustion (i.e. burned gas). With this approach, it is possible to precisely define the local repartition between unburned and burned zone and the position of the flame front in each CFD-cell.

To keep track of EGR and burned gas compositions, the concept of lambda EGR and lambda Burned are used. According to this formulation, the combustion of a rich mixture, for example, produces a rich burned mass.

Combustion products are then described using databases where properties, like thermal enthalpy of the gas in the burned zone, are described as a function of the thermal state (T, p) and the lambda of burned mass.

For the calculation of fuel-specific databases, the atom-composition of the fuel as $C_nH_mO_rNq$ and its lower heating value are used. More detail about the calculation method can be found in [7].

Table 3.1: Scalars definition in QuickSim.

Scalar name	Description
w_{Air_U}	Mass fraction of fresh air
w_{F_U}	Mass fraction of fresh vaporized fuel
w_{Water_U}	Mass fraction of water
$w_{EGR\_Air\_U}$	Mass fraction of air that has previously produced EGR (burned gas of the previous operating cycle)
$w_{EGR\_F\_U}$	Mass fraction of vaporized fuel that has previously produced EGR (burned gas of the previous cycle)
w_{Air_B}	Mass fraction of air that has previously produced burned gas
w_{F_B}	Mass fraction of vaporized fuel that has previously produced burned gas
w_{Water_B}	Mass fraction of water that has previously produced burned gas

3.1.2 Injection Modelling

Validation and calibration of the injection models used in QuickSim are extensively discussed by Wentsch in [53]. In the following, a brief description is reported.

Each injector nozzle is defined as cone-shaped volume in which droplets, with different size and velocity, are initialized. The diameter of each droplet is calculated according to the Rosin-Rammler-distribution. Droplet velocity, instead, is determined as a function of the injection pressure and an empirical

loss coefficient. To better adapt liquid fuel description (i.e. pressure of saturation and boiling curve) to the required level of accuracy, the fuel can be model either as single or multi component. An overview of the implemented models is shown in Appendix Table A.1.

3.1.3 Combustion Modelling

The function of combustion models is to calculate the local burning rate and the heat release as function of the local thermodynamic properties of the working fluid. In QuickSim, four heat-release models are available:

- Spark-ignition/flame propagation: the burn rate is calculated as a function of the flame front propagation.
- Auto-ignition: volume reaction of the cell. Used for HCCI, SACI or similar combustions.
- Diffusive flame: based on diffusive flame propagation typical of CI combustion
- Post-oxidation of exhaust gases: volume reaction based on burned species concentration (i.e. CO), air concentration and temperature.

This work focuses on the first two of the mentioned models and, in the following, a brief description of their state of the art in QuickSim is presented.

3.1.4 Flame Propagation Model - State of the Art

In SI engines, after the spark-plug has been triggered, the flame propagates through the unburned zone with a relative laminar flame speed S_L and when the flame front has reached a dimension comparable to the turbulent eddies it accelerates to the turbulent flame speed S_T. Numerically, if the flamelet approach is used, the turbulent flame front can be described as a laminar flame with increased flame surface A_f (Figure 3.4). Accordingly, laminar and turbulent flame speed can be related by the wrinkling factor K as follows:

$$K = \frac{A_{f,L}}{A_{f,T}} = \frac{S_T}{S_L} \qquad \text{eq. 3.1}$$

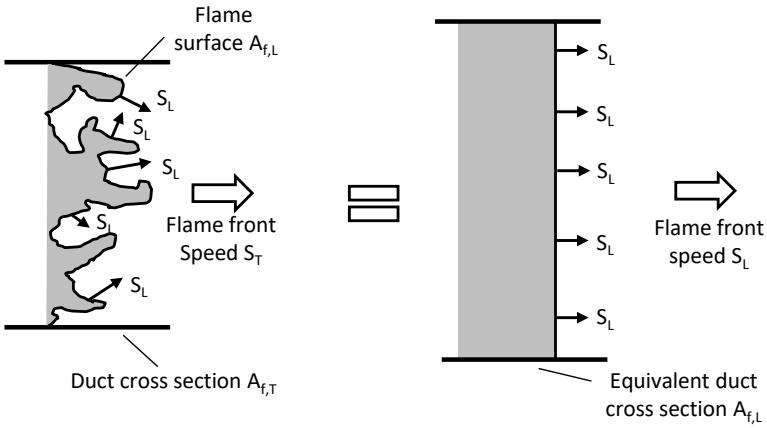

Figure 3.4: Schematic of turbulent flame propagation.

This formulation is finally used for the calculation of the turbulent laminar flame speed while the factor K is determined by semi-empirical formulations like the one proposed by Herweg and Maly [24]. The only remaining variable to be specified is the laminar flame speed which can be either calculated through chemical reaction schemes (very time consuming) or read from semi-empirical formulation or databases.

To reduce simulation time, the semi-empirical formulation from Gülder reported in eq. 3.2 was used so far. It consists of empirical and semi-empirical correlations which, through different coefficients, is able to consider the influence of temperature, pressure, lambda, and EGR mass fraction on the laminar flame speed. The equation can be used only with those fuels for which experimental coefficients are available, and it does not take into account the influence of water concentration and EGR composition. More information can be found in [19].

$$S_L(\lambda, p, T_{unb}, x_{exh}) = ZW(\frac{1}{\lambda})^{\eta} exp[-\zeta(\frac{1}{\lambda} - \phi_{st})^2)](\frac{T_{unb}}{T_{ref}})^{\alpha}(\frac{p}{p_{ref}})^{\beta}(1 - F_{exh}x_{exh}) \quad \text{eq. 3.2}$$

In equation eq. 3.2, lambda of the fresh charge λ, stoichiometric air to fuel ratio of the fuel ϕ_{st}, temperature of the unburned zone T_{unb}, pressure p and EGR concentration X_{EGR} are the input variables, and all others are experimentally validated coefficients. It can be noticed that the influence of temperature and pressure are expressed through power functions, while EGR concentration has a linear correlation.

One of the primary purposes of this work is to replace this empirical formulation with databases which are calculated by solving detailed chemical reaction mechanisms in Cantera. In this way, without affecting 3D-CFD simulation time, it is possible to improve the accuracy of results, increase the range of fuels that can be reproduced and consider the influence of water concentration and EGR composition. The methodology used for the calculation of laminar flame speed databases is discussed more in detail in Chapter 5.

3.1.5 Auto-ignition Model - State of the Art

As already mentioned, the autoignition process has been implemented as volume reaction of the cell. No models are currently present to identify combustion start and speed.

In this work, a locally-resolved auto-ignition model has been developed to reproduce the pre-reaction state of the mixture and to identify autoignition onset. The model can be used not only to initialize HCCI and Diesel combustions but also to identify Knock occurrence in SI engines.

3.2 Cantera

Cantera is a suite of object-oriented software tools for problems involving chemical kinetics, thermodynamics and transport processes.

In this work, the software is used for the calculation of induction time and laminar flame speed. In the following, a brief description of the approaches used is reported. For more details, please refer to [20].

3.2.1 0D-Reactors for the Calculation of Induction Delay Time

For the calculation of fuels induction time, a 0D constant volume reactor is used to reproduce the typical experimental environment. In this volume, all state variables are homogeneously distributed and the system is generally unsteady, i.e., all states are functions of time. In particular, transient state changes due to chemical reactions are possible. However, thermodynamic (but not chemical) equilibrium is assumed to be present throughout the reactor at all instants of time. Furthermore, the reactor is assumed to be isolated, i.e. no heat or mass transfer with the external occurs.

A user-defined reaction mechanism model specifies the number of reactions and species included in the equations. Temperature, pressure and initial composition are used as inputs.

3.2.2 One Dimensional Flames

Under steady conditions, a balance between convection, diffusion and reaction processes exists inside the reaction zone. Consequently, a simple one-dimensional analysis can be used to obtain approximated expressions for laminar flame speed (S_L). The amount of reactions and species included in the equations are specified by a user-defined reaction mechanism model. S_L can be then calculated by solving governing conservation equations for the overall mass, species, and energy. Temperature, pressure and initial composition are used as inputs and the numerical resolution of the differential equations is obtained using a damped modified Newton solver with internal time integration [21].

4 Detailed Description of Real Fuels

Due to the molecular complexity of common fuels, experimental and computational investigations of fuel reaction kinetic during combustion is not practically possible. Therefore, fuels can be numerically reproduced only by surrogates of simple molecular composition. Surrogates of different complexity can be used and the lower is the amount of species considered, the smaller and faster is the chemical reaction mechanism that can be used to solve reaction kinetics. Commonly, the main factor influencing the choice of chemical mechanism is indeed its impact on CFD simulation time.

The most widely used surrogates for gasoline fuels are a mixture of n-heptane and isooctane, commonly called primary reference fuel (PRF), a ternary mixture of PRF plus toluene (i.e. TRF) or a mixture of ethanol plus TRF. However, due to the increasing interest in alternative fuels, the surrogates used in the past years are not suitable for future investigations as a drastic simplification in fuel description may strongly limit simulation predictability.

In the following sections, the investigations conducted on chemical reaction mechanisms and surrogate compositions are reported. The goal is to determine which is the level of surrogate complexity necessary to describe with sufficient accuracy the most important characteristics of commercial and high-performance fuels.

The analysis mainly focuses on the calculation of the inputs of the combustion models, i.e. laminar flame speed and autoignition delay time of the fuel. All other properties, like those affecting vaporisation of the fuel, and the corresponding models were the subject of a study conducted by Wentsch in [53] and are here not discussed.

© The Editor(s) (if applicable) and The Author(s), under exclusive license to Springer Fachmedien Wiesbaden GmbH, part of Springer Nature 2021
F. Cupo, *Modeling of Real Fuels and Knock Occurrence for an Effective 3D-CFD Virtual Engine Development*,Wissenschaftliche Reihe Fahrzeugtechnik Universität Stuttgart, https://doi.org/10.1007/978-3-658-31628-0_4

4.1 Choice of Chemical Reaction Mechanism

Many chemical mechanisms for gasoline surrogates are available in the literature and they mainly differ for the number of species, chemical reactions and validation range [60]. This last point is of crucial importance, especially for the simulation of internal combustion engines due to the broad variation in pressure and temperature that occur during combustion. Depending from engine configuration and operating point, during combustion, pressure can vary from 20 to more than 120 bar while temperature of the unburned gas can increase from 600 to 1000 K. As example, Figure 4.1 shows the variation in temperature and pressure during compression and combustion in a downsized turbocharged SI engine at 2000 rpm and 20 bar IMEP.

However, as already explained in Chapters 2.2 and 2.3, the validation of these mechanisms is currently limited by the thermodynamic conditions at which experimental measurements of auto-ignition delay (IDT) and laminar flame speed (LFS) can be performed.

For what concerns the laminar flame speed measurements, it is indeed difficult to find any experiment conducted at temperatures higher than 400 K and pressures higher than 10 bar [34]. On the other side, measurement of ignition delay time can be conducted with temperatures up to 1200 K and pressures up to 50 bar [15]. Consequently, it is not practically possible to validate a chemical mechanism for both LFS and IDT in those thermodynamic conditions that are typically found in ICEs during combustion. For this reason, independently from the mechanism used for CFD simulations, further calibration of the combustion models with experimental data is often required.

For the calculation of laminar flame speed and auto-ignition time, different chemical mechanisms have been tested. Table 3 reports some information about some of those considered. To find the more accurate mechanism, the results of calculations have been compared with experimental data under different thermal conditions and mixture compositions. It is essential to highlight that the mechanisms with more than 350 chemical species are usually considered to have a too high computational time to be directly implemented in the 3D-CFD simulations. The mechanism developed at LLNL, for example, has a CPU time three times higher than the CRECK mechanism, which has

half so many species. Therefore, a compromise between results accuracy and computational time is often needed. For this reason, no mechanism with more than 350 species is here considered.

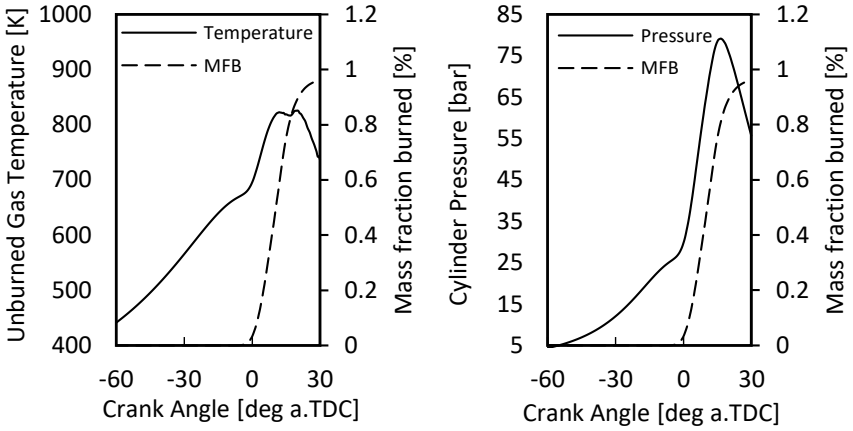

Figure 4.1: Variation in temperature (left) and pressure (right) during compression and combustion in a downsized turbocharged SI engine at 2000 rpm and 20 bar IMEP.

Table 4.1: Chemical reaction mechanisms considered in this work.

Mechanism	Chemical species	Reactions
CRECK [42]	156	3370
LLNL [36]	324	5739
Cai [5]	335	1613

4.1.1 Comparison of Reaction Mechanisms with Experimental Measurements

Surrogates containing isooctane, n-heptane, toluene and ethanol have been considered in order to compare the mechanisms under different mixture conditions

and to ensure that the interaction among the most important chemical species is correctly reproduced.

In Figure 4.2, 4.3 and 4.4, the three mechanisms are compared against laminar flame speed measurements conducted on PRF, TRF and TRF+Ethanol surrogates respectively. The mechanisms that performed better are the one developed at the Lawrence Livermore National Laboratory (LLNL) [36], including 324 species and 5739 reactions and the one developed by Cai et al. [5], with 335 species and 1613 reactions. It is interesting to notice that for pressures higher than environmental, the Cai´s mechanism shows significantly lower accuracy, as shown in Figure 4.3. The issue may be the model extrapolation at high pressure.

In Figure 4.5 is reported the laminar flame speed of a commercial E10 fuel measured at 358 K and 1 bar by Dirrenberger [12]. The mechanisms have been tested according to the following surrogate composition: 43.8 vol% isooctane, 14.4 vol% n-Heptane, 31.8 vol% toluene. Once again, LLNL and Cai models show good agreement with experimental data.

Similar conclusions can be made for the calculation of autoignition delay time. As reported in Figures 4.6 and 4.7, LLNL mechanism showed to be the most accurate option.

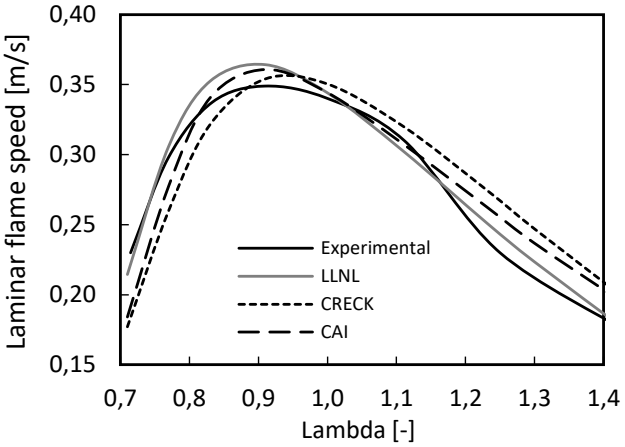

Figure 4.2: Laminar flame speed of a PRF fuel (90% isooctane and 10% n-Heptane) at 298K and 1 bar. Experimental data from [27].

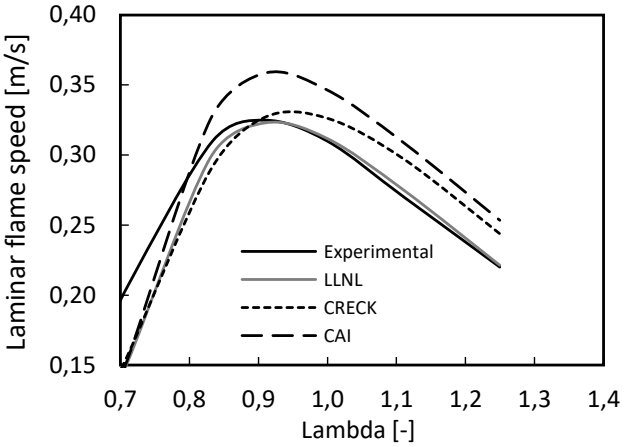

Figure 4.3: Laminar flame speed of TRF fuel (77.4% isooctane, 17.6% n-heptane and 5% Toluene) at 358 K and 4 bar. Experimental data from [34].

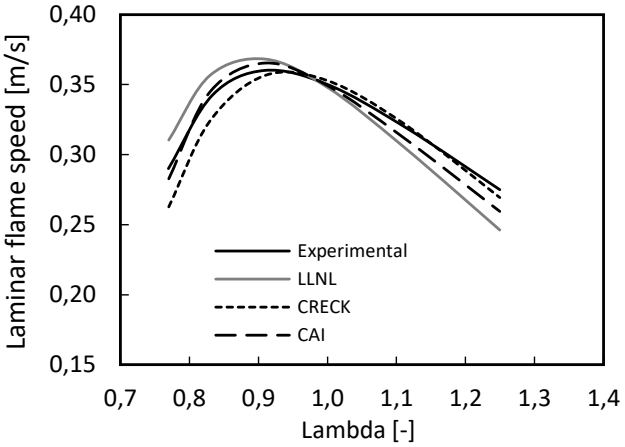

Figure 4.4: Laminar flame speed of TRF+Ethanol fuel (75% isooctane, 10% n-heptane and 15% Ethanol) at 298 K and 1 bar. Experimental data from [32].

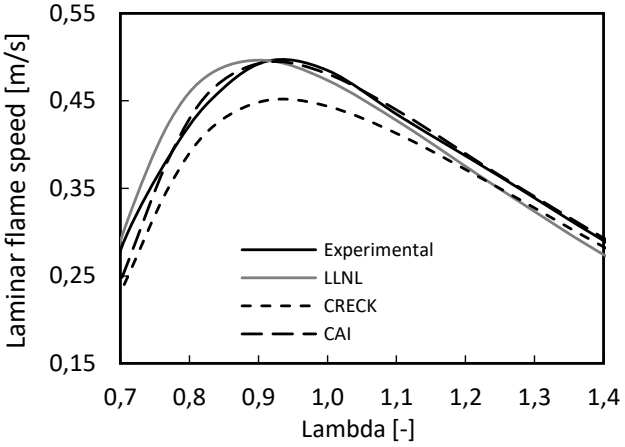

Figure 4.5: Laminar flame speed of a commercial E10 gasoline [12] compared to TRF+Ethanol surrogate at 358 K and 1 bar.

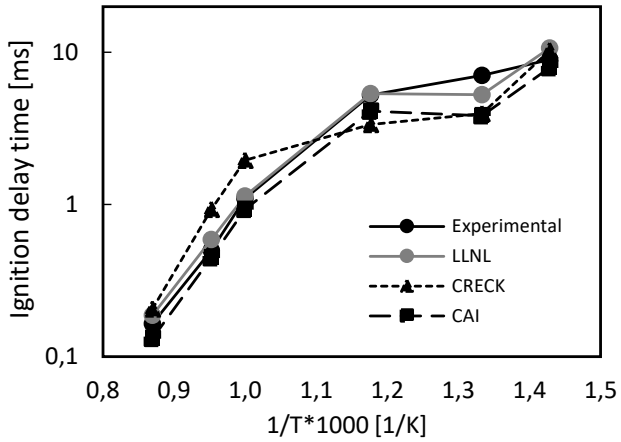

Figure 4.6: Ignition delay time of TRF+Ethanol fuel (62% isooctane, 18% n-heptane, 20% ethanol) at 30 bar and lambda 1. Experimental data from [15].

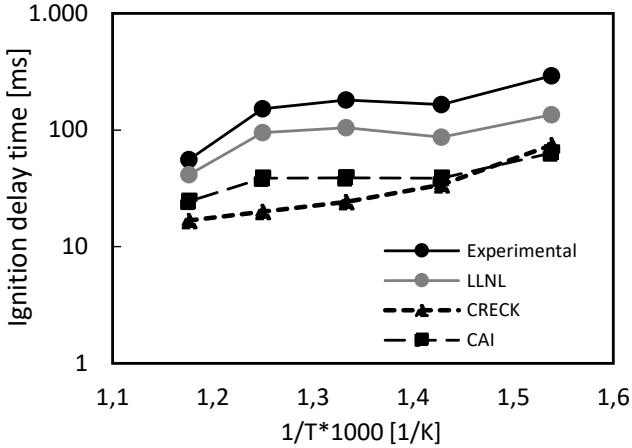

Figure 4.7: Ignition delay time of mixture composed by 65% isooctane and 35% toluene at 12 bar and in stoichiometric conditions. Experimental data from [36].

4.1.2 Reaction Mechanism Extrapolation to High Temperatures and Pressures

Chemical mechanisms use different extrapolation approaches to estimate kinetics at high temperatures and pressures (i.e. outside the T-p validation range) and this explains why under these conditions the mechanisms deliver remarkably different results. As already mentioned, this is an extremely important aspect to keep in consideration because the extrapolation is done exactly in the range of thermodynamic conditions typically found in an ICEs during combustion.

In Figure 4.8, the laminar flame speed dependency on temperature and pressure for three reaction mechanisms is reported. The calculations are performed with a TRF+Ethanol surrogate (53% isooctane, 11% n-heptane, 31% toluene and 15% Ethanol) at 1 bar and stoichiometric conditions on the left side and 375 K and stoichiometric conditions, on the right.

It can be noticed that the chemical mechanisms analysed show similar temperature extrapolation trends (fig 4.8, left) with a maximum variation of 2%. On the other side, they have considerably different behaviours at high pressures (fig 4.8, right) with differences up to 30%. In particular, the LLNL mechanism shows a lower laminar flame speed as the pressure increases which means that, under engine relevant conditions, this model is expected to show lower laminar flame speeds compared to the other mechanisms. A comparison with the same surrogate, high pressure and temperature is shown in Figure 4.9 (calculations at 800 K and 50 bar).

Due to the absence of corresponding experimental data under these conditions, it is unfortunately not possible to verify which mechanism is more accurate. Therefore, independently from the mechanism used, further calibration of combustion models inputs used in the CFD simulations is often required.

Furthermore, to match all the fuel properties relevant for predicting the combustion behaviour of a real fuel, a large palette of possible surrogate components is desirable (as it is better explained in the next chapters). Accordingly, the LLNL mechanism was chosen. Other than delivering accurate results for both laminar flame speed and ignition delay time, it includes a wide range of

linear and branched hydrocarbons as well as aromatic and olefinic components [35, 36].

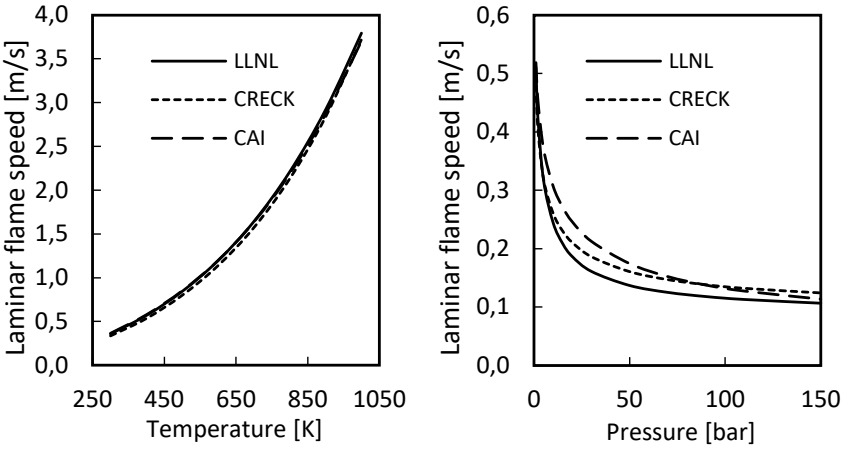

Figure 4.8: Laminar flame speed as a function of temperature (left) and pressure (right) for different mechanisms and TRF+Eth. surrogate.

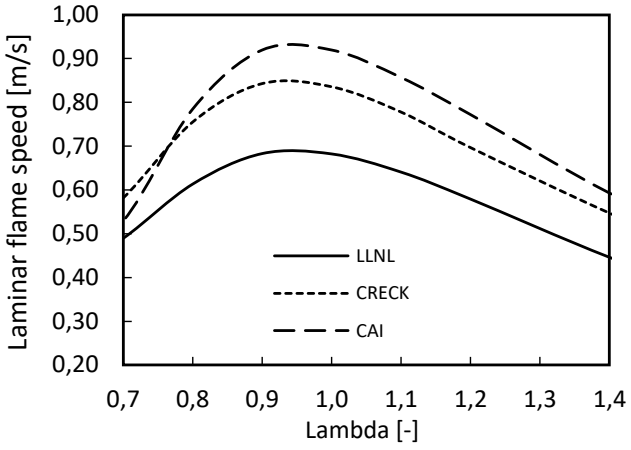

Figure 4.9: Mechanisms comparison for Laminar flame speed of a TRF+Ethanol surrogate at 800 K and 50 bar.

4.2 Detailed Surrogate Formulation

As shown in the chemical analysis reported in Table 4.2, commercial E10 (RON 95) fuels are mostly composed by alkanes (mainly iso- and n-alkanes) and aromatics. Together, they represent more than 80% in volume of the entire composition. For these reasons, most of the experimental researches conducted in the last decade showed that simple compositions like (PRF, TRF or TRF + Ethanol) are suitable to reproduce with sufficient accuracy properties like the laminar flame speed and auto ignition delay time of commercial fuels [5, 12].

Table 4.2: Chemical composition and most representative species of a commercial E10.

Hydrocarbon group	**Concentration [vol%]**	**Representative species**
Iso- and n-Alkanes	44.3	Iso-octane, n-heptane
Cycloalkanes	6.0	Cyclopentane
Aromatics	34.7	Toluene
Olefins	5.0	Isooctene
Oxygenates	10.0	Ethanol

However, these simple surrogates are not adequate for a fuel investigation because their ability in describing fuel characteristics is limited. They cannot accurately describe the influence of chemical species like olefins and cycloalkanes which, if present in high concentrations (like in high performance, motorsport fuels and in many e-fuels), remarkably influence both knock resistance and laminar flame speed of the fuel. For this reason, in the last years, there is a trend to represent real fuels with an increasing number of chemical species [45].

Another critical aspect to consider is how the surrogate composition is chosen. Many approaches can be found in the literature and, in most of them, the surrogate is composed in such a way that it matches some specific fuel characteristics (e.g. RON, MON, A/F ratio, H/C ratio, etc.) [12, 17, 40]. However, some characteristics like RON and MON do not behave linearly due to interaction among chemical components which means that it is often not possible to correctly predict utilising simple formulations [37].

In the following, surrogates of different complexity are compared for both commercial and high-performance fuels. The goal is to understand, which is the most accurate approach that can be used to define surrogates valid for any type of fuel.

4.2.1 Surrogate Composition for Commercial Fuels

As already mentioned, to reproduce commercial fuels like Super E10 (whose composition is reported in Table 4.2), simple surrogates up to 4 components are commonly used. The aim of the following investigation is to understand if, for this fuel, the use of more complex surrogates including olefins and cycloalkanes has a relevant impact on the calculation of laminar flame speed and ignition delay time.

Table 4.3 reports the compositions that have been tested. As explained in [40], to determine a surrogate composition, it is necessary to define several constrains equal to the number of chemical species included in it. For any type of surrogate, a fist constraint is the unity for the sum of the compound fractions. Then, the number of physical targets of a surrogate with n compounds is reduced to (n - 1). Other constraints are defined by matching the following fuel properties:

- RON (for all surrogates)
- H/C ratio (for TRF, TRF+Eth and 6-components surrogates)
- Ethanol content (for TRF+Eth and 6-components surrogates)
- Olefin content (for 6-comp. surrogate)
- Cycloalkanes content (for 6-comp. surrogate)

RON of the mixture is estimated as the average of compound values weighted by the volume fractions [40].

In this analysis, only the fuel properties relevant for the calculation of laminar flame speed and autoignition delay time have been considered. Differences in liquid vaporisation are indeed not of interest for this calculations.

In Tables 4.4 and 4.5, the chemical composition and the properties of the surrogates are compared to those of the real fuel. It can be noticed that a surrogate with at least 4 components is necessary to match most fuel characteristics with sufficient accuracy. Furthermore, the 6 components surrogate does not show any further improvement in accuracy compared to TRF+Ethanol. This result can be explained by considering that cycloalkane and olefin content is not enough to significantly affect fuel macro properties.

Table 4.3: Surrogates for E10, RON 95 fuel.

	PRF	**TRF**	**TRF+Eth.**	**6 comp.**
Isooctane [vol%]	96.7	60.3	43.8	34.7
n-heptane [vol%]	3.3	11.0	14.4	14.3
Cyclopentane [vol%]	0	0	0	6.0
Isooctene [vol%]	0	0	0	5.0
Toluene [vol%]	0	28.7	31.8	30.0
Ethanol [vol%]	0	0	10.0	10.0

Table 4.4: Chemical composition of the tested surrogates compared to E10.

	E10 Fuel	**PRF**	**TRF**	**TRF +Eth.**	**6 comp.**
Iso-, n-Alkanes [vol%]	44.3	100	71.3	58.1	49.0
Cycloalkanes [vol%]	6.0	0	0	0	6.0
Olefins [vol%]	5.0	0	0	0	5.0
Aromatics [vol%]	34.7	0	28.7	31.9	30.0
Oxygenates [vol%]	10.0	0	0	10.0	10.0

Table 4.5: Chemical properties of the tested surrogates compared to E10.

	E10 Fuel	**PRF**	**TRF**	**TRF +Eth.**	**6 comp.**
RON [-]	96.3	96.3	96.3	96.3	96.3
MON [-]	85	96.3	90.8	87.9	86.5
Molar mass [g/mol]	91.2	113.7	104.4	90.7	88.4
A/F ratio stoich. [-]	13.85	15.07	14.53	13.85	13.85
H/C ratio [-]	1.86	2.25	1.86	1.86	1.86
O/C ratio [-]	0.03	0	0	0.03	0.03

In Figure 4.10 are compared the calculated laminar flame speed of each surrogate with the experimental measurements conducted by Dirrenberger et al. [12] on a similar commercial fuel at 358 K and 1 bar. All the calculated surrogates show good agreement with the experimental data, with an average difference around 5%. It can be concluded that, for commercial fuels, surrogate complexity as a limited impact on laminar flame speed.

However, for what concerns ignition delay time, the surrogate formulation has a significant influence on ignition delay time, as shown in Figure 4.11. In detail, it can be noticed that in the range between 1.0 and 1.3 (which corresponds to 1000 and 750 K) all the surrogates show similar behaviour with the exception of the PRF which, since it is composed only by alkanes, shows a significant negative temperature coefficient (NTC) region. In the range between 1.3 and 1.8 (which corresponds to 750 and 550 K), also a small concentration of knock-resistant chemical species (especially oxygenates and olefins) shows a considerable influence on the calculated autoignition delay time. In this temperature range, the difference between TRF+Eth. and 6-components surrogates is higher than 15%. Consequently, the 6 comp. surrogate has, during compression phase and beginning of combustion, significantly lower production of radicals and therefore higher autoignition resistance (i.e. lower knock occurrence).

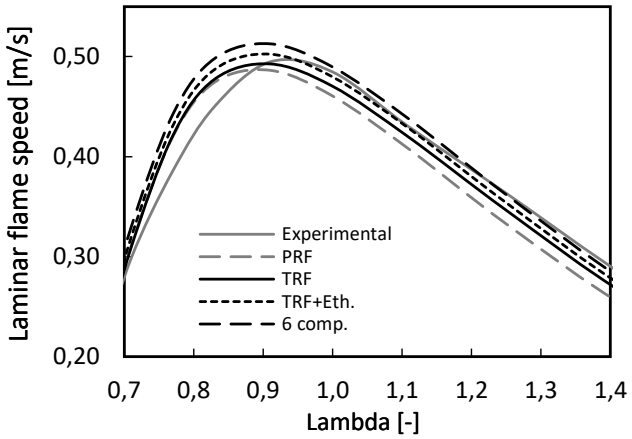

Figure 4.10: Laminar flame speed of E10 fuel at 358 K and 1 bar. Experimental measurements compared to different surrogate formulations.

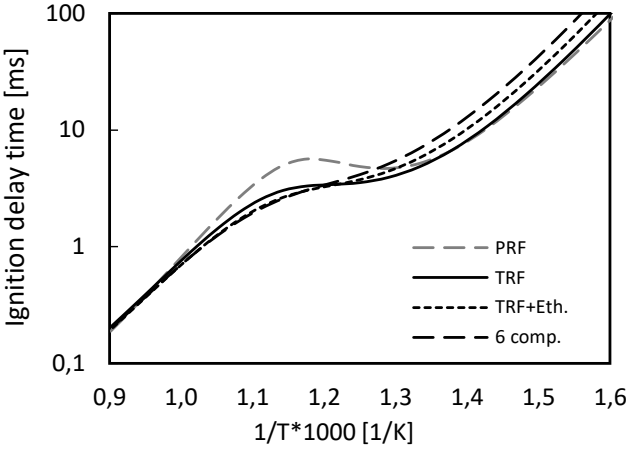

Figure 4.11: Ignition delay time of E10 fuel calculated according to different surrogate formulations at 50 bar, lambda 1.

Unfortunately, for what concerns the autoignition delay time, the results of the calculation could not be compared with experimental measurements because no data were found in the literature for similar fuels. Therefore, it can only be stated that due to the presence of oxidants and olefins, surrogates deliver significantly different results.

Finally, in agreement with what stated in the literature, it can be concluded that a surrogate with at least four species should be used (TRF + Ethanol/ETBE) to represent a commercial fuel with sufficient accuracy. If no oxygenates are present, it can be reduced to three (i.e. TRF).

4.2.2 Surrogate Composition for Alternative and High Performance Fuels

One of the most interesting aspects of e-fuels for SI engines is that their composition can be chosen according to requirements. E-fuels can be of different nature and composition but they are all produced according to the same principles: overcome current limits of commercial fuels while being CO_2 neutral. In designing a fuel, the following aspects are often considered:

- Very simple composition, with 90 vol% of the fuel composed by less than 10 chemical species.
- High cycloalkanes content due to its very high laminar flame speed and good knock resistance.
- Minimised aromatics content (lower than 20 vol%) to reduce particulate emissions.
- High olefins content for motorsport applications, to further enhance knock resistance.
- Use of oxygenates like ethanol or ETBE for increasing Knock resistance. Ethanol, however, has a very low energy content which may impact fuel consumption. Ethanol effect on combustion is analysed in details in Chapter 7.
- Low use of iso and n- Alkanes due to their extremely low resistance to knock (especially n-alkanes).

The result is a fuel which, in comparison to what can be currently found in the fuel stations, has:

- Lower variation in composition and simplified reproducibility through surrogates.
- High resistance to knock (with RON higher than 98) which allows to rise combustion efficiency and therefore reduce fuel consumption.
- High energy content.
- Reduced particulate emissions.

In the contest of fuel design, different high-performance fuels have been tested in the past years at FKFS for both motorsport and series applications. An example is the fuel study presented in Chapter 9, which was conducted on a WRC-derived engine operating with the innovative SACI strategy. During these investigations, it was found that, differently from traditional compositions, their laminar flame speed and autoignition delay time cannot be accurately reproduced through TRF surrogates [10]. For this type of fuels, the quantity of cycloalkanes and olefins present in the mixture is high enough to make the fuel behave significantly different compared to traditional alkane-based compositions.

In the following, the approach used to create the surrogates for the high-performance fuels tested with the SACI combustion strategy is presented.

To analyse these fuels, two types of surrogate have been tested. The first reproduces the exact composition of the real fuel (in vol%) while, the second is a TRF whose composition was determined by matching RON and H/C of the fuel. More details are reported in Table 4.6, where the values are normalised due to confidentiality reasons. It can be noticed that a significant difference in molar mass and MON is present. While, due to the absence of oxygenates, the TRF surrogate is able to correctly reproduce fuel stoichiometric air to fuel ratio, H/C and O/C ratios.

By comparing the respective laminar flame speed and autoignition time, it becomes clear that the two surrogates have completely different behaviour, as shown in Figure 4.12. In particular, it is shown that due to the high concentration of cycloalkanes and olefins, the detailed surrogate shows significant

higher laminar flame speed and ignition delay time (for temperatures between 500 and 850 K). It should also be noticed that, by having a significantly lower amount of alkanes, the reference surrogates have a remarkably smaller NTC zone in the ignition delay time curve.

Table 4.6: Chemical properties the considered surrogates. Values are expressed as variation compared to real fuel characteristics.

	Exact composition	**TRF**
RON [%]	0%	0%
MON [%]	0%	16%
Molar mass [%]	0%	34%
A/F ratio stoich. [%]	0%	0%
H/C ratio [%]	0%	0%
O/C ratio [%]	0%	0%

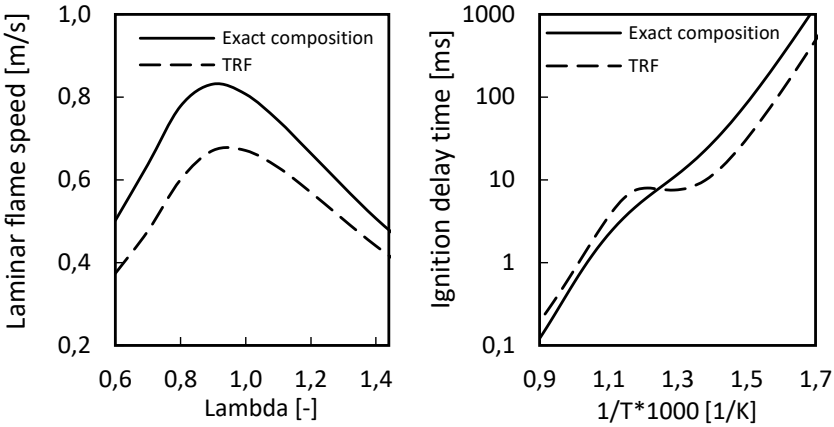

Figure 4.12: Surrogates comparison for LFS at 800 K and 50 bar (left) and for IDT at 50 bar and lambda 1 (right).

It can be concluded that, to accurately describe the characteristics of different kinds of fuels, an extended surrogate formulation is needed. It is important that all the main hydrocarbon groups are represented in the surrogate and that

their volume concentration match. In particular for cycloalkanes, oxygenates and olefins. Furthermore, as it is shown in the next chapters, such detailed surrogate formulation considerably increases CFD-simulations accuracy and makes a virtual fuel investigation possible.

5 Implementation of Fuel Characteristics in QuickSim

As stated in chapter 4, in order to better reproduce fuel characteristics, it is necessary to use surrogates of increased complexity compared to traditional approaches. The higher is the number of species to be included in the surrogate, the higher is the complexity of the reaction kinetic model that must be used. To reduce the calculation burden, thermodynamic properties of the mixture and information on chemical reactions (such as laminar flame speed and ignition timings) are read from external databases and not directly calculated in the 3D-CFD simulation.

In this chapter, the methodology used for the implementation of look-up tables in QuickSim is described. It follows a comparison between Gülder formulation and reaction kinetics for the estimation of laminar flame speed.

5.1 Approach for the Calculation of Look up Tables

Fuel-specific inputs for the combustion processes are prepared using Cantera. In this specific case, the focus is on laminar flame speed and ignition delay time. For their calculation, the detailed mechanism developed by LLNL, containing 323 species [36], is used.

According to QuickSim structure, which was already discussed in Chapter 3, six variables must be considered in the calculations of laminar flame speed and ignition delay time: temperature, pressure, lambda of fresh charge, mass fraction of EGR, lambda of EGR and mass fraction of water. For each of these variables, a range of interest was defined according to typical conditions found in ICE engines, Table 5.1.

For better understanding, it is essential to clarify that here EGR is used to identify the whole mass of previous cycles. It includes both the residual gases and the gases recirculated through external circuits. As it is better explained in

© The Editor(s) (if applicable) and The Author(s), under exclusive license to Springer Fachmedien Wiesbaden GmbH, part of Springer Nature 2021
F. Cupo, *Modeling of Real Fuels and Knock Occurrence for an Effective 3D-CFD Virtual Engine Development*,Wissenschaftliche Reihe Fahrzeugtechnik Universität Stuttgart, https://doi.org/10.1007/978-3-658-31628-0_5

the following sections, the lambda of EGR is used to track the composition of the fresh charge from which it was produced.

Table 5.1: Range of thermodynamic and mixture conditions included in the look-up table.

Temperature	500 - 1000 [K]
Pressure	10 - 250 [bar]
EGR%	0 - 30 [%]
Lambda EGR	0.6 - 1 [-]
Water %	0 - 30 [%]
Lambda %	0.3 - 3.0 [-]

To avoid extrapolation errors, a high number of combinations must be calculated, which results in a look-up table with more than 5 million values. To efficiently read such table within the CFD-simulation, an addressing approach is used. Through which, the software knows in advance, which is the row that should be read and thus saving considerable CPU time.

Furthermore, it is not practically possible to directly calculate all required combinations with reaction kinetics because it would be very time consuming. With the reaction mechanism from LLNL, the calculation time for laminar flame speed is in the range of 8-10 minutes per each point. Even though it is possible to calculate more points in parallel, the overall calculation time remains significantly high.

A solution to the problem can be the use reaction kinetics only for a few significant variables combination and then estimate the remaining points through extrapolation functions. If, for example, the influence of EGR on laminar flame speed can be approximated with a linear equation, it is sufficient to use reaction kinetics only for few points to estimate the trend and then extrapolate the remaining combinations.

In the following, the influence of each variable on the calculated laminar flame speed and ignition delay time for a TRF+Ethanol surrogate (composition is reported in Table 4.4) is discussed. It can be noticed that for almost all cases,

it is possible to define an extrapolation function that catches the trend with sufficient accuracy.

5.1.1 Variables Influence on Laminar Flame Speed

Figures 5.1, 5.2 and 5.3 show the results of reaction kinetics next to extrapolation functions. It can be noticed that laminar flame speed decreases linearly with an increase in water concentration, EGR concentration and lambda EGR. For the thermodynamic conditions here considered (800 K, 80 bar and lambda 1), calculations show that laminar flame speed is not stable for a concentration of EGR and water higher than 30%.

Furthermore, it can be noticed that the trends as a function of temperature and pressure can be approximated with a power function. The trend of laminar flame speed as a function of lambda has the typical bell shape with a maximum for lambda close to 0.95. In this case, a polynomial function is required.

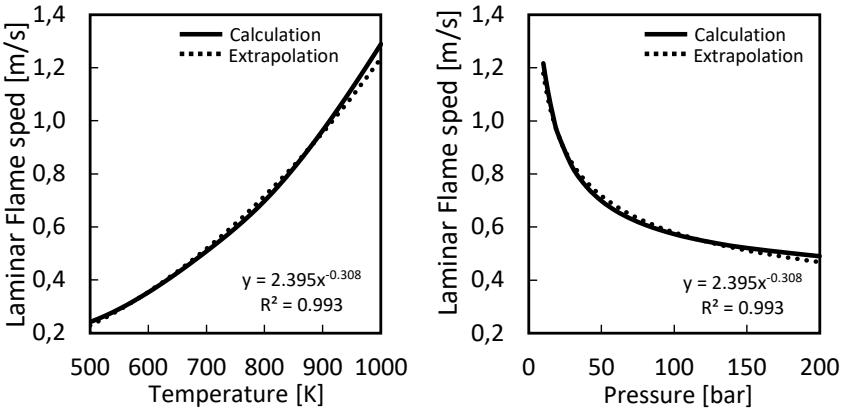

Figure 5.1: Influence of temperature on LFS at 80 bar and lambda 1 (left). Influence of pressure on LFS at 800 K and lambda 1 (right).

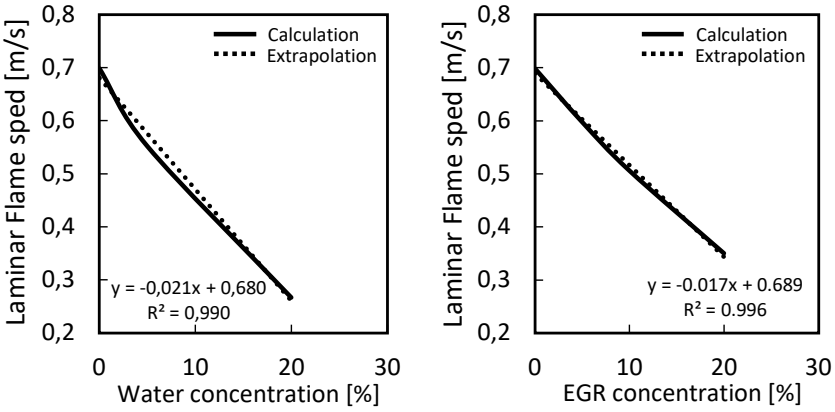

Figure 5.2: Influence of water concentration on LFS at 800 K, 80 bar and lambda 1 (left). Influence of EGR concentration on LFS at 800 K, 80 bar and lambda 1 (right).

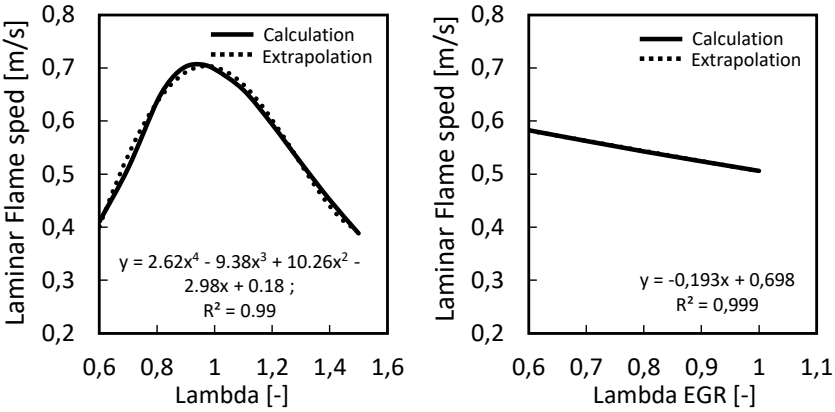

Figure 5.3: Influence of lambda on LFS at 800 K, 80 bar and lambda 1 (left). Influence of lambda EGR on LFS at 800 K, 80 bar and lambda 1 (right).

5.1.2 Variables Influence on Ignition Delay Time

As for the laminar flame speed, autoignition delay time changes according to a power function for a change in pressure (Figure 5.4) and linearly as function of water concentration, EGR concentration and lambda EGR (Figures 5.5 and 5.6). It should also be noticed that the curve showing ignition delay time as a function of the temperature has an "S" shape and it is difficult to correctly extrapolate this trend with a function because the shape changes accordingly to fuel type. The higher is the paraffin content in the fuel, more marked is the "S" shape. This means that to predict this trend properly, the whole temperature interval should be calculated with reaction kinetics.

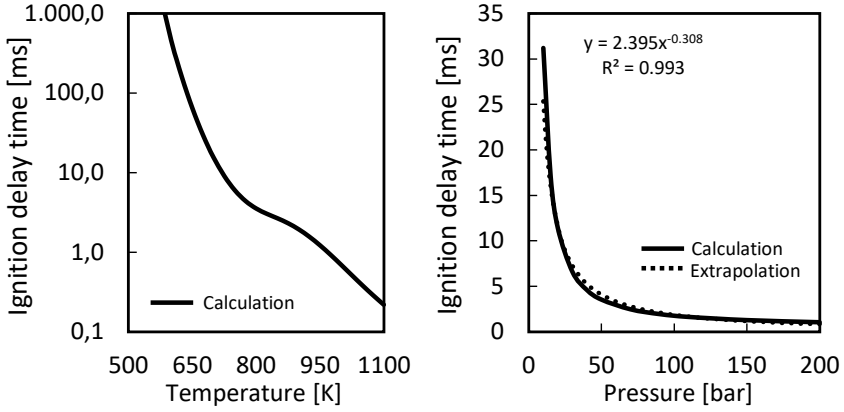

Figure 5.4: Influence of temperature on IDT at 80 bar and lambda 1 (left). Influence of pressure on IDT at 800 K and lambda 1 (right).

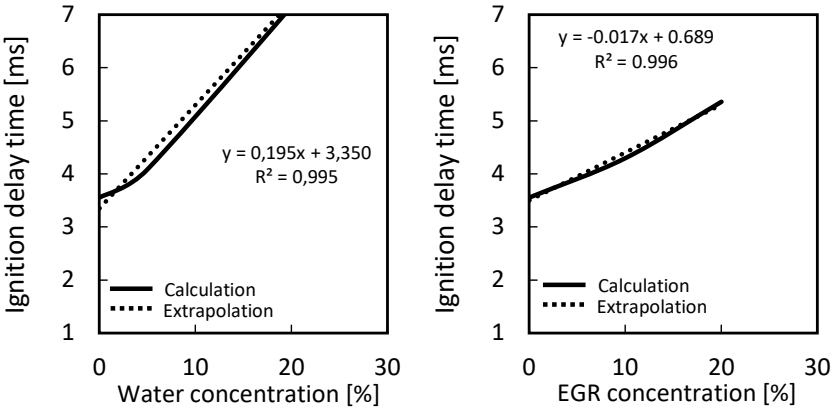

Figure 5.5: Influence of water concentration on IDT at 800 K, 80 bar and lambda 1 (left). Influence of EGR concentration on IDT at 800 K, 80 bar and lambda 1 (right).

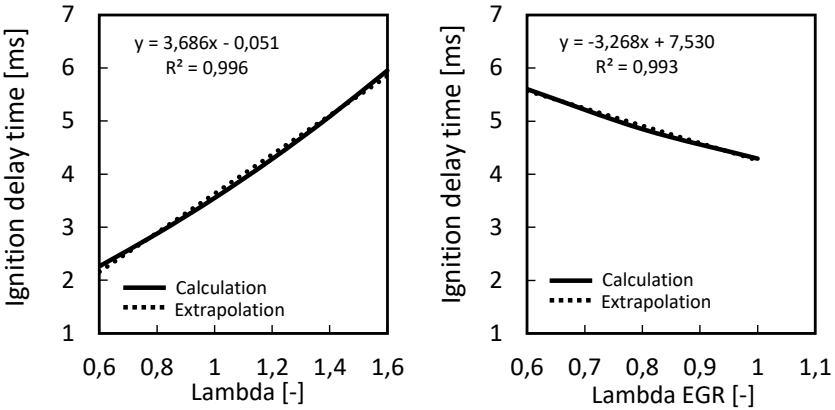

Figure 5.6: Influence of lambda on IDT at 800 K, 80 bar and lambda 1 (left). Influence of lambda EGR on IDT at 800 K, 80 bar and lambda 1 (right).

5.2 Influence of EGR Composition

In QuickSim, the lambda of EGR is used to track the composition of the fresh charge from which it was produced. The combustion of a rich mixture will then produce a rich EGR. By including the Lambda of EGR as a variable, it is possible to distinguish between inert and active EGR. The first is composed of fully oxidized products of combustion (mainly CO_2, H_2O, N_2 and O_2), while the second is produced by a rich mixture and it contains also species as CO, $H2$ and OH. These species participate in further oxidation as soon as oxygen is available, influencing both laminar flame speed and ignition delay time. The contribution of active species has more and more importance as the air available in the mixture increases. As shown in Figure 5.7, in excess of air (lambda higher than 0.95), the difference in laminar flame speed can be as big as 20%. The calculations are performed with the TRF + ethanol surrogate, whose composition is reported in Table 4.3.

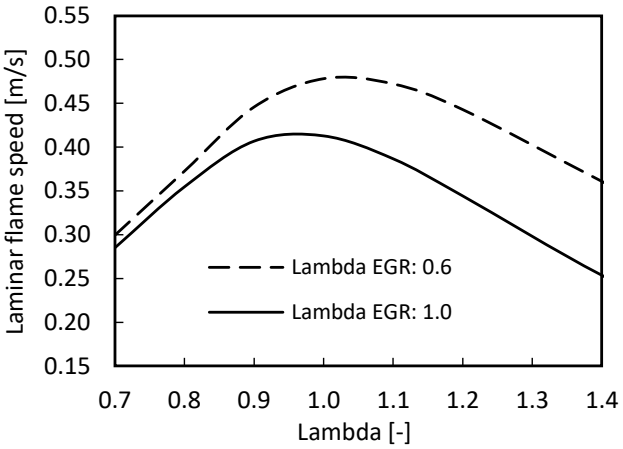

Figure 5.7: Effect of EGR composition on laminar flame speed for a TRF+Ethanol surrogate. Values calculated at 750 K, 50 bar and 10% EGR.

5.3 Comparison of Empirical Formulations with Reaction Kinetics

As mentioned in Chapter 3, in the past, the laminar flame speed in QuickSim was estimated using Gülder formulation (eq. 3.2). In order to keep into account the influence of temperature, pressure, lambda, and EGR mass fraction, different coefficients are used.

This formulation, however, has different drawbacks. It can be used only with those fuels for which experimental coefficients are available and it does not take into account the influence of water concentration and EGR composition.

Figures 5.8 reports a comparison between Gülder's equation and kinetic reaction calculations. Here, the two modelling approaches are shown next to experimental measurements conducted by Dirrenberger et al. [12] on commercial E10 gasoline with a RON of 95. The six-components surrogate (whose composition is reported in Table 4.3) and the LLNL chemical mechanism are used. As shown, relevant approximations can be introduced by using Gülder´s formulation, which is found to give reliable results only for lambda values lower than stoichiometric. Consequently, this formulation is not suitable for all lean combustion modes, like SACI and Diesel.

Moreover, big discrepancies between reaction kinetics and Gülder formulation can be found at high pressure and temperature. For reaction calculations, a six-components surrogate (whose composition is reported in Table 4.3) is used. As shown in Figure 5.9, the empirical approach shows a laminar flame speed significantly higher than any other reaction model tested so far.

Due to the broader validation range and fuel flexibility, the introduction of look-up tables calculated with reaction mechanisms is expected to bring a significant improvement in simulation accuracy.

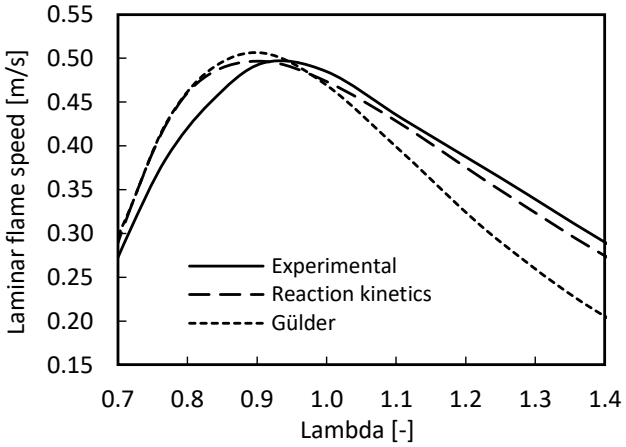

Figure 5.8: Comparison of Gülder formulation with reaction kinetics for a commercial E10 fuel at 358 K, 1 bar and 0% EGR. Experimental measurements from [12].

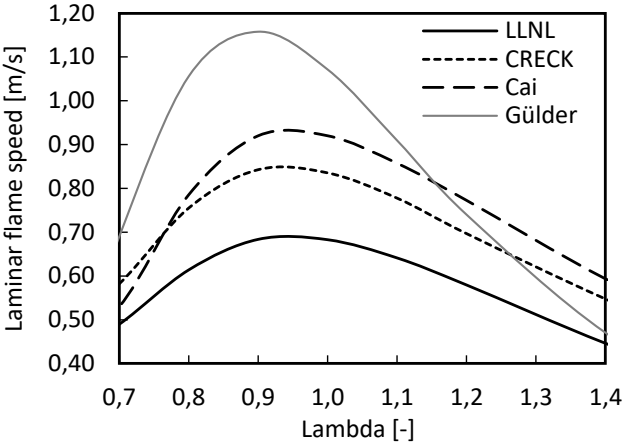

Figure 5.9: Comparison of Gülder formulation with different reaction models at 800 K, 50 bar.

6 Locally-Distributed Auto-Ignition Model and Knock Detection

In QuickSim, to optimize simulation time, the working fluid is described by few scalars and the combustion processes are based on heat-release models (more details can be found in Chapter 3.1). Since no detailed chemical reaction is directly implemented in the simulation environment, in order to reproduce phenomena like autoignition of fresh charge, a dedicated model must be implemented.

In this chapter, the approaches used to implement a locally-resolved autoignition model and a knock detection criterion are discussed.

These models were tested and calibrated on a wide range of engines and, in the last years, they have been successfully used in QuickSim for detecting knock conditions in SI engines.

6.1 Modelling of Local Auto Ignition

As already introduced in Chapter 2.3.2, the ignition delay time of an air-fuel mixture can be estimated by evaluating the integral formulation proposed by Livengood and Wu (eq. 2.4) which represents the degree of chemical reaction progress and thus the pre-reaction state of the mixture.

The integral, according to its original formulation, is calculated considering the average mixture conditions in the cylinder. However, this approach has two main drawbacks. First, autoignition occurs due to the formation of radicals that depend on local charge conditions and significant approximations are made if, for example, average cylinder temperature and lambda are considered. Secondly, phenomena like knock in SI engines occur only if a sufficient amount of the mixture auto-ignites. Therefore, it is also essential to quantify the quantity of charge in autoignition conditions so that knock occurrence can be correctly detected.

© The Editor(s) (if applicable) and The Author(s), under exclusive license to Springer Fachmedien Wiesbaden GmbH, part of Springer Nature 2021
F. Cupo, *Modeling of Real Fuels and Knock Occurrence for an Effective 3D-CFD Virtual Engine Development*,Wissenschaftliche Reihe Fahrzeugtechnik Universität Stuttgart, https://doi.org/10.1007/978-3-658-31628-0_6

To overcome these disadvantages, a local integral counter has been implemented in QuickSim as additional scalar and this is updated in every cell of the 3D-CFD model at each time step. In this way, it is possible to consider fluid mixing and to calculate the location and the quantity of charge in autoignition conditions.

For a correct implementation of Livengood and Wu integral, it is of significant importance to correctly estimate local temperature increase in the cell during combustion. As shown on the right-hand side of Figure 6.1, during any type of combustion process, local heat release generates high-temperature gradients. The difference in temperature between unburned and burned mass can be as high as 2000 K. As explained in detail by Chiodi in [7], it is numerically difficult to reproduce the increase in temperature of the unburned zone during combustion propagation.

If we consider a general 3D-cell j at the flame front during combustion (schematically shown on the left of Figure 6.1), it can be divided into unburned and burned regions while no reaction zone is present. With a burned mass fraction $0 < w_{B,j} < 1$, the cell temperature (which is per definition in the central node of the cell) as a value in-between the unburned and burned zone, respectively. Since cell temperature and most of the other variables at the central node (e.g. the density) are representative neither for the unburned zone nor for the burned zone, it is a remarkable cause of inaccuracy. Especially for those 3D-CFD models that expressively require information about the unburned zone (laminar flame speed, self ignition, local burn rate, etc.) or the burned zone (e.g. modelling of the burned gas properties).

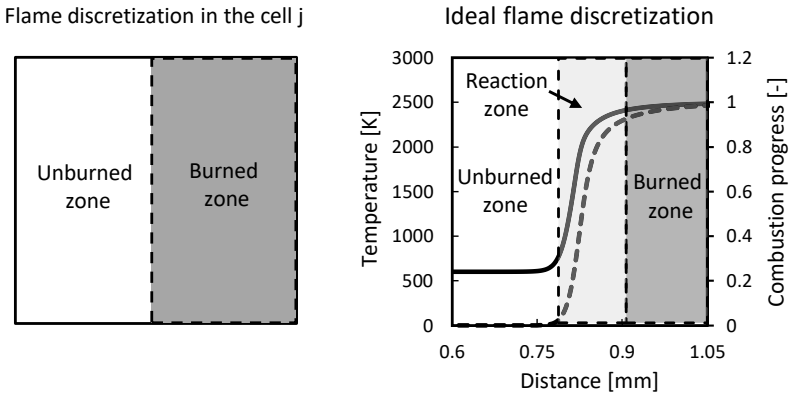

Figure 6.1: Flame discretization in a general 3D-cell of QuickSim compared to ideal flame discretization.

To correctly estimate local temperature increase in the cell during combustion, the following approaches have been investigated:

- Consider as reference temperature the average temperature of the cell. The approach is numerically stable, but it implies a considerable overestimation of local temperature as the combustion in the cell advances. Furthermore, the actual volume of the cell is not taken into account. This means that the temperature increase due to combustion is only a function of the burned mass fraction within the cell and not its dimensions. It follows that the results may be influenced by mesh structure.
- Consider as reference temperature the average temperature of the whole unburned zone. The approach is numerically stable, but it implies a loss of local temperature details which would lead to a considerable underestimation of local temperature increase at the flame front.
- Consider as reference temperature the average temperature of the neighbour unburned cells. The approach is geometrically very complex and can be inconsistent in many cases.
- Use a local CFD two-zones model which allows a continuous separation of each cell involved in the combustion in burned and unburned zone with a

similar procedure like the one used in the real working process analysis for the whole combustion chamber.

Among them, the latter approach is the most promising as it allows to estimate, in the cell, a local unburned mass temperature which increases as the combustion proceeds.

6.2 Model Validation with 0D-Reactor

The auto ignition model was intensively tested against chemical calculations performed with Cantera to prove the accuracy of the results under ideal homogenous conditions. The goal was to identify the limits of the integral formulation without the influence of local mixture conditions. These calculations were performed by creating two virtual compression machines, the first 0-D reactor in Cantera, and the second 3-D reactor in QuickSim. In both cases, adiabatic walls and fully pre-mixed mixture are set to ensure identical calculation conditions. The calculations consisted in compressing the charge until autoignition occurrence. A schematic representation of the two reactors and the validation procedure is shown in Figure 6.2.

The integration approach showed good accuracy under different charge conditions but, as shown in Figure 6.3 and 6.4, its main limitation is the impossibility to evaluate the effect of pre-reactions as those responsible for the so-called cold flame. The heat released by these reactions is responsible for the increase in pressure that can be noticed shortly before autoignition occurs. More sophisticated formulations of the original Livengood and Wu's integration formula have been developed in the past to take into account the effect of these reactions. One example is the one proposed by Fandakov in [14]. However, these phenomena strongly depend on fuel composition (paraffin content) and thermodynamic conditions. As shown in Figures 6.4, pre-reactions do not always lead to an advance in autoignition timing. At this stage, the influence of this phenomena on simulation accuracy needs further investigations. However, in many cases, like for e-fuels that have a low paraffin content, this aspect is considered to be less relevant for future fuel investigations.

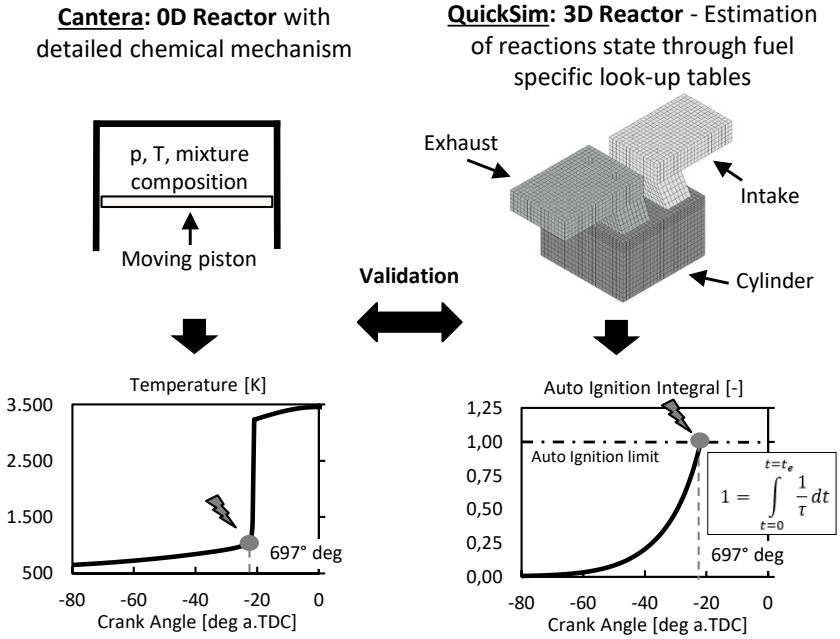

Figure 6.2: Schematic representation of 0D and 3D reactors used for the validation of the autoignition model.

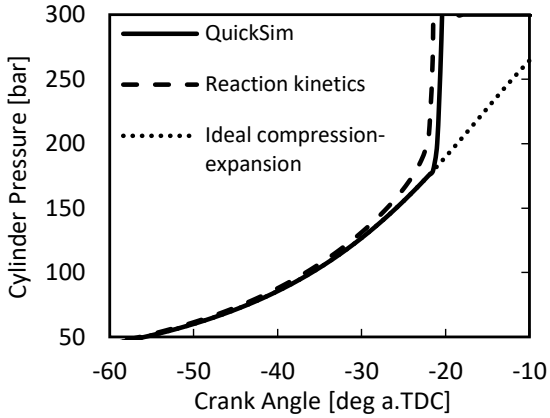

Figure 6.3: Autoignition timing calculated with reaction kinetics and QuickSim. Initial conditions: 600 K – 15 bar – lambda 1.

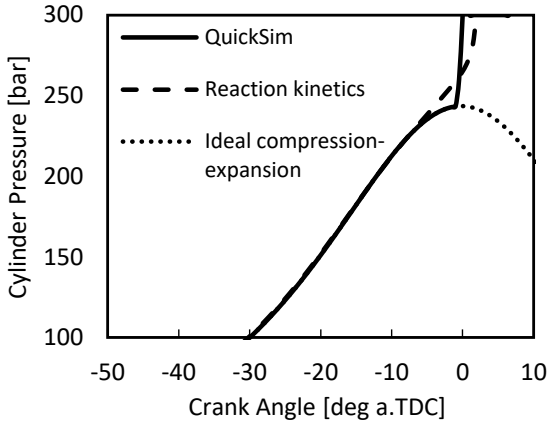

Figure 6.4: Autoignition timing calculated with reaction kinetics and QuickSim. Initial conditions: 470 K – 15 bar – lambda 1.

6.3 Phenomenological Knock Detection Criterion

At the test bench, knock limit is found by advancing the ignition point until a previously defined knock rate limit (expressed as percentage of analysed working cycles in which knock is detected) is reached [13]. It is known that depending from engine application, different knock tolerances are accepted. For series engines, for example, a knock rate around 5% is accepted while for race engines it can be considerably higher due to lower durability requirements.

Unfortunately, it is numerically difficult to correctly reproduce pressure oscillations occurring at the test bench and, therefore, a different approach is usually used to detect knock in CFD-simulations.

As experimentally established, an engine is in critical knock conditions only if a sufficient amount of unburned mass auto-ignites. Thanks to the locally-resolved auto-ignition model previously introduced, it is possible not only to identify the amount of mass in autoignition conditions but also its location at each time step. Besides, to establish a knock criterion, it is necessary to find a critical value of mass in autoignition over which the operating point is considered to be in knock.

However, the mass in autoignition cannot be easily estimated experimentally, and it is not practically possible to have a direct comparison of simulation results with test bench measurements. Nevertheless, as shown in the next chapters, if the simulation reproducing a knock-critic operating point is taken as reference, the calculated mass in autoignition can be successfully used to compare different engine configurations and fuel types, predicting which case is less knock critical.

In the following, the working principle of knock investigations is introduced. A single-cylinder engine running at 2500 rpm with an IMEP of 15 bar is considered. More information about engine configuration can be found in Table 7.1.

Once the reference case is set, different strategies and geometries can be compared according to the calculated mass in autoignition. In Figure 6.5, for example, are compared the calculated mass in autoignition obtained with different spark timings. The case with IP at 9.5 deg b.TDC is here considered as

reference since, according to test bench measurements, it is at knock limit. By further advancing the IP, the amount of unburned mass that goes in autoignition increases above the reference value. The opposite happens if the IP is delayed.

In Figure 6.6 is qualitatively shown how the locally-resolved auto-ignition integral develops in time during combustion. Few crank angles after the spark plug has been triggered, a considerable increase in autoignition integral takes place all around the flame front. Few degrees later (8 deg a.TDC), the integral reaches the value of 1 (i.e. local autoignition) in the areas below the exhaust valves, ahead of the flame front. This crank angle corresponds to the point at which the mass in autoignition shown, in Figure 6.5, increases exponentially.

In the following chapters, some of the investigations conducted in the last years with the support of knock detection criteria are presented.

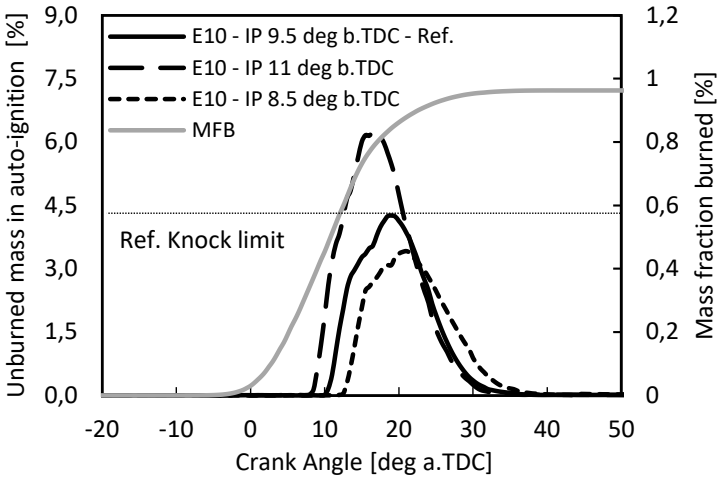

Figure 6.5: Mass in autoignition for different spark timings.

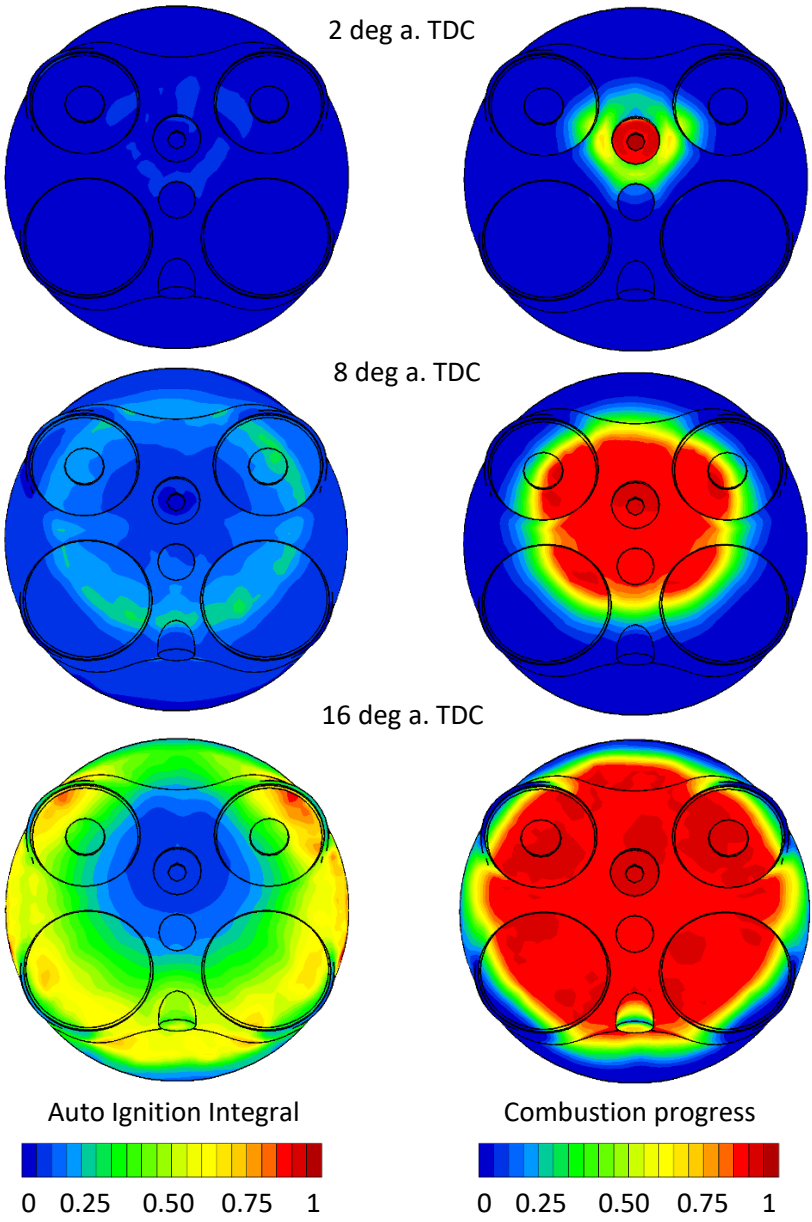

Figure 6.6: Development of auto ignition during combustion in a SI engine at knock limit.

7 Influence of Ethanol on Combustion and Knock

Bioethanol is one of the most used bio-fuels and it is mainly blended with standard gasoline to both improve its quality and to reduce its price. Thanks to the ability of ethanol to mix homogeneously with gasoline, in many countries it is possible to find at the pump station gasolines that are blended with 5% (E5) or 10% (E10) of ethanol.

In this section, the investigation conducted on three fuels with different ethanol content is presented. 3D-CFD engine simulations are used to better understand their differences in knock behaviour and evaluate the potential increase in engine efficiency. Finally, the advantages and disadvantages of ethanol-based fuels are discussed.

7.1 Engine Configuration and Fuels Description

The engine considered is a downsized, turbocharged, direct injection, SI engine and the investigated operating point is, according to experimental data, at the knock limit. More information on engine configuration and operating point are reported in Table 4.

As discussed in more detail in [52], the simulation was extensively calibrated with test bench data under different operating conditions.

© The Editor(s) (if applicable) and The Author(s), under exclusive license to Springer Fachmedien Wiesbaden GmbH, part of Springer Nature 2021
F. Cupo, *Modeling of Real Fuels and Knock Occurrence for an Effective 3D-CFD Virtual Engine Development*,Wissenschaftliche Reihe Fahrzeugtechnik Universität Stuttgart, https://doi.org/10.1007/978-3-658-31628-0_7

Table 7.1: Engine configuration and reference operating point according to experimental data.

Bore x Stroke	719 x 820 mm
Displacement Volume	333 cm3
Compression ratio	10.5
Engine Speed	2500 rpm
IMEP	15 bar
Peak Pressure	79 bar
MFB 50%	10° deg a.TDC
Injection system	DI

Considering test bench operating point as a reference, three fuels with different RON have been virtually investigated at constant IMEP. Some of the most relevant properties of these fuels are reported in Table 7.2. They can be easily distinguished according to oxygenates content which is typically added to increase the knock resistance of the mixture. Oxygenates are mainly represented by ethanol for fuels E10 and E20 while, for the Super Plus, by ETBE (Ethyl-tert-butylether). The last is an additive produced by mixing ethanol and isobutylene, and it is often added to gasoline instead of ethanol to improve its knock resistance.

Table 7.2: Main properties of the analysed fuels.

	E10	**Super Plus**	**E20**
RON [-]	95	98	103
LHV [MJ/kg]	41.7	42.4	40.7
Density at 15°C [kg/m3]	756.9	749.2	755.5
Vapor pressure at 38° C [kPa]	55.4	59.4	51.4
Heat of vaporization at 38° C [kJ/K]	395.9	339.5	455.2
Stoich. Ratio [-]	13.8	14.1	13.5
Alkanes [vol%]	50%	44%	48.8%
Olefins [vol%]	5%	10%	5.8%
Aromatics [vol%]	35%	34%	25.9%
Oxygenates [vol%]	10%	12%	20%

Due to the absence of ethanol, Super Plus shows the highest Low Heating Value (LHV) and the lowest heat of vaporization. Another important aspect to highlight is that the E20 here considered is not a commercial fuel like the others. This mixture was prepared by mixing an E0 - RON 95 fuel with ethanol and this explains the very high RON. Compared to E10, the mixing principle is different. For E10, ethanol is used to improve the knock resistance properties of fuels with very low RON in such a way to make it compliant with legislation limits (e.g. RON 95 in Europe). For this reason, the ignition delay time of the fuels here considered does not increase linearly with higher ethanol content, as shown in Figure 7.1. The laminar flame speed, on the other side, is not significantly affected by the presence of ethanol. The difference between fuels is indeed lower than 5% (Figure 7.2).

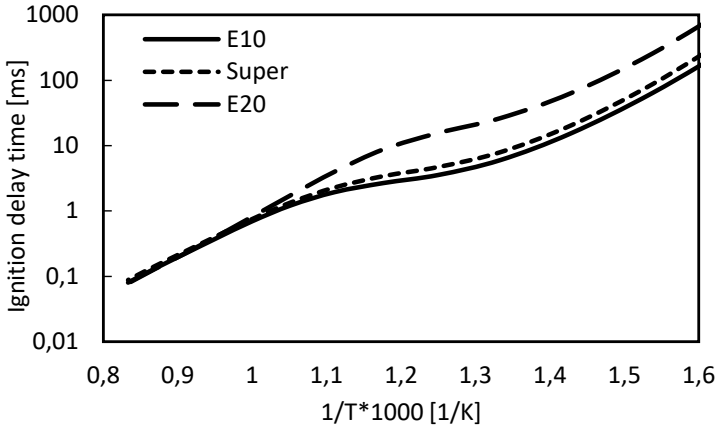

Figure 7.1: Calculated ignition delay time of the analysed fuels at 50 bar, lambda 1, and 0% EGR.

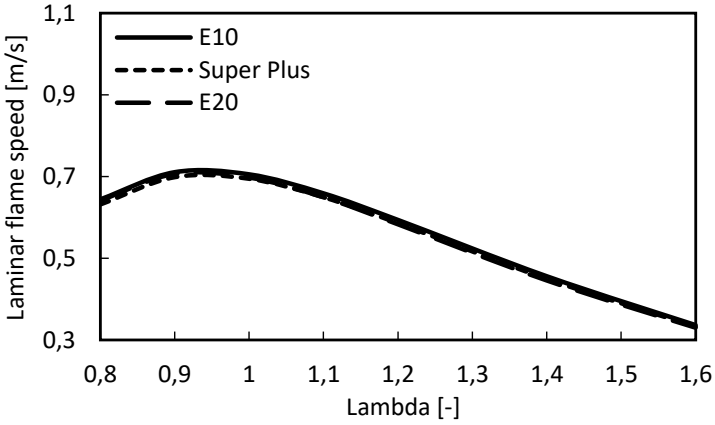

Figure 7.2: Calculated laminar flame speed of the analysed fuels at 800 K, 50 bar, and 0% EGR.

7.2 Fuel Investigation

If fuels with different ethanol content are compared at constant IMEP, two aspects should be considered. First, ethanol decreases the fuel stoichiometric ratio of the mixture, which implies that, at constant air consumption and target lambda, more fuel must be injected. Secondly, ethanol increases the heat of vaporization of the fuel, which, combined with a higher mass of fuel injected, significantly decreases the temperatures at ignition point. As shown in Table 7.3 and Figure 7.3, at constant IMEP, fuel E20 brings a decrease in temperature of almost 30 degrees compared to Super Plus. The combination of higher autoignition resistance and temperature decrease help to enhance knock resistance of the E20 and not only. Such a decrease in temperature may also be beneficial in terms of fuel consumption and emissions because less enrichment is needed at high load for components protection.

Table 7.3: Results of engine simulations for each fuel.

	E10	**Super Plus**	**E20**
Air Cons.[kg/h]	32.7	32.5	33.0
Fuel Cons. [kg/h]	2.33	2.28	2.42
IP [deg b.TDC]	9.5°	9.5°	9.5°
IMEP [bar]	15	15	15
MFB50 [deg a.TDC]	10°	10°	10°
Lambda at IP [-]	1	1	1
Temp at IP [K]	658	665	636

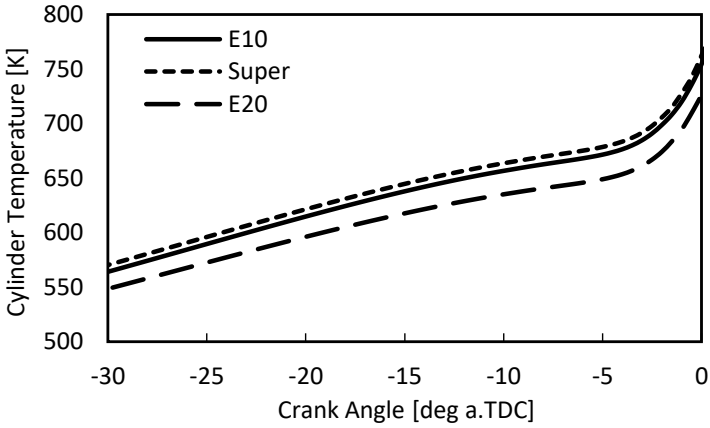

Figure 7.3: Cylinder temperature during compression phase for each fuel.

In Figure 7.4, are compared the values of mass in autoignition conditions obtained for each fuel and spark timing. The test bench case "E10 – IP 9.5°deg b.TDC" is considered as knock-limit reference. If, with the same fuel, the ignition point is advanced to 11°deg b.TDC, knock is detected as the amount of unburned mass in autoignition is well above the limit value. Accordingly, it is possible to state that:

- No mass is in autoignition conditions before the fraction of burned mass reaches 50%, which is line with what experimentally established at the test bench for commercial fuels [13].
- The higher knock resistance of the Super Plus can be eventually exploited to further increase power output. By advancing the ignition point to 11°deg b.TDC, for example, the amount of mass in autoignition conditions is indeed still comparable to the reference case.
- Fuel E20, on the other hand, do not show any significant amount of autoignition in the considered operating conditions. As already mentioned, this is due to the lower temperature at IP and much higher knock resistance.

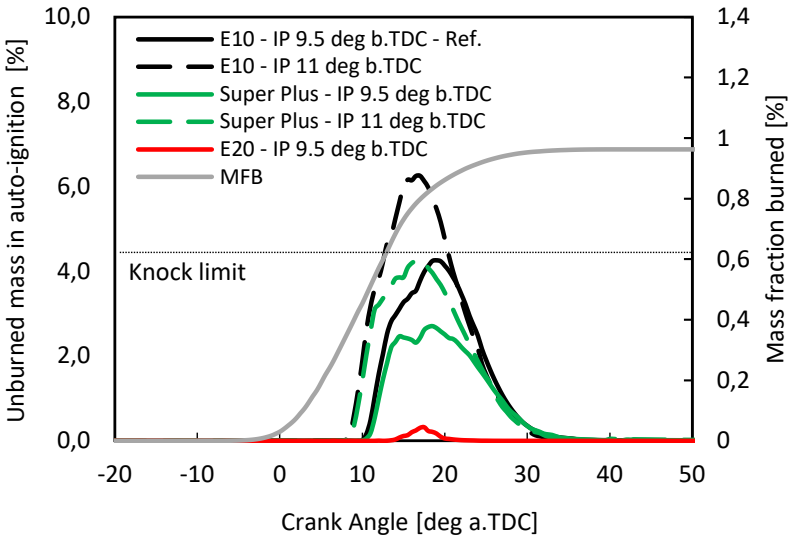

Figure 7.4: Unburned mass in autoignition conditions and mass fraction burned for different fuels and ignition points.

Once the most critical cases have been identified, the next step is to find the areas in which the fresh charge auto-ignites. This information allows a deeper understanding of how different factors like engine geometry, mixture formation and flame propagation affect knock occurrence.

In Figure 7.5 are reported the values of autoignition integral and mass fraction of unburned fuel at different crank angles for 15 bar IMEP, IP at 9.5°deg b.TDC and fuel E10. The distribution of mass fraction of unburned fuel is used to identify the position of the flame front during combustion (areas approaching a value of zero) and the fuel distribution in the end gas. Those regions in which autoignition is occurring are marked with an ignition integral value of 1. It is here interesting to notice that the most critical regions are located under the intake valves where the flame front comes at last due to the not centred position of the spark plug.

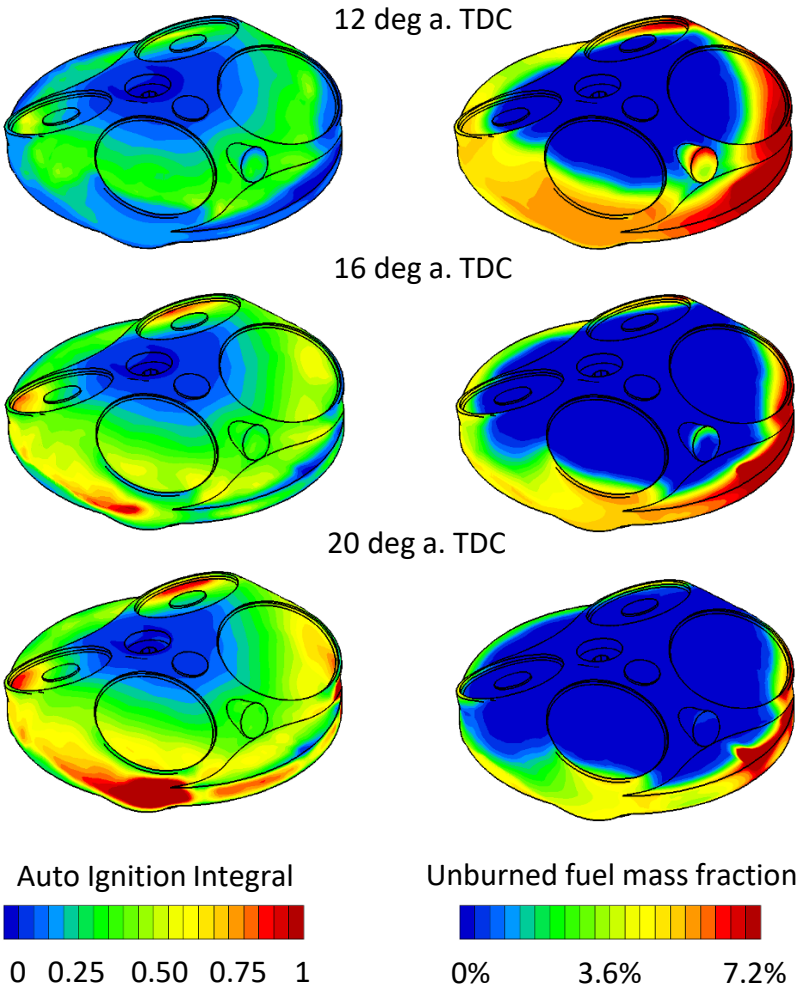

Figure 7.5: Distribution of autoignition integral and fuel unburned at different crank angles for 15 bar IMEP, IP 9.5°deg b.TDC, fuel E10.

By comparing the autoignition integral distribution at 20°deg a.TDC, between two cases with different IP (Figure 7.6), it is possible to see that for the reference spark timing (IP at 9.5°deg.TDC), the area with an autoignition integral of 1 is smaller, and it forms a well-defined ring, surrounding the flame front.

In Figure 7.7 are compared auto-ignition integral and fuel distributions obtained at 20°deg a.TDC with different fuels. As expected, areas with relatively rich mixture have lower temperatures and, therefore, show a lower tendency to auto-ignite (i.e. low value of autoignition integral). This aspect is most relevant in the case with fuel E20, which has the worse mixture homogeneity.

One of the main drawbacks of the presence of ethanol is indeed its high heat of vaporization, which slows down the fuel vaporization with consequent disadvantage in charge homogeneity, as shown in Figure 7.8 and 7.9.

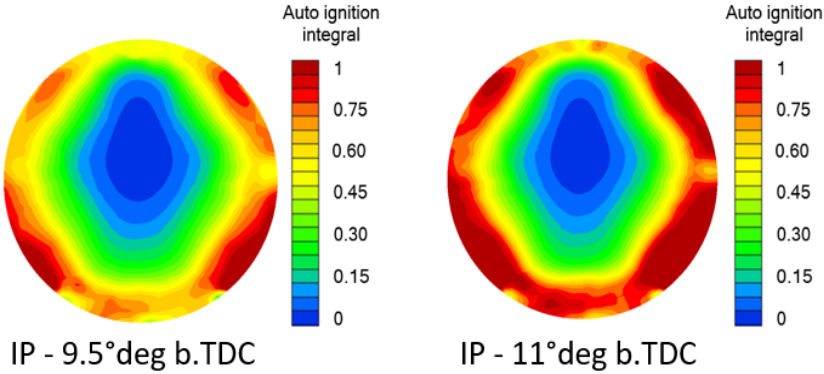

Figure 7.6: Autoignition integral distribution at 20°deg a.TDC for reference and advanced IP, Fuel E10. Section at 2 mm under cylinder head.

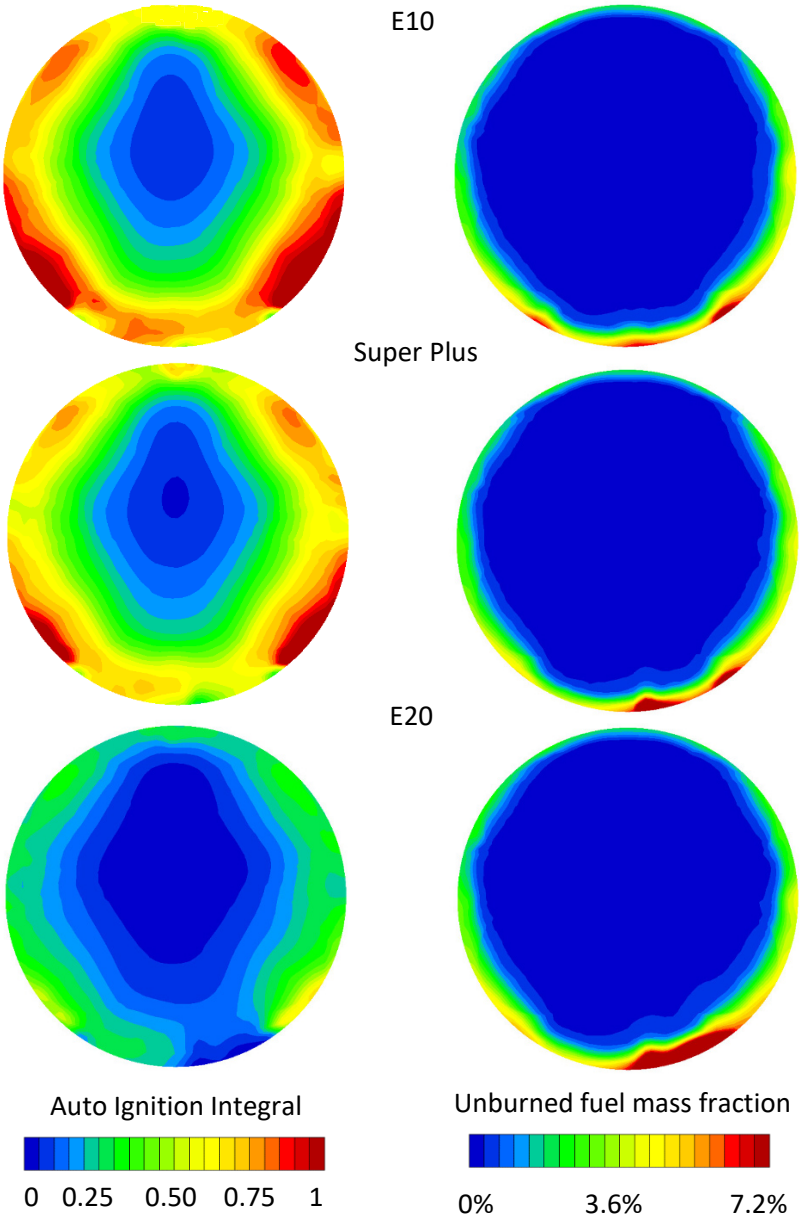

Figure 7.7: Autoignition integral distribution and fuel unburned mass fraction for different fuels at 20°deg a.TDC and IP at 9.5°deg b.TDC. Cylinder section at 2 mm under cylinder head.

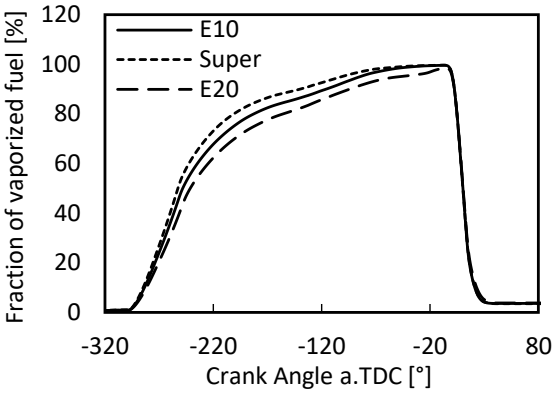

Figure 7.8: Fraction of vaporized fuel mass for different fuels.

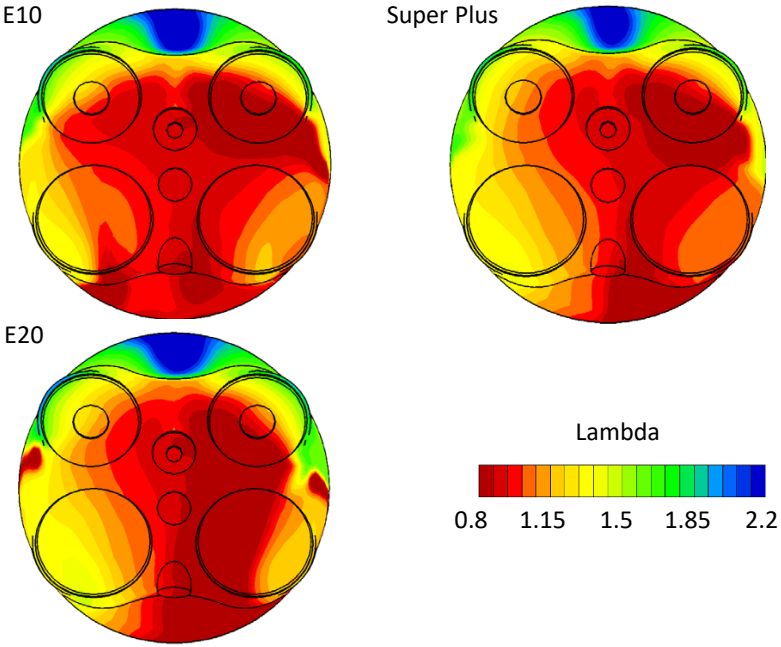

Figure 7.9: Lambda distribution at IP (9.5 deg b.TDC) for different fuels.

8 Knock Analysis for the Optimization of Water Injection

To reduce both harmful emissions (CO, HC, NO_x, etc.) and gases responsible for greenhouse effects (especially CO_2), gasoline engines must run efficiently (i.e. with low fuel consumption) and with stoichiometric air to fuel ratio in order maximise the conversion efficiency of the three-way-catalyst. In-cylinder gas temperature is one of the main factors which limits combustion efficiency and the area of the engine map in which a stoichiometric mixture can be used. At low engine speed, knock occurrence requires a late combustion phasing while, at high speed, it is often necessary to enrich the mixture for components protection. Among others, water injection is a promising technology able to target both aspects.

The investigation on water injection here presented is just a part of a research project conducted at the University of Stuttgart in the last years. The focus of this section is not to discuss in detail the full potential of water injection but to describe how the models introduced in the last chapters have been effectively utilised to analyse and optimise water injection strategies. The knock detection model was indeed an essential tool in the development process as it helped to virtually predict, according to the different in-cylinder conditions, the potential advance in spark time in case of water injection. For more details on the extensive work conducted at the University of Stuttgart on water injection, please refer to [18, 52].

In the following chapter, two studies conducted with direct water injection are reported. The first focuses on the validation of the results of the simulation. The second shows more in details the potential benefits of direct water injection on knock occurrence.

© The Editor(s) (if applicable) and The Author(s), under exclusive license to Springer Fachmedien Wiesbaden GmbH, part of Springer Nature 2021
F. Cupo, *Modeling of Real Fuels and Knock Occurrence for an Effective 3D-CFD Virtual Engine Development*,Wissenschaftliche Reihe Fahrzeugtechnik Universität Stuttgart, https://doi.org/10.1007/978-3-658-31628-0_8

8.1 Benefits of Water Injection

The implementation of water injection can be realised through different engine layouts and injection strategies. Its effectiveness is strictly dependent on base engine features and load point, which implies that many configurations must be analysed to find the optimal strategy. Consequently, the support of engine simulations becomes essential to reduce development time and cost.

One of the most important properties of water is its high heat of vaporisation, which is six times higher than that of gasoline. Like Ethanol, water can be very effective in decreasing in-cylinder gas temperature allowing for an earlier centre of combustion and a lower exhaust gas temperature. Thus, avoiding fuel enrichment for component protection. Furthermore, water has a 30% higher density and three times higher surface tension compared to gasoline which implies a delayed droplets breakup and therefore vaporisation.

Moreover, it is well known that water efficiency in cooling the charge is quite far from the theoretical contribution. The reason for the low cooling effect of the injected water has to be addressed in the low amount of evaporated water mass. When it vaporises, it cools down the surrounding area and, due to its high heat of vaporisation, the reduction in temperature is preventing further evaporation of water droplets present in this region [52].

During the project conducted at the University of Stuttgart, different injections strategies have been analysed. Compared to indirect strategy, direct water injection (DWI) in the cylinder shows better results in improving combustion efficiency as all the vaporisation occurs inside the cylinder itself [23]. On the other hand, indirect water injection (IWI) implies much lower costs. Consequently, a good water injection strategy can be identified as the one which increases water evaporation and, at the same time, reduces wall wetting (especially at the liner where water can mix with lubricants).

In general, limiting factors for applying water injection are the higher system complexity, the needed space to install the system and the necessity to refill the water tank.

8.2 Experimental Setup and Calibration of Combustion Models

At the test bench, both direct and direct injectors have been tested. The high-pressure injector for direct water injection is a conventional solenoid valve commonly used for gasoline, and it is located directly below the intake ports. Due to its lateral position, an injector with an asymmetrical spray pattern is selected, and its maximum injection pressure is 200 bar. The indirect injector, instead, is positioned in the intake manifold, and it allows a maximum injection pressure of 10 bar. More information about engine configuration are reported in Table 8.1.

Table 8.1: Technical data of the single cylinder research engine.

Displaced Volume	333 cc
Stroke - Bore	82 mm - 71.9 mm
Compression ratio	10.75:1
Direct Water Injection (DWI)	up to 200 bar, 120° b.TDC
Indirect Water Injection (IWI)	up to 10 bar, 360° b.TDC
Fuel	E10 with RON 95

The entire real engine at the test bench, including intake and exhaust system, has been reproduced in the 3D-CFD model. Figure 8.1 shows the corresponding simulation model, which contains approximately 420,000 cells. The extension of the 3D-CFD domain to both intake and exhaust vessels remarkably reduces the influence of the boundary conditions. Here, the pressure signals can be assumed as constants over time. On the other hand, more simulation cycles (usually 6-8 cycles) must be performed to reach the convergence of scavenging process and to correctly estimate water accumulation in the runners, in case of indirect water injection.

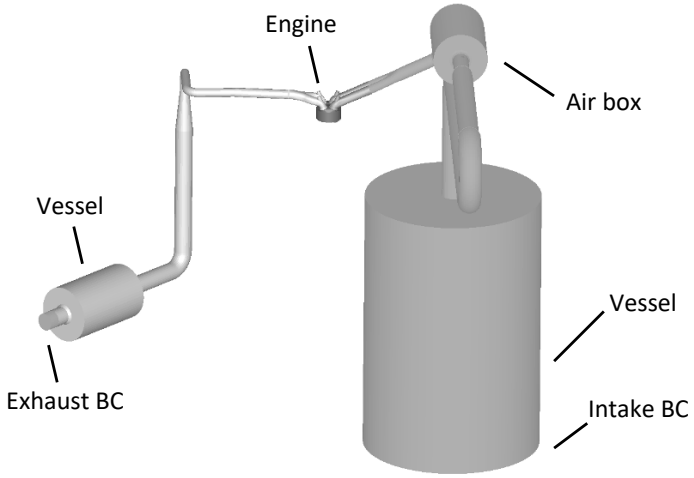

Figure 8.1: 3D-CFD model used to reproduce test bench environment.

In the following investigations, the case without water and with spark time at knock limit is considered as reference. Then, two further cases with direct water injection are reported. In the first, the reference ignition point is used. In the second, a new spark advance is found by advancing the ignition point until the new knock limit is reached.

For the validation of combustion models, the experimental measurements conducted at 2500 rpm, lambda 1 and 15 bar are here considered. In this case, the boost pressure is regulated to reach 1.2 bar while the engine throttle valve is fully opened. Direct water injection (DWI) at 100 bar is considered while a mass corresponding to a water to fuel ratio of 20% is injected. Table 8.2 summarizes all the information about the operating point considered.

Table 8.2: Operating point considered for validation of the simulation.

Engine Speed	2500 rpm
Target IMEP	15 bar
P_2 and P_3	1.2 and 1 bar
T_2	40 °C
Water injection	Direct injection (100 bar)
Start of water injection	120°CA b.TDC
Water/fuel ratio	20%
Average Lambda	1
Fuel	E10 with RON 95

In Figure 8.2, the pressure traces measured at the test bench are compared with the results of the simulation. The case with water injection and reference IP shows much slower combustion and 15 bar lower peak pressure compared to the reference case. It can also be noticed that the oscillations in pressure signal have disappeared, meaning that no knock is occurring. If, with the same water injection strategy, the spark time is advanced to 13°CA b.TDC, a new knock limit is reached with a cylinder pressure considerably higher than in the reference case.

Good agreement was found between experimental data and simulation results meaning that the estimated influence of water on laminar flame speed and ignition delay time is correctly estimated.

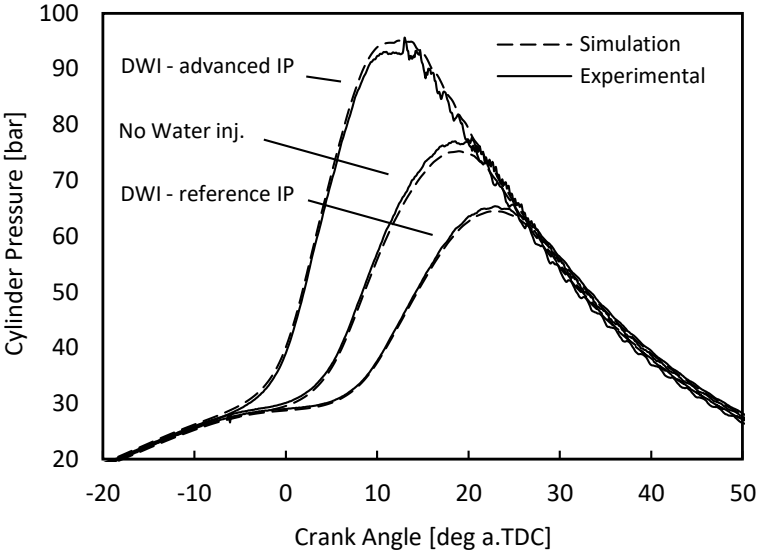

Figure 8.2: Comparison of experimental measurements and simulation results, with and without water injection.

8.3 Water Injection Influence on Knock Occurrence

In the following, an analysis conducted on an operating point with extremely late IP due to knock and direct water injection is presented. The scope is to analyse in detail the effects of water on combustion and to identify the potential advantage in efficiency that can be obtained by advancing the spark timing.

An operating point at 2000 RPM and 20 bar IMEP is considered. Without water, the test bench shows that knock takes place if an ignition time earlier than 0° CA b.TDC is used. At this operating point, direct water injection at 200 bar with a water to fuel ratio of 30% is investigated. More information about the operating point can be found in Table 8.3.

Table 8.3: Operating point considered for knock investigation.

Engine Speed	2000 rpm
Target IMEP	20 bar
P_2 and P_3	1.8 and 1 bar
T_2	40 °C
Water injection	Direct injection (200 bar)
Start of water injection	120°CA b.TDC
Water/fuel ratio	30%
Target Lambda	1
Fuel	E10 with RON 95
Reference IP	0° CA b.TDC

The reference case without water injection is compared to two cases with water injection. In the first, the reference ignition point is used. In the second, a new spark advance is found by advancing the ignition point until either knock or optimal centre of combustion is reached.

As shown in Figure 8.3, the case with water injection and reference IP shows 50° C lower in-cylinder gas temperature at ignition point which, in combination with a global water concentration of 2%, leads to a considerably lower laminar flame speed and then peak in pressure (Figures 8.3 and 8.4). As reported in Table 8.4 and Figure 8.5, the case with water injection and reference IP shows slower and less efficient combustion that did not show any significant influence on gas exhaust temperature (T_3). Nevertheless, as shown in Figure 8.5, the injection of water drastically reduced the amount of mass in autoignition conditions which implies that, in this conditions, the spark timing can be further advanced.

According to the results of the simulation, in the case with water injection, the ignition point can be advanced until the optimal position of the MFB50% is reached, without detecting any knock occurrence. In Figure 8.5, it is shown that even with an IP advanced to 13 deg b.TDC the percentage in unburned mass that goes in autoignition is considerably lower than in the reference case. With the advanced combustion, not only efficiency and IMEP increased but

also a considerable reduction in T3 is obtained. The peak in T3 decreased of circa 70°C.

Table 8.4: Simulation results obtained with and without water injection.

	No water inj.	**DWI**	**DWI and advanced IP**
IP [deg b.TDC]	1	1	13
IMEP [bar]	19.8	18.8	20.6
Indicated eff. [%]	30.4	28.9	31.5
MFB50% [deg a.TDC]	21.4	23.6	9.9

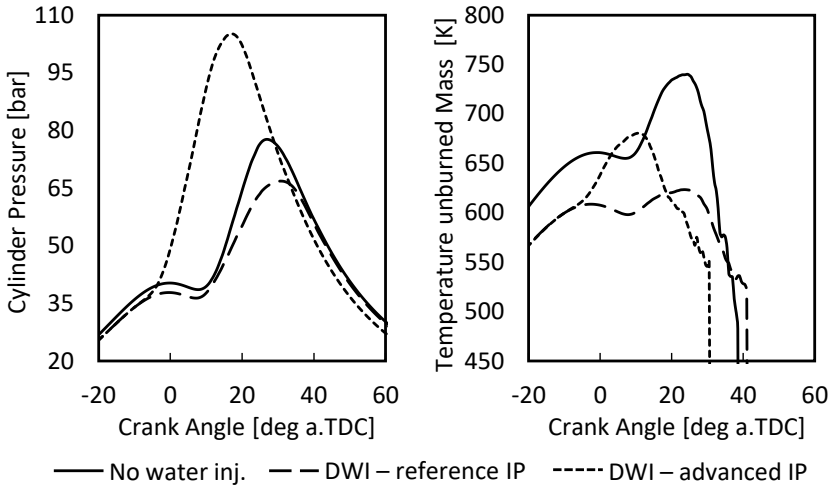

Figure 8.3: Comparison of cylinder pressure (left) and unburned mass temperature (right).

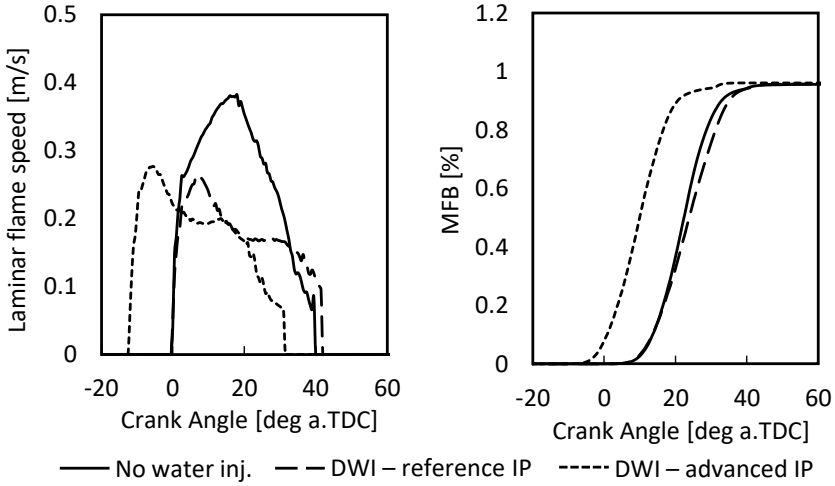

Figure 8.4: Comparison of laminar flame speed (left) and fraction of mass fuel unburned (right) during combustion.

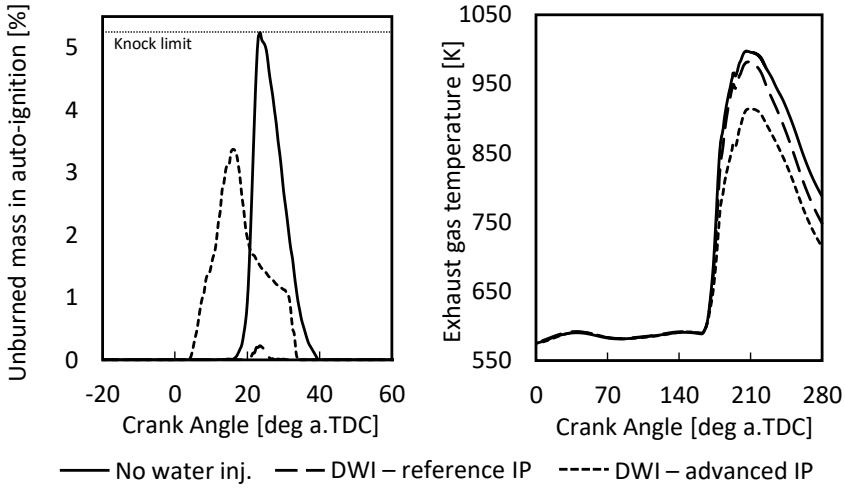

Figure 8.5: Comparison of unburned mass in autoignition during combustion (left) and exhaust gas temperature (right).

9 Virtual Fuel Design for SACI Operation Strategy

The combustion engine of the future must be more efficient and during the history of ICEs, very often Motorsports played a central role in the development of innovative solutions. Highly motivated by competition, the solutions can be tested, implemented and validated within a very short development time, thus establishing Motorsports as a genuine innovation driver. In the last years, the strategies adopted to increase engine performance remarkably changed. Due to different recent regulations – e.g. the introduction of an air restrictor in the World Rally Championship (WRC) or the limitation of the fuel consumption imposed in the World Endurance Championship (WEC) or the Formula One World Championship (F1) - engine power can be raised only by increasing engine efficiency. Accordingly, the development targets in Motorsports have changed. Thus, new motorsport solutions may become increasingly interesting for mass production engines in the future, too [9, 30, 54, 55].

Following this approach, in the last years, Volkswagen Motorsport GmbH, the Technische Universität München (TUM) and the Research Institute of Automotive Engineering in Stuttgart (FKFS) developed, in a joint research project, the innovative combustion concept SACI (Spark Assisted Combustion Ignition) on a WRC-derived engine. This application shows very high-performance levels while remarkably reducing fuel consumption. To better understand how fuel properties can affect this type of combustion, the engine was subject to a fuel investigation whose final goal was to define, through a virtual fuel investigation, a new fuel composition that would further improve engine performance.

© The Editor(s) (if applicable) and The Author(s), under exclusive license to Springer Fachmedien Wiesbaden GmbH, part of Springer Nature 2021
F. Cupo, *Modeling of Real Fuels and Knock Occurrence for an Effective 3D-CFD Virtual Engine Development*,Wissenschaftliche Reihe Fahrzeugtechnik Universität Stuttgart, https://doi.org/10.1007/978-3-658-31628-0_9

9.1 SACI Operating Strategy, Simulation and Experimental Setup

Spark Assisted Compression Ignition (SACI) operating strategy relies on a lean mixture by means of injecting fuel during the early intake stroke into the combustion chamber [43]. The mixture is compressed to a level safely below the critical autoignition threshold. An external ignition source is used to start a propagating flame front which further compresses the unburned mixture inside of the cylinder. This initiates a compression ignition by crossing the autoignition threshold (Figure 9.1). The autoignition threshold is dependent upon the air-fuel mixture, fuel type and amount of residual gas.

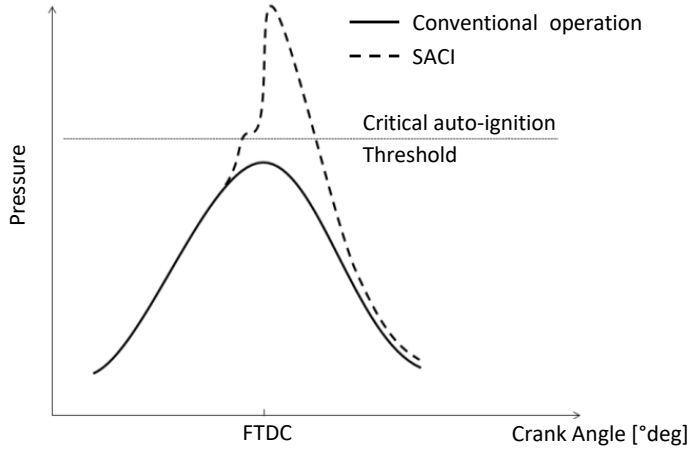

Figure 9.1: Technical principle of SACI combustion strategy.

This specific application uses a passive pre-chamber spark plug featuring several orifice holes and a separated chamber to ignite the highly diluted mixture (Figure 9.2). The ignition inside the pre-chamber spark plug results in the combustion of the trapped mixture, sending hot gaseous jets, radicals, and pressure waves towards the main combustion chamber. In this way, the pre-chamber amplifies the effects of the spark plug. This effect is sufficient to exceed the autoignition threshold of the main charge and a rapid, stable, and almost complete combustion process even at high dilution levels is obtained. This opera-

tion mode leads to substantial improvements in terms of indicated efficiency up to very high load operating conditions [8, 29].

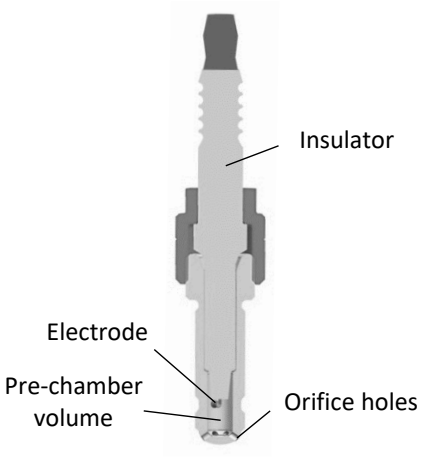

Figure 9.2: Pre-chamber spark plug used in the combustion system for SACI operation.

The experimental investigations on SACI combustion strategy were conducted on a single-cylinder research engine located at the engine laboratory of the Chair of Internal Combustion Engines at the Technische Universität München. The research engine was originally built to carry out development work concerning injection, combustion optimisation, and component testing. It was derived from Volkswagen Motorsports proven 1.6l DI-SI WRC race engine used between 2013 and 2016 in the FIA World Rally Championship (WRC). The specifications of its single-cylinder derivate used in this study are shown in Table 9.1.

Table 9.1: Technical specifications of the single cylinder research engine.

Displaced volume	400 cm^3
Stroke	73.8 mm
Bore	83 mm
Compression ratio	From 12.0:1 to 18:1
Number of valves	4
Max engine speed	8000 rpm
Injection	Direct with one multi-hole injector
Max boost pressure	4 bar abs.
Max eff. power	> 75 hp
Indicated efficiency	> 45% (with SACI)

The entire real engine at the test bench, including intake and exhaust system, has been reproduced in the 3D-CFD model. Figure 9.3 displays the test bench, whereas Figure 9.4 shows the corresponding simulation model.

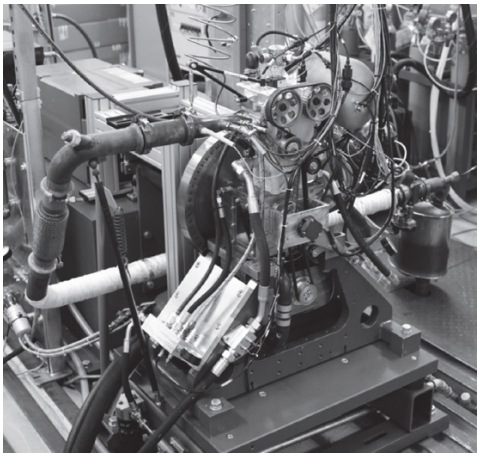

Figure 9.3: Research engine at the Technische Universität München.

The extension of the 3D-CFD domain to both the air tank and the exhaust muffler remarkably reduces the influence of the boundary conditions. Here,

the pressure signals can be assumed as constant over time. On the other hand, more simulation cycles (usually 6-8 cycles) must be performed to reach the convergence of the scavenging process.

Although the extended mesh contains approximately 240,000 cells, the simulation of one operating cycle takes no longer than 3 to 4 hours as single thread calculation. If High-Performance Computing (HPC) is used, the simulation time can be further reduced by a factor of 4 with a 16 cores CPU. In both cases, the computational time remains considerably lower compared to conventional 3D-CFD simulations [8].

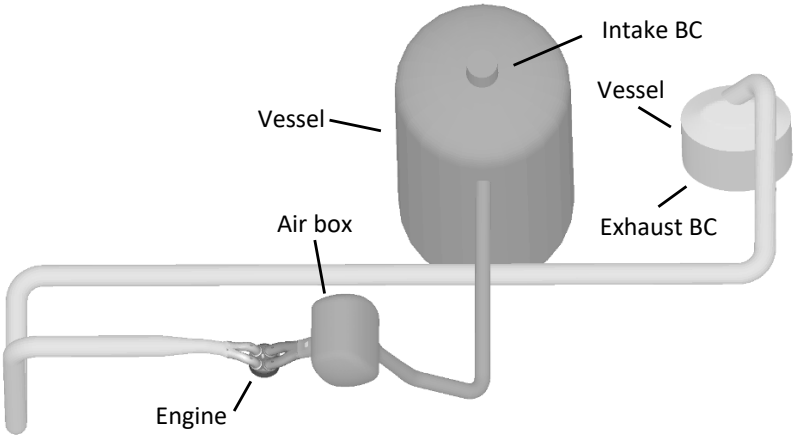

Figure 9.4: QuickSim model of research engine with test bench environment.

During the development phase, the joint research project faced several challenges with the ignition behaviour of the mixture. Charge air motion and mixture formation are essential processes when using a passive pre-chamber spark plug. They define the quality of the mixture inside of the pre-chamber as well as its scavenging. Ideally, both processes should be consistent over a wide range of engine loads and speeds to ensure a stable trigger of CI combustion.

A virtual engine development routine between the FKFS and TUM was indispensable to acquiring the results shown in the experimental results section of this work. Before testing the most promising fuels on the test bench,

the QuickSim 3D-CFD-simulation tool enabled the development of different piston crown geometries, intake ports, pre-chamber designs, and cam-timing strategies. Charge air motion and mixture formation were subsequently tailored to the requirements of the SACI combustion strategy. As a result, operation in SACI mode was possible in a stable and reproducible manner.

9.1.1 Experimental Validation of Simulation Models

To combine compression ignition and spark ignition combustion modes, new combustion models were adapted and calibrated using data from the test bench. Figure 9.5 shows the experimental pressure trace compared with the results of the simulation for the operating point described in Table 9.2. Results of the simulation show a good agreement with the test bench. Maximal pressure and pressure gradients during the combustion are very similar, which confirms a good capability of the simulation tool to predict also very complex combustion concepts.

Table 9.2: Operating condition of the single cylinder at the test bench.

Engine Speed	7000 rpm
Compression ratio	12.0:1
Intake pressure	2 bar
Intake Temperature	65 °C
Exhaust pressure	1.8 bar
Lambda	1.65
Fuel RON Number	102
EOI	225 b. TDC
IP	12 °deg b.TDC

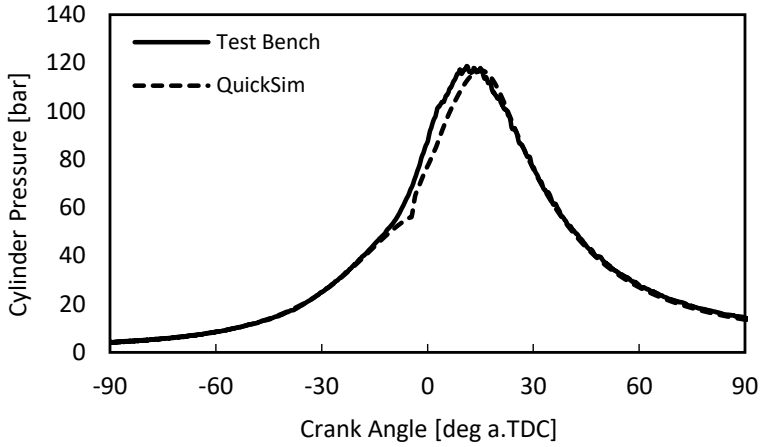

Figure 9.5: Comparison of experimental pressure trace with the results of the simulation.

9.2 First Analysis – Fuels Comparison at the Test Bench

The goal of this investigation is to increase engine performance (higher IMEP by the same fuel consumption in kg/h) by optimizing fuel composition. The analysis can be split into two parts: a first learning phase in which few existing fuels are compared to better understand how the engine reacts to different fuel characteristics (in terms of resistance to autoignition, laminar flame speed, and LHV) and a second phase in which a new virtually developed composition is created and tested.

No composition can perfectly fit every engine type. For instance, if a pure HCCI operating condition is used, it may be desirable to have a fuel with rapid autoignition characteristics while for high-performance engines, fast combustion and high resistance to knock are requested. The application here studied is particularly interesting because differently from conventional SI engines, a relevant part of the released energy comes from self-ignition of the mixture.

The analysis at the test bench was conducted with constant engine parameters, and merely the ignition point was adapted in each case to maximise power output in a knock limited region. More details are reported in Table 9.3.

The compositions tested in this study are representative of specifically designed high-performance fuels (RON higher 100). The properties of these fuels are summarised in Table 9.4 and all the reported values - due to confidentiality reasons - are normalised to those of Fuel 1. The information shown in this table is similar to what is typically found in the technical datasheets available at the test bench.

At a quick glance, these fuels appear to be very similar as they have the same RON number and an LHV difference lower than 0.5%.

Table 9.3: Engine operating parameters used for fuel comparison.

Engine Speed	6000 rpm
Fuel pressure	200 bar
Fuel consumption	Constant
p_2 and p_3	Constant
Pressure difference (p_2 - p_3)	0.2 bar
IP	Adapted according to knock limit
Lambda	Constant, $1.5 < \lambda < 2$

Table 9.4: Composition and main properties of the analysed fuels. Fuel 1 is considered as reference.

	Fuel 1	**Fuel 2**	**Fuel 3**	**Fuel 4**	**Fuel 5**
n-Alkanes	Ref.	+0.0%	+0.0%	+0.0%	+0.0%
iso-Alkanes	-	+10%	+0%	+3%	+3%
cycloalkanes	-	-8%	+2%	+9%	+2%
Olefins	-	+0%	+0%	-10%	-5%
Aromatics	-	-2%	-2%	-2%	+0%
Oxygenates	-	+0%	+0%	+0%	+0%
RON	-	+0.0%	+0.0%	+0.0%	+0.0%
MON	-	+1.5%	+0.0%	+0.7%	+0.8%
LHV	-	+0.4%	+0.2%	+0.2%	+0.0%

However, the experimental tests showed a completely different reality. Considering the indicated efficiency and the IMEP, which are shown in Figure 9.6, differences up to 5% were obtained. Fuel 1 is the one that performed best, and, for this reason, it is here considered as reference.

To understand the cause of these differences, it is necessary to take into consideration some of the fuel properties that affect the combustion process. Figure 9.7 compares the values of laminar flame speed and ignition delay time calculated with Cantera. Considering that the quantity of energy introduced is the same since the difference in LHV is very small (lower than 0.5%) and that the fuel consumption is constant. It can be noticed that the fuel that performed better is the one with the highest resistance to auto-ignition. This phenomenon may be explained considering that the charge is in critical conditions after the ignition of the spark plug and in order to have a more controlled knock-free combustion, the fuel must have a very high resistance to auto-ignition. It is also interesting to notice that fuel 4, which has the highest laminar flame speed - a property beneficial for reducing the combustion duration - and the lowest resistance to autoignition, is the one that obtained the lowest IMEP.

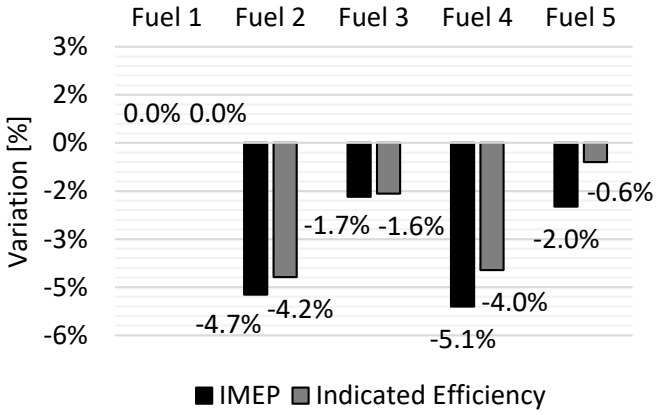

Figure 9.6: Variation in IMEP and indicated efficiency compared to Fuel 1.

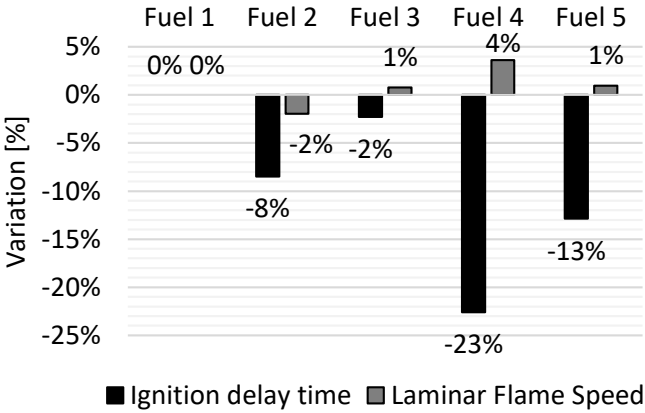

Figure 9.7: Variation in ignition delay time and laminar flame speed compared to Fuel 1. Values calculated at 750 K, 50 bar, lambda 1.

9.3 Optimization of Fuel Composition – Virtual Fuel Design

The idea behind the virtual fuel design is to exploit the chemical calculations done with Cantera to find a fuel composition that better satisfies engine requirements (in this case IMEP increase at limited fuel flow rates). This fuel is then tested virtually by means of engine simulations performed with QuickSim and, if significant advantages are obtained, it is finally tested at the test bench.

The virtual fuel design is performed by changing the mass fraction of the chemical species within predefined limits (that for example may come from technical regulations or supplier requirements). Afterwards, Cantera is used to calculate laminar flame speed and ignition delay time of each composition. This process is also relatively fast as it gives the possibility to analyse more than 500 fuel compositions in one day using a conventional computers. The results of these calculations are then filtered according to the desired constraints. In this case, the main limiting parameters are: aromatic content, olefin content and LHV since the analysis at the test bench is based on constant fuel consumption. Accordingly, the goal of the investigation was to find a composition that would increase the resistance to autoignition while keeping the LHV as high as possible.

The virtual fuel investigation conducted with Cantera showed that significant improvements in ignition delay time can be obtained but at the cost of lower laminar flame speed and LHV. In Figure 9.8 is shown how they change as the concentration of isooctane is changed at the costs of toluene. As the isooctane concentration increases and that of toluene decreases, lower resistance to autoignition but higher laminar flame speed and LHV are obtained. It should also be noticed that all trends are linear but a much more significant variation in ignition delay time is obtained (maximum 30% compared to 1% of laminar flame speed and LHV.). This implies that, according to requirements, a compromise between high knock resistance and fast-burning velocity with high energy content must be found.

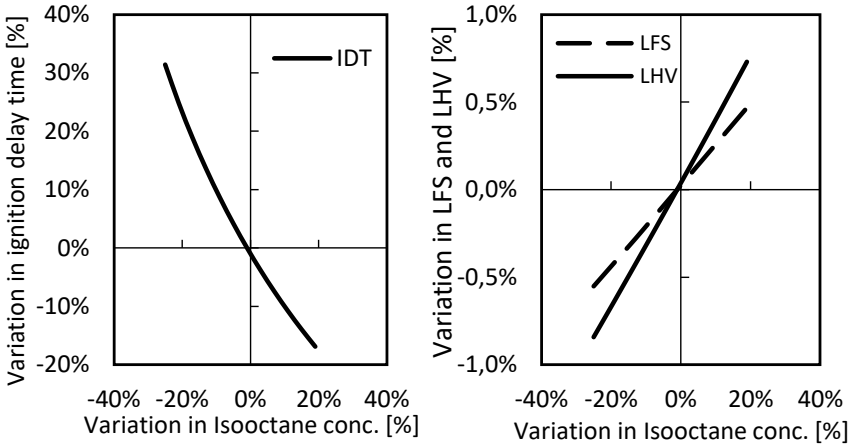

Figure 9.8: Variation in ignition delay time (left), laminar flame speed and LHV (right) as a function of isooctane concentration.

9.3.1 Proposed Fuel Composition

The composition and the properties of the chosen fuel (named as Fuel 6) are reported in Table 9.5 and they are expressed as variation compared to Fuel 1. This fuel was the most promising compromise among 2000 compositions virtually investigated. The most important differences in Fuel 6 are in the quantities of alkanes and aromatics. As is commonly known, aromatics have good resistance to autoignition but low LHV and flame speed compared to alkanes and therefore a compromise is needed. Due to extremely low LHV, ethanol was not included in the mixture. As reported in Figure 9.9, the new composition shows a significant increase in autoignition resistance (10% increase) while keeping similar flame speed and LHV (0.5% lower) compared to reference fuel 1.

Table 9.5: Composition and main properties of Fuel 6 compared to Fuel 1.

	Fuel 1	**Fuel 6**
n-Alkanes	Ref.	+0.0%
iso-Alkanes	-	-4.9%
cycloalkanes	-	+0.3%
Olefins	-	+0.6%
Aromatics	-	+4.0%
Oxygenates	-	+0.0%
RON	-	+0.0%
MON	-	-0.6%
LHV	-	-0.5%

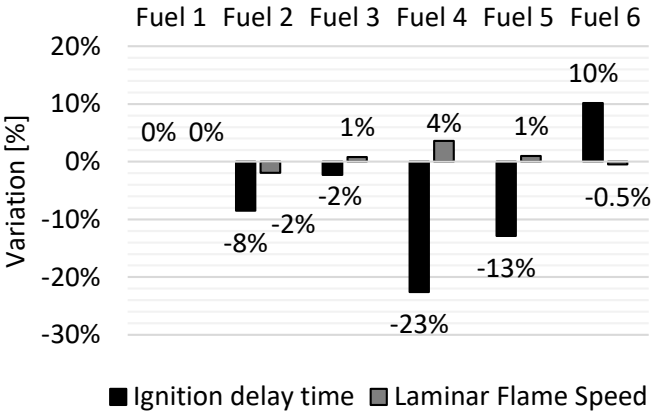

Figure 9.9: Variation in ignition delay time and laminar flame speed compared to Fuel 1. Values calculated at 750 K, 50 bar, lambda 1.

9.4 Validation at the Test Bench

QuickSim 3D-CFD-engine simulations confirmed the expectations found with the virtual reactor in Cantera and the fuel selection criteria. Fuel 6, due to its higher knock resistance, gives more stable combustion with consequently higher IMEP potential. For a similar cylinder pressure profile and IMEP, fuel 6 shows a lower amount of unburned mass in autoignition conditions compared to fuel 1. Slightly higher combustion duration of Fuel 6 is to be expected given the lower flame laminar speed. This advantage in combustion stability and autoignition resistance can be then exploited when, for the same operating point, the maximum IMEP is reached. The results showed that with the new fuel composition it is possible to obtain a higher cylinder pressure while still having a lower amount of unburned mass in autoignition conditions.

After this first virtual study, the new fuel was prepared and tested experimentally according to the same operating conditions previously introduced. As reported in Figure 9.10, fuel 6 showed a significant increase in IMEP (optimisation target) between 2.3% and 3% at different engine speeds, compared to the reference fuel 1. The indicated efficiency increased as well but to a lower extent: a peak increase of 2.5% is obtained at 5000 and 7000 rpm while no significant difference was found at 4000 rpm.

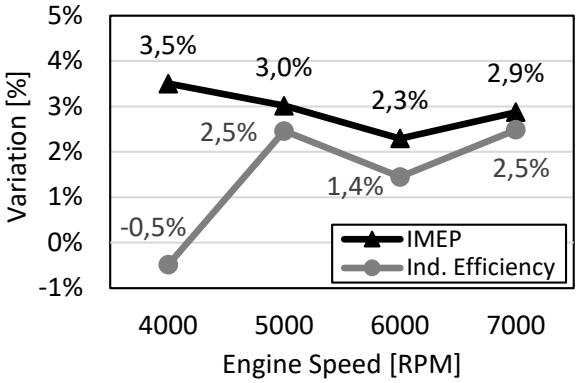

Figure 9.10: Variation in IMEP and indicated efficiency obtained at the test bench with fuel 6 in comparison with fuel 1.

10 Conclusion and Outlook

This work aims to improve the current simulation capabilities of the 3D-CFD tool QuickSim. By introducing a detailed fuel description and new combustion models, a more accurate description of the influence of fuel characteristics on combustion phenomena is achieved.

For what concerns fuels description, it is shown that, due to the increasing interest in alternative fuels, the simple surrogates used in the past years are not suitable for future investigations. If the same surrogate describes different fuels, simulation predictability is strongly limited. Detailed fuel description is a mandatory starting point for an effective virtual fuel investigation through CFD simulations.

According to the results of the fuel investigations performed on commercial and high-performance fuels, it is shown that to accurately reproduce a wide range of fuel characteristics, an extended surrogate formulation is needed. Accordingly, it is necessary to include, in the surrogate, at least one chemical species for each relevant hydrocarbon group present in the fuel. Depending on their concentration, components like cycloalkanes, oxygenates and olefins can have a substantial impact on fuel behaviour and, for more accurate results, their volume concentration in the surrogate should match the one in the fuel. However, it implies that a detailed chemical reaction mechanism is required to solve reaction kinetic and, due to its high computational time, a tabulated approach is needed to avoid a significant increase in CFD-simulation time.

The ignition delay time calculated with Cantera is used as input for a newly developed locally-distributed autoignition model based on the well known Livengood and Wu integral formulation. Differently from the original formulation, the integral is solved in every 3D-cell of the simulation domain and not according to average cylinder conditions. Such an approach brings to a more precise estimation of radicals formation and gives the possibility to calculate the location and quantity of the charge in autoignition conditions so that phenomena like knock onset can be correctly detected.

© The Editor(s) (if applicable) and The Author(s), under exclusive license to Springer Fachmedien Wiesbaden GmbH, part of Springer Nature 2021
F. Cupo, *Modeling of Real Fuels and Knock Occurrence for an Effective 3D-CFD Virtual Engine Development*,Wissenschaftliche Reihe Fahrzeugtechnik Universität Stuttgart, https://doi.org/10.1007/978-3-658-31628-0_10

The combination of detailed fuel description and new combustion models allowed to successfully investigate fuels with different ethanol content and to predict the influence of water injection on combustion and knock. Besides, it is shown that a detailed fuel description can, other than improving simulation accuracy, also be used for a virtual fuel design to support the research of the fuel composition that better fits engine requirements.

The introduction of a locally-distributed autoignition model opened new scenarios in the development of combustion models in QuickSim. In the future, this model can be used not only for knock detection but also for the initialization of HCCI, Diesel and any other combustion process.

For what concerns the numerical description of future alternative fuels, the current most significant limitation is the development and validation of respective reaction kinetic models. To better support the studies on e-fuels, the development of kinetic models should focus on accurately reproduce the characteristics of oxygenates and cycloalkanes.

Bibliography

[1] J. D. Anderson. *Computational Fluid Dynamics*. McGraw-Hill Education - Europe, 1995.

[2] A. Babajimopoulos, D. N. Assanis, D. L. Flowers, S. M. Aceves, and R. P. Hessel. A fully coupled computational fluid dynamics and multi-zone model with detailed chemical kinetics for the simulation of premixed charge compression ignition engines. *International Journal of Engine Research*, 6, 2005.

[3] M. Badami, V. Bevilacqua, F. Millo, M. Chiodi, and M. Bargende. Gdi swirl injector spray simulation:a combined phenomenological-cfd approach. *SAE Technical Papers*, 2004.

[4] M. Bargende. Berechnung und analyse innermotorischer vorgänge. Lecture notes, 2013.

[5] L. Cai and H. Pitsch. Optimized chemical mechanism for combustion of gasoline surrogate fuels. *Combustion and Flame*, 162, 2015.

[6] CD adapco. *Methodology - STAR-CD Version 4.20*, 2013.

[7] M. Chiodi. *An Innovative 3D-CFD-Approach towards Virtual Development of Internal Combustion Engines*. PhD thesis, University of Stuttgart, 2011.

[8] M. Chiodi, A. Kaechele, M. Bargende, D. Wichelhaus, and C. Poetsch. Development of an innovative combustion process: Spark-assisted compression ignition. *SAE Int. J. Engines*, 10, 2017.

[9] M. Chiodi, A. Perrone, P. Roberti, M. Bargende, and et al. 3d-cfd virtual engine test bench of a 1.6 liter turbo-charged gdi-race-engine with focus on fuel injection. *SAE Int. J. Engines*, 6, 2013.

[10] F. Cupo, M. Chiodi, M. Bargende, and et al. Virtual investigation of real fuels by means of 3d-cfd engine simulations. 2019.

© The Editor(s) (if applicable) and The Author(s), under exclusive license to Springer Fachmedien Wiesbaden GmbH, part of Springer Nature 2021

F. Cupo, *Modeling of Real Fuels and Knock Occurrence for an Effective 3D-CFD Virtual Engine Development*,Wissenschaftliche Reihe Fahrzeugtechnik Universität Stuttgart, https://doi.org/10.1007/978-3-658-31628-0

[11] A. Diez, R. J. Crookes, and T. Løvås. Experimental studies of autoignition and soot formation of diesel surrogate fuels. *Proceedings of the Institution of Mechanical Engineers, Part D: Journal of Automobile Engineering*, 227, 2013.

[12] P. Dirrenberger, P. Glaude, R. Bounaceur, H. L. Gall, , and et al. Laminar burning velocity of gasolines with addition of ethanol. *Fuel*, 115, 2014.

[13] M. Eberbach, M. Bargende, H. J. Berner., F. Altenschmidt, and M. Schrenk. Methane based fuels and high octane liquid fuels during knocking combustion. *12. Gasfahrzeugtagung*, 2019.

[14] A. Fandakov. *A Phenomenological Knock Model for the Development of Future Engine Concepts*. PhD thesis, University of Stuttgart, 2018.

[15] M. Fikri, J. Herzler, R. Starke, C. Schulz, and et al. Autoignition of gasoline surrogates mixtures at intermediate temperatures and high pressures. *Combustion and Flame*, 152, 2008.

[16] J. Fröhlich. *Large Eddy Simulation turbulenter Strömungen*. Vieweg+Teubner Verlag, 2007.

[17] B. Gauthier, D. Davidson, and R. Hanson. Shock tube determination of ignition delay times in full-blend and surrogate fuel mixtures. *Combustion and Flame*, 139, 2004.

[18] M. Gern, G. Kauf, A. Vacca, T. Franken, and A. Kulzer. Ganzheitliche methode zur bewertung der wassereinspritzung im ottomotor. 2019.

[19] O. L. Gülder. Correlations of laminar combustion data for alternative s.i. engine fuels. 1984.

[20] D. G. Goodwin, R. L. Speth, H. K. Moffat, and B. W. Weber. Cantera: An object-oriented software toolkit for chemical kinetics, thermodynamics, and transport processes. Version 2.4.0, 2018.

[21] J. F. Griffiths. *Flame and combustion*. Blackie Academic & Professional, 1995.

[22] M. Grill. Objektorientierte prozessrechnung von verbrennungsmotoren. 2006.

[23] C. Heinrich, H. Doerksen, A. Esch, and K. Kraemer. Gasoline water direct injection (gwdi) as a key feature for future gasoline engines. *5th International Conference on Knocking in Gasoline Engines, Berlin, Germany*, 2018.

[24] R. Herweg and R. R. Maly. A fundamental model for flame kernel formation in s. i. engines. 1992.

[25] J. Heywood. *Internal Combustion Engine Fundamentals*. McGraw-Hill Education, 1988.

[26] E. Hu, G. Yin, Z. Gao, Y. Liu, and et al. Experimental and kinetic modeling study on 2,4,4-trimethyl-1-pentene ignition behind reflected shock waves. *Fuel*, 195, 2017.

[27] S. Jerzembeck, N. Peters, P. Pepiot-Desjardins, and H. Pitsch. Laminar burning velocities at high pressure for primary reference fuels and gasoline: Experimental and numerical investigation. *Combustion and Flame*, 156, 2009.

[28] V. Knop and S. Jay. Latest developments in gasoline auto-ignition modelling applied to an optical cai (tm) engine. 61, 2006.

[29] D. Koch, V. Berger, A. Bittel, M. Gschwandtner, and et al. Investigation of an innovative combustion process for high-performance engines and its impact on emissions. 2019.

[30] D. Koch, G. Wachtmeister, M. Wentsch, M. Chiodi, C. Poetsch, and et al. Investigation of the mixture formation process with combined injection strategies in high-performance si-engines. *16th Stuttgart Symposium, Stuttgart – Germany*, 2016.

[31] Y. H. Liao and W. Roberts. Laminar flame speeds of gasoline surrogates measured with the flat flame method. *Energy & Fuels*, 30, 2016.

[32] Y.-H. Liao and W. L. Roberts. Laminar flame speeds of gasoline surrogates measured with the flat flame method. *Energy & Fuels*, 30, 2016.

[33] J. Livengood and P. Wu. Correlation of autoignition phenomena in internal combustion engines and rapid compression machines. *Symposium (International) on Combustion*, 5, 1955.

[34] O. Mannaa, M. S. Mansour, W. L. Roberts, and S. H. Chung. Laminar burning velocities at elevated pressures for gasoline and gasoline surrogates associated with ron. *Combustion and Flame*, 162, 2015.

[35] M. Mehl, J. Y. Chen, W. J. Pitz, S. M. Sarathy, and C. K. Westbrook. An approach for formulating surrogates for gasoline with application toward a reduced surrogate mechanism for cfd engine modeling. *Energy & Fuels*, 25, 2011.

[36] M. Mehl, W. J. Pitz, C. K. Westbrook, and H. J. Curran. Kinetic modeling of gasoline surrogate components and mixtures under engine conditions. *Proceedings of the Combustion Institute*, 33, 2011.

[37] N. Morgan, A. Smallbone, A. Bhave, M. Kraft, and et al. Mapping surrogate gasoline compositions into ron/mon space. *Combustion and Flame*, 157, 2010.

[38] A. Naidja, C. Krishna, T. Butcher, and D. Mahajan. Oxidation of fuels in the cool flame regime for combustion and reforming for fuel cells. *Progress in Energy and Combustion Science*, 2002.

[39] B. Noll. *Numerische Strömungsmechanik*. Springer, 1993.

[40] C. Pera and V. Knop. Methodology to define gasoline surrogates dedicated to auto-ignition in engines. *Fuel*, 96, 2012.

[41] Y. Ra and R. D. Reitz. A reduced chemical kinetic model for ic engine combustion simulations with primary reference fuels. *Combustion and Flame*, 155, 2008.

[42] E. Ranzi, A. Frassoldati, R. Grana, A. Cuoci, and et al. Hierarchical and comparative kinetic modeling of laminar flame speeds of hydrocarbon and oxygenated fuels. *Progress in Energy and Combustion Science*, 38, 2012.

[43] D. L. Reuss, T. W. Kuo, G. Silvas, V. Natarajan, and V. Sick. Experimental metrics for identifying origins of combustion variability during spark-assisted compression ignition. *International Journal of Engine Research*, 9, 2008.

[44] P. Risberg. *Describing the Auto-Ignition Quality of Fuels in HCCI Engines*. PhD thesis, School of Industrial Engineering and Management Royal Institute of Technology - Stockholm, 2006.

[45] S. M. Sarathy, G. Kukkadapu, M. Mehl, and et al. Ignition of alkane-rich face gasoline fuels and their surrogate mixtures. *Proceedings of the Combustion Institute*, 35, 2015.

[46] R. Scarcelli, T. Wallner, N. Matthias, V. Salazar, and S. Kaiser. Mixture Formation in Direct Injection Hydrogen Engines: CFD and Optical Analysis of Single- and Multi-Hole Nozzles. *SAE International Journal of Engines*, 4, 2011.

[47] S. Schneider, M. Chiodi, H. Friedrich, and M. Bargende. Development and experimental investigation of a two-stroke opposed-piston free-piston engine. 2016.

[48] S. Schneider, M. Chiodi, H. Friedrich, and M. Bargende. Analysis of si and hcci combustion in a two-stroke opposed-piston free-piston engine. 2017.

[49] R. Schwarze. *CFD-Modellierung*. Springer Berlin Heidelberg, 2012.

[50] L. Sileghem, V. Alekseev, J. Vancoillie, K. V. Geem, and et al. Laminar burning velocity of gasoline and the gasoline surrogate components iso-octane, n-heptane and toluene. *Fuel*, 112, 2013.

[51] G. Stiesch. *Elektronisches Management motorischer Fahrzeugantriebe*. Vieweg+Teubner Verlag, 2010.

[52] A. Vacca, M. Bargende, M. Chiodi, and et al. Analysis of water injection strategies to exploit the thermodynamic effects of water in gasoline engines by means of a 3d-cfd virtual test bench. 2019.

[53] M. Wentsch. *Analysis of Injection Processes in an Innovative 3D-CFD Tool for the Simulation of Internal Combustion Engines*. PhD thesis, University of Stuttgart, 2018.

[54] M. Wentsch, M. Chiodi, M. Bargende, C. Poetsch, and et al. Virtuelle motorentwicklung als erfolgsfaktor in der f.i.a. rallye-weltmeisterschaft

(wrc). *12th International Symposium on Combustion Diagnostics, Baden-Baden - Germany*, 2016.

[55] M. Wentsch, A. Perrone, M. Chiodi, M. Bargende, and D. Wichelhaus. Enhanced investigations of high-performance si-engines by means of 3d-cfd simulations. 2015.

[56] C. K. Westbrook. Chemical kinetics of hydrocarbon ignition in practical combustion systems. *Proceedings of the Combustion Institute*, 28, 2000.

[57] E. Winklhofer, H. Philipp, P. Kapus, and W. F. Piock. Anomale verbrennungseffekte in ottomotoren. *Haus der Technik Kongress, Essen*, 2004.

[58] D. E. Winterbone and A. Turan. *Advanced Thermodynamics for Engineers*. Butterworth-Heinemann, second edition edition, 2015.

[59] R. Worret, S. Bernhardt, F. Schwarz, and U. Spicher. Application of different cylinder pressure based knock detection methods in spark ignition engines. 2002.

[60] X. Zhen, Y. Wang, and D. Liu. An overview of the chemical reaction mechanisms for gasoline surrogate fuels. *Applied Thermal Engineering*, 124, 2017.

Appendix

Table A.1: Models implemented in QuickSim.

Phenomena	**Adopted Model**
Simulation methodology	Multiphase RANS
Turbulence	$k-\varepsilon$
Droplet drag	Function of the droplet Reynolds number
Secondary droplet breakup	Reiz-Diwakar
Wall impingement	Bai
Fluid	Euler-Lagrange

© The Editor(s) (if applicable) and The Author(s), under exclusive license to Springer Fachmedien Wiesbaden GmbH, part of Springer Nature 2021
F. Cupo, *Modeling of Real Fuels and Knock Occurrence for an Effective 3D-CFD Virtual Engine Development*,Wissenschaftliche Reihe Fahrzeugtechnik Universität Stuttgart, https://doi.org/10.1007/978-3-658-31628-0